The representation of the Kalahari Thermal Low and its induced circulations over southern Africa in observations and models.

Bellinda Mashoene Monyela

Thesis presented for the degree of

Doctor of Philosophy

Department of Oceanography

Faculty of Science

February 2024

SUPERVISORS

Prof. Mathieu Rouault

Nansen-Tutu centre for Marine Environmental Research & Department of Department of Oceanography, University of Cape Town, South Africa

Dr. Georges-Noel Tiersmondo Longandjo

Department of Oceanography, University of Cape Town, South Africa

FUNDING AND SCHOLARSHIPS

I highly acknowledge and appreciate the funding and scholarship from National Research Foundation (NRF) Grant holder Award under the ocean and atmospheric science SARCHI, Science Faculty Need-Based Fellowship and Mamokgethi Phakeng Fellowship.

DEDICATION

I would like to dedicate this thesis to mme ~ Leshirana Grace Monyela and mmane Mmatshaba Lesufi. Thank you for always being there for me!

I would also like to acknowledge and honour those who have been an integral part of my journey and have departed to another space!

My Dad – Matome Monyela (2001)

My Sister – Hilda Mamabolo (2003)

My Beloved Uncle – Mashadi Monyela (2005)

My Sister – Angelina Mamabolo (2007)

My Brother – Johannes Mamabolo (2009)

My Uncle – Selebalo Phasha (2009)

My friend – Samuel Leputu (2011)

My great grandmother – Semile Saka Phasha (2013)

My aunt – Florah Monyela (2019)

My paternal grandmother - Angelina Sthandwa Monyela (2020)

My maternal grandmother – Mmudi Matheba (2021)

My great uncle – Mmakotseng Matheba (2021)

My friend – Samuel Motimele (2022)

My aunt – Lauretta Mamogobo (2022)

My supervisor – Mathieu Rouault (2023)

My uncle – Rangwane Peter Monyela (2023)

uMakhi Wam! – Dr Precious (Mfazi)

Mahlalela (2023)

I will always comfort myself with Difela tsa Sione – Hymn 307 – Motse O re o Hlolegetseng.

ACKNOWLEDGEMENTS

I will forever be indebted to the unwavering support and, guidance of Professor Mathieu Rouault. You left me at a very delicate time of my thesis, but you at least left me under good hands.

Dr Georges-Noel, I cannot put into words how grateful I am. The unending conversations and revisions after revisions were torturous, yet you remained by my side and believe in my ability to deliver this work ~ Asante sana!

Prof Chris Reason, thanks for stepping up in my time of need.

Professor Isabelle Ansorge, thank you so much for everything you have done for me.

Mrs Cashifa Karriem, *skat* you have been very helpful and encouraging, may you not stop with me.

Mrs Nadia Jabaar, you have been a great help with finding resources beyond my scope of work.

Dr Raymond Romans you were always available to aid me with any technical issues.

"*Ya šika le tše digarago le yona ya gara*". I would not have survived this journey without the following people: Dr Natalie Ragoasha, Dr Ramontsheng Rapolaki, Dr Ntombifuthi Nzimande, Dr Precious Mahlalela, Mmapula Ramushu, Sinazo Maqezu, Zizo Stimela, Dr Philile Mbatha, Koketso Molepo, Jane Mello, Mamateane Mashao-Nkoana, Courtney Odendaal, Ilhaam Patel, Ivyne Mabaso, Mpho Senamela, Dr Kathy an der Westhuizen, Jonas Mamabolo, Dr Joseph Olusegun Adebayo, Mmachela Desire Kgarose, Lillian Maboya, Sive Xokashe, Munashe Madzimure, Dr Tshiamiso Makwela, Dr Zwido Khangale, Masefako Molepo, Paballo Chauke, Chuene Lefala, and Tebogo Phala.

Bonolo, Cia, Amogelang, Atlegang, Omphile and Matome, this is for you.

DECLARATION

I, Bellinda Mashoene Monyela, am presenting this thesis in full fulfilment of requirements for my PhD Degree under the supervision of Dr Georges-Noel Longandjo. I know the meaning of plagiarism and declare that all of the work in the dissertation, save for that which is properly acknowledged, is my own. I hereby grant the University of Cape Town free licence to reproduce for the purpose of research either the whole or any portion of the contents in any manner whatsoever of the above dissertation.

Signed by Candidate: Signed by candidate Date: 08/02/2024.

ABSTRACT

Many studies investigated the impacts of different drivers on southern Africa's precipitation. But the influence of the Kalahari thermal low (KTL) on the southern Africa precipitation is overlooked and deserve more attention. In austral summer, the Botswana high and the Angola low are highly dependent to each other. Here, we reconcile these two most important features of the southern Africa's climate as part of the same robust atmospheric feature, the KTL. The KTL is the semi-permanent heating source in southern Africa that displaces poleward from its initiation in September until its maturation in January and recedes rapidly to disappear near where it originated in March. However, the relationship between the KTL and Angola low shows two distinct behaviours at different timescales. At seasonal timescale (annual cycle), the Angola low, driven by the KTL, responds as a thermal low. But at the interannual timescale, the reversal of the relationship suggests that the Angola low behaves as a tropical low and forms as a Gill-like response to the diabatic heating related to KTL. The KTL has a strong negative correlation with southern Africa precipitation. This teleconnection is explained by the leading mode of variability, but it is controlled more by the heat dome mechanism rather than by the advection of the mid-tropospheric dry air into the convective region. During the warm phase of KTL, the anomalous surface warming induces a tropospheric subsidence that develops later into a heat dome, conducive to drought. In the cold phase, the reduced mid- tropospheric divergence favours the development of an anomalous moisture flux convergence that triggers the deep convection and leads to more rainfall. Furthermore, the accurate representation of the Hadley circulations over southern Africa revealed the coexistence of both shallow and deep Hadley circulations over southern Africa. The deep mode is characterized by a strong convection that occurs over the tropical southern Africa (between 25^{o}–15^{o}S). The shallow mode is associated with the thermally-driven shallow meridional circulation (SMC) over subtropical southern Africa (between 35^{o}–25^{o}S) and formed by the divergent flow. Its upper branch is constituted by the mid-tropospheric northerly jet (MTNJ) and the lower branch being formed by the low-level southerly jet (LLSJ). This vertical structure of the SMC has been mistaken by the observed opposite recirculation that is widely reported in the literature. This recirculation is dominated by the rotational wind, with its upper branch constituted by the subtropical southerly jet (STSJ) that connects the dry subtropical southern Africa

to the wet tropical southern Africa. The SMC contributes substantially to the moisture budget, with limited supply from the mid-tropospheric circulation. However, the mid-tropospheric air is predominantly advected westward towards the Atlantic Ocean by the AEJ-S rather than northward into the convective region by the STSJ as argued in the literature. Current climate models from CMIP6 not only underestimate the intensity of the KTL and its spatial structure, but also fail to reproduce the physical mechanisms through which the KTL controls the regional moisture budget.

Contents

LIST OF ACRONYMS

AEJ - S: African Easterly Jet, South

AEJ – N: African Easterly Jet, North

AMIP: Atmospheric Model Intercomparison Project

AL: Angola Low

CONV: Convergence

COLs: Cut – Off Lows

CRU: Climate Research Unit

CMIP: Coupled Model Intercomparison Project

DIV: Divergence

ENSO: El Nino Southern Oscillation

EOF: Empirical Orthogonal Functions

ERA5: European Centre for Medium Range Weather Forecast

ITCZ: Intertropical Convergence Zone

JRA55 – Japanese 55-year Reanalysis

GCMS: Global Climate Models

GISST: Global Sea Ice and Sea Surface Temperature

GPCC: Global Precipitation Climatology Centre (GPCC)

KTL: Kalahari Thermal Low

LLSJ: Low-level Southerly Jet

MERRA: Modern-Era Retrospective Analysis for Research and Applications

MCCs: Mesoscale Convective Complexes

MCT: Mozambique Channel Trough

MTNJ: Mid-tropospheric northerly jet

NCEP: National Centre for Environmental Project

OISST: Optimum Interpolation Sea Surface Temperature

SAH: South Atlantic High

SARI: South African Rainfall Index

SAH: Sahara Heat Low

SAMM: Shallow Atlantic Midlatitude Mode

SICZ: South Indian Convergence Zone

SIH: South Indian High

SIOD: Subtropical Indian Ocean

SMC: Shallow Meridional Circulation

SRI: Summer Rainfall Index

SST: Sea Surface Temperature

STSJ: Subtropical southerly jet

TTT: Tropical Temperate Troughs

WRI: Winter Rainfall Index

1 Introduction

1.1 Motivations

Thermal Lows (also known as heat lows) are low–pressure systems in the lower atmosphere caused by localised intense heating of the Earth's surface Johnson (2003). Since, these low–pressure systems are intimately related to surface conditions, the maximum temperature amplitudes and atmospheric conditions associated with them are usually confined below 500 hPa (Johnson, 2003). The converging circulation associated with the intense surface heating produces a vertical motion in the lower troposphere, which in turn, is capped by a sinking motion at mid-troposphere (Johnson, 2003). Previous studies (Lindzen and Hou, 1988, Zhang et al., 2004, Zhang et al., 2008) showed that over the tropics, a thermal low drive the formation of a shallow meridional circulation (SMC) in the mid-lower troposphere. Albeit, a local phenomenon, the SMC is defined as a vertical meridional overturning circulation like the commonly known deep circulation, except its return flow is in the lower troposphere (i.e., below 500 hPa, Zhang et al.,2004).

To understand the SMC dynamics, Nolan et al. (2007) simulated the idealised Hadley Circulation driven by moist convection in the tropical regions. The authors found that even in the absence of deep convection, the SMC is well reproduced, but it is driven by the reversal of pressure gradient above the atmospheric boundary layer with a strong return flow in the mid-troposphere. The key difference between the SMC and the deep circulation is that the SMC has maximum wind and return flow at the lower troposphere (Zhang et al., 2004). But over nearly all monsoon regions during local summer, the SMCs are superimposed on the deep circulations that produce rainfall (Nie et al., 2010). These shallow circulations further transport dry subtropical mid-tropospheric air into the tropical monsoon precipitation maxima (Zhai and Boos, 2017). Consequently, thermal lows are important climatological features over arid lands in the subtropics, especially during the local summer when solar insolation is at its highest. These regions include west Africa and Sahel (Lavaysse et al., 2009, Lavaysse et al.,

2010), Australia (Lavender, 2017, Preissler et al., 2002), southwestern North America (Rowson and Colucci, 1992), Iberian Plateau (Hoinka and Castro, 2003), Saudi Arabia (Blake et al., 1983), west Pakistan and northern India (Bollasina and Nigam, 2011) and Kalahari (Ryoo et al., 2022, Howard et al., 2019, Munday and Washington, 2017). In the above highlighted regions, thermal lows play a significant role in modulating weather and hydroclimate conditions. For instance, Hung and Yanai (2004) suggested that heat lows influence the monsoon systems by advecting low-level moist monsoonal air inland and further intensifying the monsoon circulation in northern Australia–Arafura Sea. Australian Heat Low controls the Australian monsoon system by creating an unstable convective environment through land-sea temperature contrast (Kawamura et al., 2002). When the land-sea temperature is coupled with additional large-scale disturbances, such as Madden- Julian Oscillation (Zhang, 2005), deep convection can occur (Kawamura et al., 2002). Over Asia, the Arabian Heat Low has a two–way relationship with the southwest Asian monsoon. The Arabian Heat Low is maintained by the monsoon through adiabatic warming and large-scale descent, while the thermal advection of the Arabian Heat Low into the western Arabian Sea confines and sustains low-level moisture within the monsoon (Fonseca et al., 2022). Over West Africa, during the monsoonal season (i.e., from May to September) the variation of Saharan (also called West African) Heat Low impacts the rainfall anomalies on an interannual and interdecadal scale (Biasutti et al., 2009). As one of the dynamic components of the West African monsoon systems (Lavaysse et al., 2010, Lavaysse et al., 2009, Martin and Thorncroft, 2014, Thorncroft et al., 2011, Zhai and Boos, 2017), the Saharan Heat Low increases the monsoon flow south of the heat low and the northerly Harmattan winds west of the heat low, respectively. A strong upward motion over the Saharan Heat Low strengthens and impacts the structure of the northern African Easterly Jet (AEJ-N) at around 700 hPa (Lavaysse et al., 2009). Besides, the Saharan Heat Low and Atlantic cold tongue modulate the annual evolution of the moisture flux and associated convergence over the West African monsoon systems (Thorncroft et al., 2011). At an interannual timescales, the rainfall variability over Sahel is closely related to the strength of the Sahara Heat Low in observations and climate models (Haarsma et al., 2005, Biasutti et al., 2009, Thorncroft et al., 2011). This means that enhanced rainfall over Sahel is caused by a stronger SMC over the Sahara. However, (Hurley and Boos, 2013) and (Zhai and Boos, 2017) arguably proposed that

the southward advection of the dry mid-tropospheric air originating from Sahel into a convective region by the seasonal-mean SMC inhibits the monsoon precipitation.

Unlike west Africa where the Sahara low and its induced SMC are widely documented, in southern Africa, they were overlooked. Nie et al. (2010) was the first to highlight the existence of a SMC over southern Africa, but with little cross-equatorial flow in the mid-troposphere. Hurley and Boos (2013) further investigated the relationship between the SMC and the regional rainfall over southern Africa and found that increased precipitation is associated with a weakened SMC. However, Zhai and Boos (2017) reported that over southern Africa, the horizontal moisture advection is produced by transient eddies rather than by the seasonal-mean circulations. Although, the Kalahari Desert is located poleward of the rainfall maximum, intense temperature in the boundary layer is associated with weak easterly jet at ~ 600 hPa, suggestive of a shallow and dry circulation (Nie et al., 2010). But, for Adebiyi and Zuidema (2016), the southern branch of the African easterly jet (AEJ-S, between 600 and 700 hPa) is diabatically driven by temperature-moisture gradient between the poleward hot-dry convection related to the thermal low and the equatorial cool-moist convection associate with intense rainfall. Interestingly, Reason (1996) found that due to the interaction of the background easterly flow with the surface heating and the topography, continental thermal low forms on the western sides of continents over tropical and subtropical latitudes. Furthermore, Munday and Washington (2017) and Howard and Washington (2018) found a strong connection between the thermal low in southern Africa and the Angola low, which in turn, impacts the regional hydroclimate. Firstly, Munday and Washington (2017) found that the Angola low, driven by surface heating, is a thermal low in austral spring before transitioning into a tropical low associated with moist instability in austral summer (DJF). Howard and Washington (2018) furthered this study to unravel that the Angola low is formed by a combined effect of dry thermal low and anchored Angola tropical low-pressure systems. This anchored mechanism to Angola region is provided by the anabatic sea-breeze circulation. But at interannual timescales, the Angola tropical low modulates the southern African precipitation, while the heat low has no bearing on precipitation variability in summer (Howard and Washington, 2018). This means that the Kalahari low has no link with the regional rainfall from November to February. But its thermally induced SMC has a strong impact on regional rainfall – strong northward advection of

dry mid-tropospheric air originating from Kalahari low into the convective region by the seasonal-mean SMC inhibits the strengthening of rainfall (Hurley and Boos, 2017; Zhai and Boos, 2018). These contrasting results suggest that the role of Kalahari low is not well understood and deserve more investigation. In addition, little is known about the influence of the Kalahari thermal low and its induced SMC on the regional moisture budget.

The previous studies (Engelbrecht et al. 2009; Cook and Vizy, 2013; Vizy et al., 2015; Vizy and Cook, 2016) suggested that the Angola Low and the Kalahari Thermal Low are expected to strengthen due to amplified surface warming in response to anthropogenic climate. Notwithstanding that, the sixth assessment report of the IPCC (((IPCC), 2022) stipulated that the mean rainfall in the summer region of southern Africa is projected to decrease by 10–20% with an increase in the number of consecutive dry rainy days under a business-as-usual model. Whilst the temperature is expected to rise. Therefore, it is very crucial to (a) further our understanding of observed variability, trends, driving mechanisms and hydroclimatic impacts of the

Kalahari Thermal Low, and to (b) examine whether state-of-the-art climate models can represent the Kalahari Thermal Low, its driving mechanisms and its impact on regional hydroclimate.

1.2 Aims and objectives.

The main objective of this dissertation is to fill the gap in the literature by highlighting the potential roles played by the Kalahari Low and its induced SMC on regional precipitation during the summer season (DJF).

To achieve this aim, this dissertation is going to address the following questions:

(i) What is the mean-state structure of the Kalahari Low and the dynamics of its induced SMC during austral summer? What are physical mechanisms through which the Kalahari low impact the southern Africa hydroclimate?

(ii) How does the thermally driven SMC induced by the Kalahari Thermal Low affect the regional moisture budget over southern Africa?

(iii) How well do some models of the recent version of the Climate Model Intercomparison Project (CMIP6) represent the Kalahari low and its induced circulation as well as its influence on regional precipitation?

1.3 Literature review / background

1.3.1 Overview of the southern African geography and climate

Southern Africa is defined here as Africa south of 15°S. Due to its position, the subcontinent is mainly semi-arid and is influenced by different weather and hydroclimatic systems from both the tropics and subtropics. Topography also plays a vital role in regulating the climate and weather in southern Africa (Tyson and Preston-Whyte, 2000). Areas of elevated terrain on the eastern and western coasts are separated by a relatively flat interior plateau of 1 – 1.5 km above sea level, the Kalahari Basin (Figure 1.1). The eastern escarpment comprises the Drakensberg-Maloti Mountain range (Figure 1.1) reaching about 3400 meters at the Lesotho and South African border. The Mozambican coastal plain flanks the Drakensberg-Maloti Mountain range on the eastern side. An interaction between the north-eastern escarpment and the propagating westerly waves at the tip of South Africa assist in developing convective storms (Garstang et al., 1987). While the eastern escarpment acts as an initiator for developing mesoscale convective systems (Blamey and Reason, 2013). The Cape Fold Belt lies on the south and west coast of South Africa. The South African coastal topography also plays a significant role in climate by promoting the ascent of air over the escarpments and blocking the propagation of synoptic systems, such as cut-off lows (Singleton and Reason, 2007). The western coast of southern Africa consists of the Bie Plateau over Angola and the Khomas Highlands in Namibia (Figure 1.1).

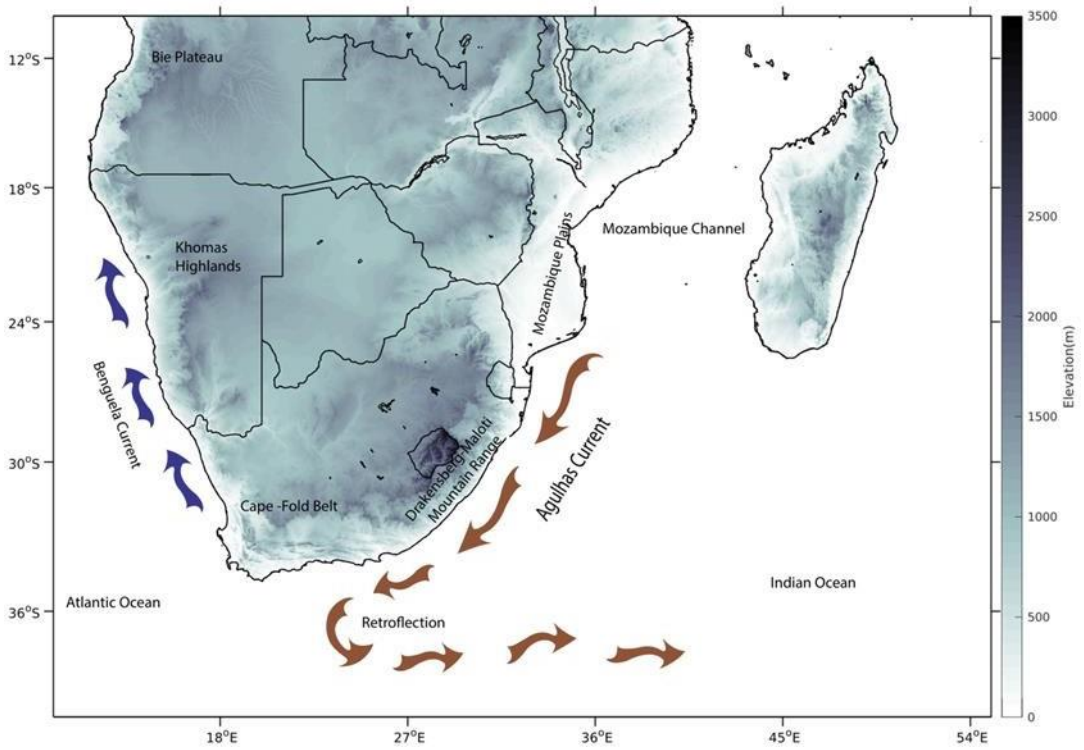

Figure 1.1: The elevation (shaded, m) of southern Africa. The brown arrows in the Indian Ocean represent the Agulhas Current while the blue arrows in the Atlantic Ocean represent the Benguela Current.

Southern Africa is flanked by two ocean currents, namely Agulhas and Benguela currents. The warm Agulhas current (Lutjeharms, 2006) flows southwards on the east coast of Southern Africa. The current retroflects back to the Indian Ocean once itaches the southern tip of the continent as the Agulhas Return Current (Beal et al., 2011). The Agulhas current systems impact the precipitation over southern Africa (Jury et al., 1993, Reason, 2001a, Imbol Nkwinkwa et al., 2021, Nkwinkwa Njouodo et al., 2018, Tim et al., 2022). The moisture fluxes and air masses that travels from the warm Agulhas current to the subcontinent, favours precipitation, especially in the southeast coast (Imbol Nkwinkwa et al., 2021). On the other hand, the cold Benguela current runs along the west coast of Southern Africa. The cold water from the Benguela current also impacts the heat and moisture content of the air masses, which leads to hazy conditions along the coast and parched conditions (e.g., Kalahari and Namib desserts) further inland (Reason, 2017).

The topography and the two contrasting oceans contribute to the complexity of the climate of southern Africa. However, most of southern Africa receives rain in summer

(depicted as SRI on Figure 1.1), primarily through deep tropical convective processes (Pohl et al., 2014) such as tropical-temperate troughs (TTT; Macron et al., 2014). In contrast, the southwestern tip and the hinterlands receive rain during the austral winter (depicted as WRI on Figure 1.2) due to the influence of the mid-latitude systems (Philippon et al., 2012), such as the passage of westerly cold front systems (Reason and Phaladi, 2005). While the southern coast (black box in Figure 1.2) receives rain throughout the year due to its orientation relative to the South Atlantic High and South Indian pressure systems and the typical tracks of cold fronts and migratory anticyclones (Mahlalela et al., 2020). Therefore, the southern coast rainfall is dependent on the climate processes that drives both the summer and winter rainfall.

1.3.2 Semi-permanent circulation systems over southern Africa

1.3.2.1 South Atlantic and Indian High

The position of South Atlantic High (SAH, Figure 1.3) and South Indian High (SIH, Figure 1.3) vary throughout the year. The SAH moves 6 ° and 13 ° meridionally and annually (Tyson and Preston-Whyte, 2000). The SAH pressure system plays a significant role in advecting moisture into the land regions of southern Africa (Reason, 2001b). The latitudinal variability of SAH and other westerlies act to reduce or enhance the advection of moisture towards the subcontinent by allowing or not allowing the southern Atlantic trade winds to bring moisture into the subcontinent south of 25° (Vigaud et al., 2009). The seasonal changes in the position of the SAH drive changesin the surface winds and the SST along the Atlantic region (Reason and Smart, 2015). The SAH also contributes to the strong upwelling on the west coast of southern Africa during austral summer. The southerly winds from the SAH drives the colder Sea Surface Temperatures (SSTs) on the Namibian Coast throughout the year.

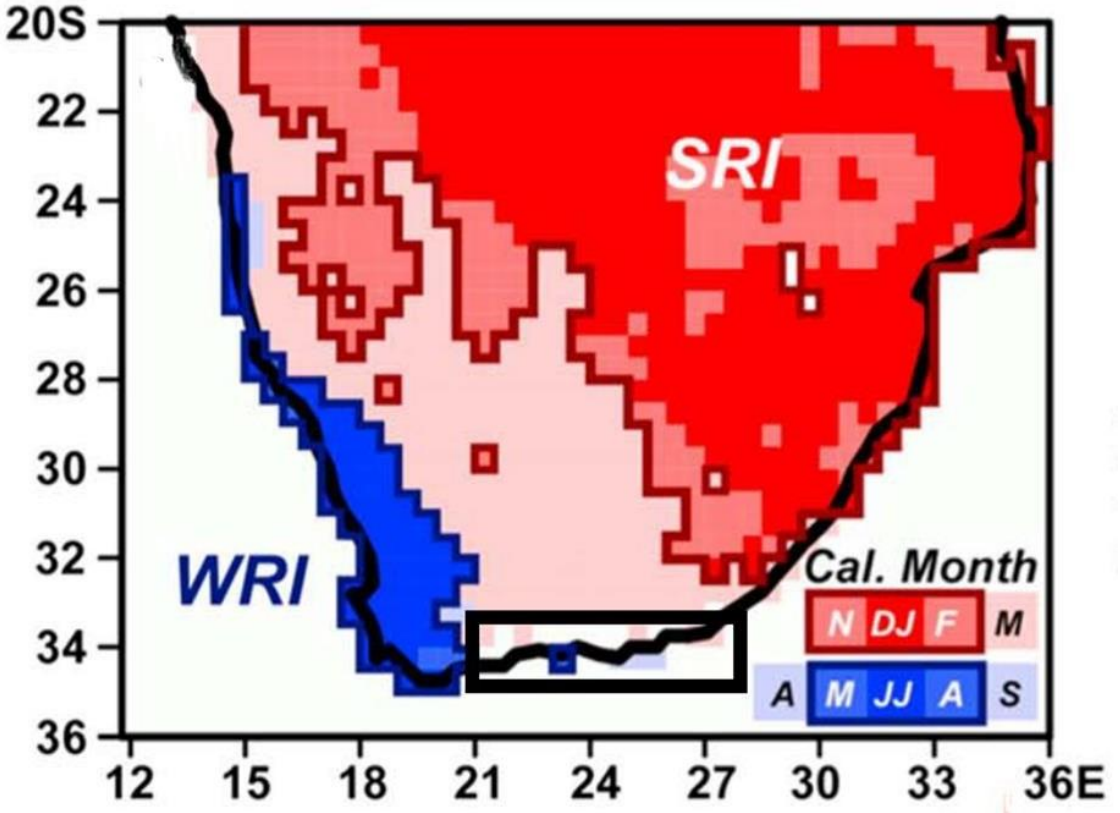

Figure 1.2: The spatial distribution of the wettest month of the year over southern Africa using Climate Research Unit (CRU) precipitation dataset. The wettest months in the summer rainfall region (SRI, red) occur between November, December, January, February. While the wettest months in the winter rainfall region (WRI, blue) occurs between May and August. The black box delineates “all year” rainfall zone. (Adapted from Dieppois et al. (2016), with some modifications).

On the other hand, SIH moves 5 º zonally and 24 º meridionally per annum (Tyson and Preston-Whyte, 2000). The meridional shift of the SIH influences the weather and climate of the east coast of southern Africa during summer and winter. (Fauchereau et al., 2003) and (Hermes and Reason, 2005) highlighted that the changes in the intensity of the SIH are linked to the dominant mode of the pressure field, Southern Annular Mode (SAM; Fogt and Marshall, 2020). Furthermore, the fluctuations in the SIHintensity are highlighted by (Behera and Yamagata, 2001) to influence the formation of the Subtropical Indian Ocean Dipole (SIOD).

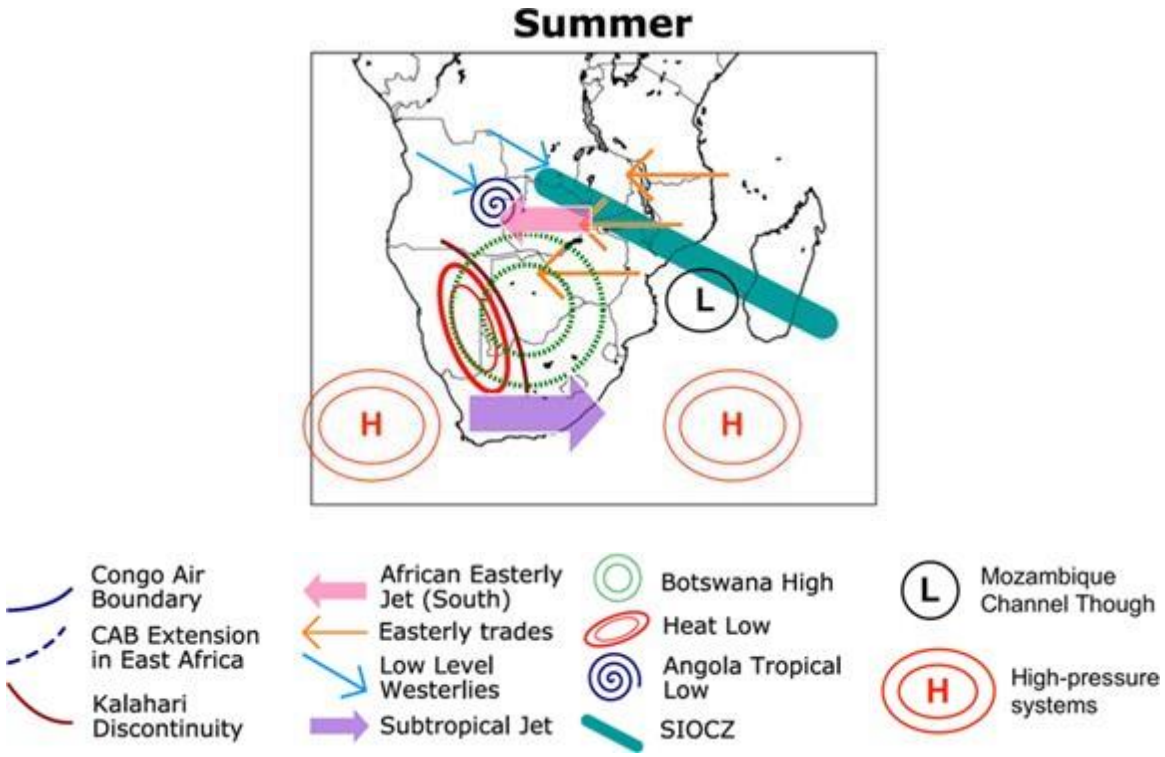

Figure 1.3: Dominant features over Southern Africa during summer. Figure adapted from Howard and Washington (2019) with some modifications.

1.3.2.2 Intertropical Convergence Zone

North of the two southern hemisphere anticyclones, lies the Intertropical Convergence Zone (ITCZ) which migrates between the southern and northern hemispheres between July and January. During austral summer, particularly in February, the ITCZ reaches its southernmost position and lies across central Mozambique and Madagascar (Reason et al., 2006). Wet January summers over southern Africa may be associated with the southward shift of the ITCZ (d'Abreton and Tyson, 1995). The increased rainfall can be attributed to an increased moisture flow from the north due to the anomalous Hadley cell. There are less frequent dry spells near the ITCZ zone across northern Madagascar, northern Mozambique and Zambia compared to more frequent dry spells over the desert and semi-deserts areas of southwest Africa (namely, Botswana, Namibia, and South Africa) during summer (Usman and Reason, 2004).

1.3.2.3 Botswana High

Botswana High (BL, Figure 1.3) pressure system is a prominent mid-tropospheric level (~ 500 hPa) feature that modulates southern African climate. The high-pressure system usually develops during early austral spring (August) and then intensifies and

moves southwards over southern Africa during austral spring and summer, and then weakens and dissipates around May. Botswana High is always situated to the south and southeast of the regions with heavy rainfall associated with the ITCZ (Driver and Reason, 2017). This is why Reason (2016) suggested that the Botswana High, which lies above the thermal low is generated in response to tropical precipitation to the northeast. The impact of Botswana High on rainfall variability was not well studied until (Unganai and Mason, 2002) found that some droughts in Zimbabwe, especially in 1982 -1984 and 1991/2 were influenced by a strong seasonal high-pressure system over Botswana and persistent blocking systems from the Indian Ocean. During these two droughts, Botswana High prevented the passage of the upper westerly waves. Botswana High is typically stronger during an El Niño phase and weaker during a La Niña phase (Driver and Reason, 2017). However, Driver et al. (2019) highlighted that the intensity of the rainfall is not always proportional to the magnitude of ENSO, because there are numerous neutral ENSO summers with large positive anomalies of Botswana High. While investigating the response of Botswana High to ENSO using a Variable Resolution Global Climate Model, Maoyi and Abiodun (2021) found that although ENSO enhances the strength of Botswana High, it however does not aid in its development.

1.3.2.4 Angola low

Angola Low (AL, Figure 1.3) is a semi-permanent low-pressure system located over southern Angola and northern Namibia during summer. The Angola Low is the primary driver of tropical moisture transport that contributes to the development of tropical temperate cloud bands. The SSTs in the tropical southeast Atlantic Ocean and Angola low influence summer rainfall over southern Africa through the near-surface westerlies that feed a stronger Angola Low, leading to increased low-level moisture at the source region of the tropical temperate troughs (Reason et al., 2006). During the genesis of Angola Low, the two oceans flanking the subcontinent and the weak surface high over Mozambique enhance a pressure gradient between Zimbabwe and Botswana. The increased pressure gradient fuels the strong lower-level easterly flow, promoting the flow of tropical easterlies north of Madagascar deep into the subcontinent (Hart et al., 2013). Munday and Washington (2017) used CMIP5 to study the circulation of Angola Low over southern Africa. The study indicated that the strength of the simulated Angola Low during summer is associated with ~ 40 % of the intermodal mean rainfall variability

across the subcontinent. Crétat et al. (2019) explored the influence of Angola Low on southern Africa and its relationship with ENSO during extended summer (NDJFM) between 1980/81 and 2014/15. The study used clustering analysis to extract different modes of the Angola Low, namely the northward Angola Low, Near Climatological Angola Low and Southward Angola Low. The study suggested that at an interannual time scale, ENSO significantly modulates the occurrences of most Angola Low modes. However, the weaker and southward Angola low was strongly correlated with regional rainfall rather than ENSO.

1.3.3 Mozambique Channel Trough

Mozambique Channel Trough (MCT, Figure 1.3) is one of the low-pressure systems located within the South Indian Convergence Zone (SICZ, (Cook, 2000)). MCT plays a role in transporting moisture from the Mozambique channel to the interior of southern Africa (Mawren et al., 2022). MCT forms in December and reaches its peak in February. The generation of MCT can be attributed to the dynamical adjustment of the easterlies over the Madagascan topography and the local air-sea interaction due to warm SST (Barimalala et al., 2018). The peak of MCT in February is associated with a southward shift of the ITCZ, southeast shift of the SIH and the maximum SST in the Mozambique Channel (Barimalala et al., 2020).

1.3.4 The role of the surrounding oceans on southern African rainfall

1.3.4.1 Indian Ocean

The Indian Ocean (Figure 1.1) is the primary source of moisture for southern African rainfall (Reason, 2001b, Fauchereau et al., 2009). For instance, a popular climate mode in the Indian Ocean called Subtropical Indian Ocean Dipole (SIOD; (Hermes and Reason, 2005, Reason, 2001b, Behera and Yamagata, 2001) controls the inter-annual rainfall variability in southern Africa. The SIOD was found by Behera and Yamagata (2001) using Empirical Orthogonal Function (EOF) extracted from Global Sea Ice and Sea Surface Temperature (GISST2.3b) observational data. The SIOD is formed by the latent heat flux exchange between the atmosphere and the ocean (Ohishi et al., 2015). The SIOD is dominant during austral summer, and it oscillates between two phases, namely, positive, and negative phases.

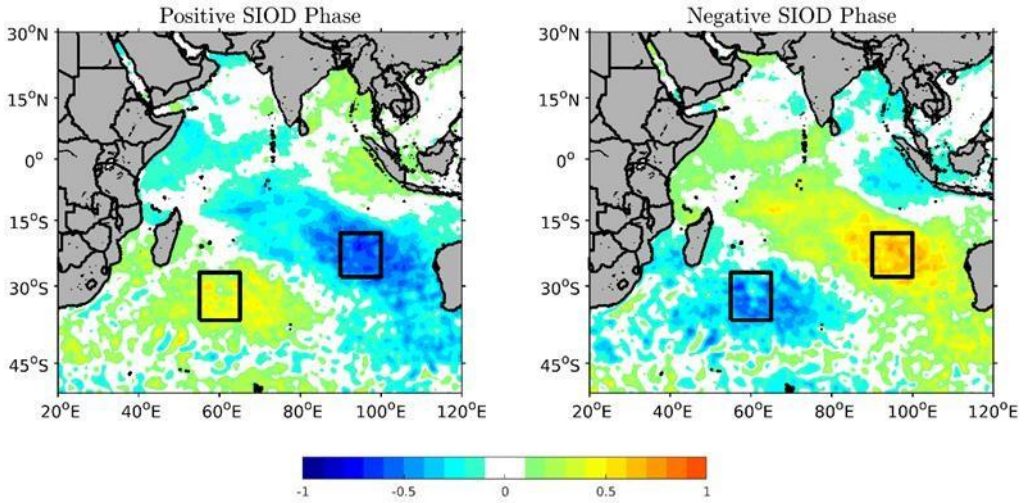

Figure 1.4: Normalised Anomalies of Sea – Surface Temperature from December to February over a 40-year climatological period (1982-2021). The black boxes represent western and eastern poles of the Subtropical Indian Ocean Dipole. The positive and negative phases of the SIOD is represent by (a) and (b). The dataset is from Optimum Interpolation Sea Surface Temperature.

The positive phase of the SIOD (Figure 1.4) is characterised by positive SST anomalies on the southwestern side of the Indian Ocean and negative anomalies on the south-eastern side of the Indian Ocean. Conversely, the negative phase of the SIOD (Figure 1.4) is characterised by negative anomalies on the southwestern side of the Indian Ocean and positive anomalies on the south-eastern side of the Indian Ocean. Many regions in the southeast of southern Africa get positive anomalous rainfall during a positive SIOD phase. An Atmospheric General Circulation Model was used by (Reason, 2001b) suggested that the favourable rain is due to a strengthened onshore flow influenced by the increased evaporation at the warm southwestern side of the positive SIOD, which increases moisture. The increased moisture then advects towards south-eastern Africa and Mozambique.

1.3.4.2 Atlantic Ocean

The South Atlantic Ocean (Figure 1.1) is the secondary source of moisture for summer rainfall over southern Africa (Tyson and Preston-Whyte, 2000, Vigaud et al., 2009, Williams et al., 2008). The SSTs in the south Atlantic Ocean are connected to the anomalous atmospheric circulations that control the southern African climate (Rouault et al., 2003). Using EOF over southern Africa during summer, Vigaud et al. (2009)

found that the South Atlantic Midlatitude Mode (SAMM) is correlated with Climate Research Unit (CRU) rainfall dataset and mimics the rainfall patterns over the South African Rainfall Index (SARI; Richard et al., 2001). The SAMM has two phases, negative and positive phases. The positive phase is correlated with surface pressure changes when the SAH shifts northwards, while the negative phase occurs when the SAH moves southwards.

1.3.4.3 Pacific Ocean

'El Niño' was a term coined by fishermen from Ecuador and Peru in the Pacific Ocean to refer to the annual warming of water during Christmas at their coasts. Nowadays, the climate science community refers to anomalous warming of the SST in the central and eastern Pacific oceans as an El Niño event. As a result, the anomalous cooling of the SST in the east and the central Pacific Ocean is referred to as a La Niña event.

Southern Oscillation is a term that explains the see-saw fluctuations of atmospheric mass (namely, sea level pressure) between the eastern and western Pacific Ocean (Cane, 2005). The positive phase of the Southern Oscillation is characterised by positive anomalous sea level pressure at Tahiti and negative anomalous sea level pressure at Darwin. The negative phase of the Southern Oscillation is oppositely characterised by negative anomalous sea level pressure at Tahiti and positive anomalous sea level pressure at Darwin. The climate mode used to measure this atmospheric phenomenon is the Southern Oscillation Index, which defines the normalised difference in sea level pressures between Darwin and Tahiti.

The prolonged phase of the Southern Oscillation is associated with a La Niña event. In contrast, the prolonged negative phase of the Southern Oscillation is associated with an El Niño event. The prominent similarity between the ocean Niño and atmospheric Southern Oscillation indices separated in space, represent the same phenomenon, hence El Niño Southern Oscillation (ENSO).

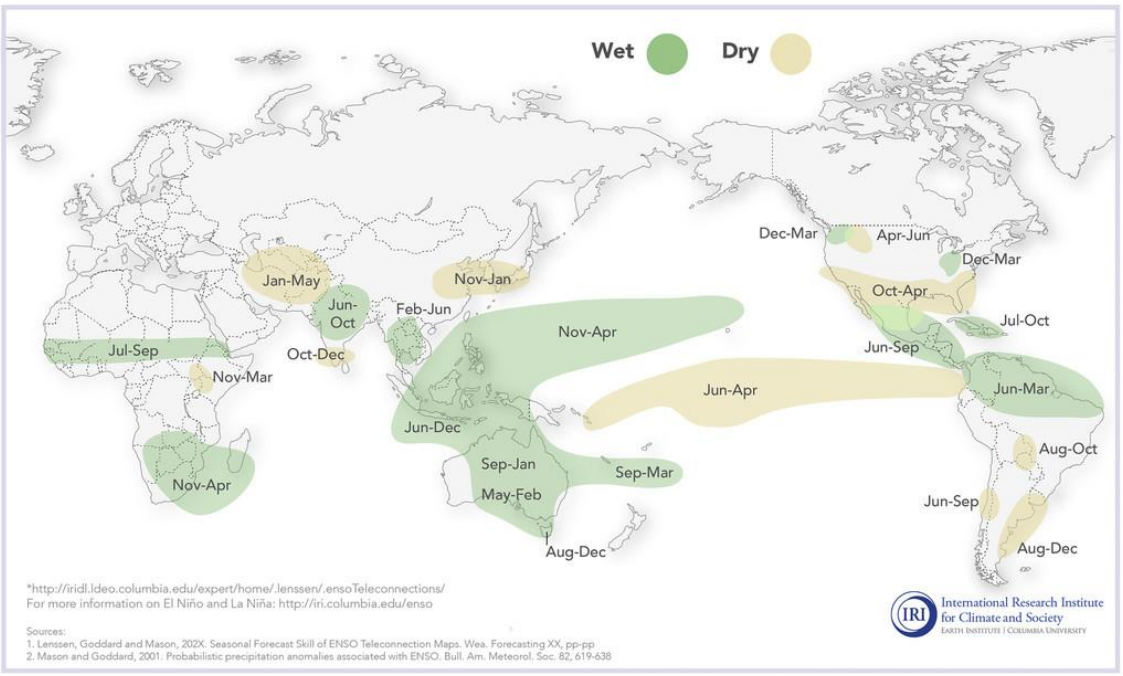

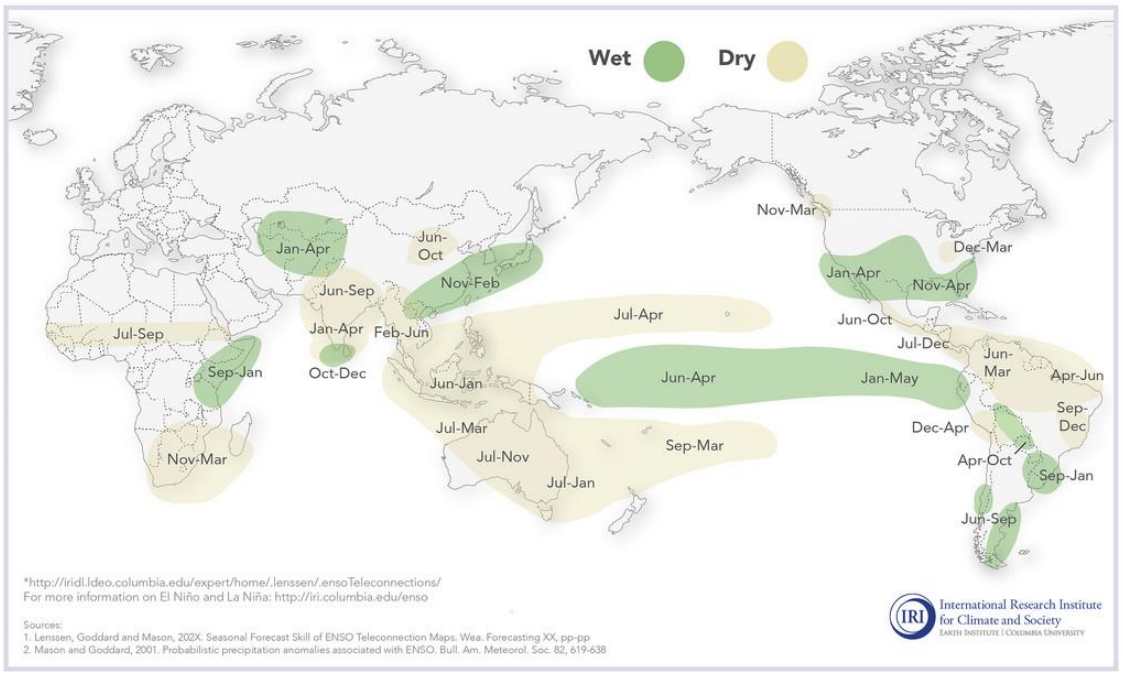

Figure 1.5: Rainfall patterns during La Nina (top) events and El Niño events. Image adapted from Lenssen et al. (2020).

The ENSO episodes (La Niña, neutral, and El Niño) are characterised by temperature, wind field, and sea level pressure differences, creating different weather and climate conditions over southern Africa and across the globe (Tyson and Preston-Whyte, 2000). For example, during La Niña, the sea surface temperature and sea level pressure in the central Pacific Ocean decrease, leading to a shallower thermocline and stronger winds. The reverse occurs during El Niño. The opposing changes in sea

surface temperature and sea level pressure during La Niña and El Niño affect the location of the major cloud bands, thus modifying the rainfall's effect on the continents (Figure 1.5). ENSO is the primary driver of the inter-annual rainfall variability in Southern Africa (Richard et al., 2001; Reason and Jagadheesha, 2005; Pohl et al.,2009; Meque and Abiodun, 2015; Dieppois et al., 2015, 2016), however, its impacts are marked by regional variations. The effects of ENSO over Southern Africa are at their maximum during the austral summer, from December to March. The impacts of ENSO are felt strongest in south-eastern Southern Africa (Richard et al., 2001). Using Regional Climate Models, Meque and Abiodun (2015) showed anomalous lower-level divergence during an El Niño over the southern African landmass that prevents moisture transport, thus reducing the seasonal summer rainfall. While during a La Niña event, the seasonal rainfall over southern Africa is enhanced due to the dominance of the anomalous convergence.

El Niño and La Niña events since the 1970s has been documented to favour droughts (Figure 1.5a) and floods (Figure 1.5b) over southern Africa during summer (Dieppois et al., 2015, Meque and Abiodun, 2015, Fauchereau et al., 2009, Richard et al., 2001). However, some other seasons post-1970 proved otherwise. The relatively weak El Niño event of 1991/2 and 2002/03 caused severe seasonal droughts over an extensive area around southern Africa (Fauchereau et al., 2009, Rouault and Richard, 2003, Rouault and Richard, 2005). Interestingly, while most of the globe experienced extreme climate anomalies during the strongest El Niño event of 1997/8, South Africa received near-average rainfall for the summer season despite a drier start of the rainy season (Richard et al., 2001, Rouault and Richard, 2003, Rouault and Richard, 2005, Tyson and Preston-Whyte, 2000). According to Reason et al. (2006), the near-normal rainfall in 1997/8 was attributed to warm SST anomalies in the south-eastern Atlantic and a well-developed Angola Low. The El Niño cases highlighted above show that not all El Niño events would lead to dry conditions in southern Africa. These cases also stress that not all strong ENSO events will lead to severe impacts over southern Africa.

Hoell et al. (2017) suggested that when the SIOD and ENSO are out of phase, their teleconnections complement each other and amplify precipitation over southern Africa. However, when SIOD and ENSO are in phase, the study suggests that the SIOD disrupts the ENSO teleconnections over southern Africa by reducing the strength of the barotropic waves and anomalous mid-tropospheric vertical motion. Hence, reduced rainfall. Hoell and Cheng (2018) further indicated that the SIOD phase

modifies the frequency of wet extremes during a La Niña phase. Southern African rain-bearing systems during Austral summer

Large-scale convective rainfall systems influence the austral summer rainfall over southern Africa due to the disturbances in the tropics and general circulation southwards of midlatitudes (Tyson and Preston-Whyte, 2000). These are some of the systems:

1.3.4.4 Tropical Temperate Troughs

Tropical temperate troughs (TTTs; Washington and Todd (1999)) are cloud bands oriented in an elongated north- western – south-eastern direction over southern Africa and contribute to significant rainfall during summer (Tyson and Preston-Whyte, 2000, Hart et al., 2013). The TTTs link the tropical disturbances with the upper-tropospheric frontal system within midlatitude westerly circulations (Fauchereau et al., 2009, Vigaud et al., 2012). Moreover, the TTTs prefer to occur in the South Indian Convergence Zone (Cook, 2000, Fauchereau et al., 2009). The midlatitudes disturbances in the Rossby wave and the excess latent heat in the Mozambique Channel are highly favourable and explain the large portion of the TTT's variability (Macron et al., 2014). When southern Africa experiences reduced rainfall in austral summer, TTTs are located further east of their origin (Usman and Reason, 2004, Reason and Jagadheesha, 2005).

1.3.4.5 Mesoscale Convective Systems

Mesoscale convective systems (MCS) are a family of thunderstorms that acts as a system. The study of MCS over southern Africa is very limited. But the system is characterised by extreme rainfall events (i.e., floods) and is known to bring relief to drought-prone regions. For example, the mesoscale convective systems over southern Africa account for 20 % of the total austral summer (November to March) rainfall in the eastern parts of South Africa (Blamey and Reason, 2013). On average 63 MCSs occur over the eastern parts of South Africa, but with substantial interannual variability (Morake et al., 2021).

1.3.4.6 Tropical Cyclones

Tropical cyclones are warm-cored low-pressure systems with an organised circulation that develops over tropical and subtropical waters. Over southern Africa, tropical cyclones typically form over the Indian Ocean in summer; and on average, six to twelve storms occur annually (Tyson and Preston-Whyte, 2000). Tropical cyclones in the Indian Ocean make land in Mozambique and Madagascar about thrice a year (Mavume et al., 2009). Only less than 5 % of tropical cyclone land on the east coast

of southern Africa (Reason and Keibel, 2004). About 45 systems from tropical lows and cyclones caused widespread heavy rainfall in the Limpopo River Basin between 1948 and 2008 after landfall over southern Africa (Malherbe et al., 2012). The tropical cyclones over the continent are associated with heavy rainfall, storm surges and loss of property and lives (Nhamo and Dube, 2021). Additionally, rainfall from tropical cyclones caused widespread flooding over the eastern part of southern Africa (Reason and Keibel, 2004) and some semi-arid parts of Botswana, Mozambique, South Africa and Zimbabwe (Malherbe et al., 2013).

1.3.4.7 Cut-off Lows

Cut Off Lows (COLs) pressure systems are important weather systems that contribute to the rainfall over southern Africa (Singleton and Reason, 2007, Omar and Abiodun, 2020, Favre et al., 2013, Ndarana et al., 2020). COLs form when a trough of cold air in the middle to upper troposphere is cut off from a westerly flow. COLs are most common between 15 º S to 40 º S, particularly in the Mozambique Channel in summer and off the west coast of South Africa and Namibia in winter (Favre et al., 2013). The COLs may contribute to the influx of moisture from the Indian Ocean into the subcontinent when they occur simultaneously with ridging high-pressure systems (Ndarana et al., 2021). One example is the COL event that occurred between the 21st to 24th of April 2019 in South Africa, which caused floods, and extensive property damage and killed 85 people (Ndarana et al., 2020). COLs are associated with persistent intense rainfall because cold air aloft promotes deep convection (Singleton and Reason, 2007). COLs were found to contribute 10 % of the annual rainfall in the Western Cape with large variability, and they reduced the severity of the prolonged droughts over the Western Cape in 2015 and 2016 (Omar and Abiodun, 2020).

1.4 Thesis Outline

In this thesis, we largely focus on the dynamics of the Kalahari thermal low and its induced SMC and their influence on the southern African hydroclimate. Each Chapter could be read separately since it is motivated by a specific question. But the mutual threads connecting these questions is to understand mechanisms that links the Kalahari thermal low and underlying precipitation over southern Africa. **Chapter 2** revisits the mean-state structure of the Kalahari Thermal low as modelled in widespread reanalysis products (ERA5, NCEP2, MERRA2, and JRA55) and analyses

of its relationship with the Angola low on annual, seasonal, and inter-annual timescales. Furthermore, the chapter investigates the regional-scale pattens of the mid-tropospheric moisture transport and convective activities associated with regional rainfall during the warmer and colder cases of the Kalahari thermal low. To the best of our knowledge, there is no study that examines the contribution of the thermally induced SMC to the regional moisture budget. Therefore, **Chapter 3** seeks to resolve this question by highlighting how the induced SMC controls the rainfall variability through the building up of the vertically integrated moisture flux divergence. In **Chapter 4**, a process-based evaluation method is applied to examine how well CMIP6 climate models represent the Kalahari thermal low and its induced SMC. **Chapter 5** summarises the main results of this dissertation by highlight the mechanisms that connect the Kalahari thermal low and the regional precipitation.

2 Representation of the Kalahari Thermal Low in Reanalyses Products: Seasonality, Interannual variability and Impacts on the southern African precipitation

2.1 Introduction

In summer, the Angola Low and the Botswana high pressure systems are the two iconic atmospheric features that dominate over southern Africa. The Angola low is a cyclonic circulation in the mid-lower troposphere over southern Africa that controls the regional precipitation (Munday and Washington, 2017, Howard and Washington, 2018, Pascale et al., 2019). Driven by intense surface heating in spring, the Angola low firstly develops as a thermal low and transitions later into a tropical low, which is associated with the moist instability in summer (Munday and Washington, 2017). To unravel the formation mechanisms of the Angola low, Howard and Washington (2018) investigated its diurnal cycle. They found combined mechanisms of dry thermal low and anabatic sea-breeze circulation that anchors the tropical low to the Angola region. On the other hand, the Botswana high is an anticyclonic circulation that forms in the mid-troposphere as a thermal response to the heat released of convective rainfall that occurs over tropical regions (Reason, 2016). This mid-tropospheric high-pressure system also regulates the interannual rainfall variability over southern Africa (Reason, 2016, Driver and Reason, 2017). It is also closely related to the surface temperature maximum over southern Africa, with its high values occurring in the eastern escapement of south Africa (Reason, 2016, Driver and Reason, 2017). However, it is still unknown how these two atmospheric features are thermodynamically linked to each other.

In the northern hemisphere, the Sahara heat low and its induced shallow meridional circulation (SMC) have been extensively studied as one of the drivers of rainfall variability in west Africa and Sahel (Zhai and Boos, 2017, Martin and Thorncroft, 2014, Thorncroft et al., 2011, Lavaysse et al., 2010, Lavaysse et al., 2009, Longandjo and Rouault, 2023). Conversely, in the southern hemisphere, (Howard and Washington, 2018) argued that the southern African thermal low fits nicely into the idealised theory

(Rácz and Smith, 1999, Spengler et al., 2005) and has no bearing on precipitation variability from November to February. This is consistent with (Johnson, 2003) who suggested that the thermal low is not associated with clouds nor precipitation. Although, many studies show a link between the Angola Low and southern African precipitation (Cretat et al. 2019, Pascale et al. 2019). Mulenga (1999) and Vizy et al. (2015) also suggest that heat lows have important control over interannual rainfall variability. No attempt has been made to date to assess the relevance of the above hypothesis in using more extensive observational datasets. Additionally, previous studies suggest that the formation of the Southern African Heat low (henceforth, referred to as Kalahari Therma Low) is linked to the African Easterly Jet South, which is driven by the Botswana High (Adebiyi and Zuidema, 2016; Reason, 2016; Vizy and Cook, 2016; Kuete et al., 2020).

Importantly, the Kalahari Thermal low is not fully documented and its role on the regional hydroclimate is still unknown. The main objective of this paper is to fill the gap in literature by trying to answer the following questions:

(a) What is the linking mechanism between the Angola low and the Botswana high at seasonal cycle and interannual timescales?
(b) What is the mean–state structure of the Kalahari Thermal Low in southern Africa and what is the possible linkage to the Angola low and Botswana high in austral summer (DJF)?
(c) How does the Kalahari Thermal Low control the regional rainfall and what are its associated atmospheric dynamics?

2.2 Data and Methodology

2.2.1. Data

In this paper, we used four different general monthly reanalyses products that are summarized in Table 2.1. The European Centre for Medium-Range Weather Forecasts (ECMWF) Reanalysis version 5 (ERA-5, Hersbach et al., 2020), the enhanced version of ERA- Interim. ERA5 is the fifth generation of atmospheric reanalysis and provides hourly estimates of large-scale numerous atmospheric, land and oceanic variables. It is based on the Integrated Forecasting System and therefore benefits from a decade of developments in core dynamics, model physics and data assimilation (Hersbach et al.,

2020). ERA5 has an enhanced horizontal resolution of 31 km compared to 80 km for ERA-interim and resolves the atmosphere into 137 levels from the surface up to 80 km. The Modern-Era Retrospective Analysis for Research and Applications, version 2 (MERRA-2) is a modern satellite era atmospheric reanalysis dataset from the Global Modelling Assimilation Office at National Aeronautics and Space Administration (Randles et al., 2017). MERRA-2 is an update of the previous reanalysis system, therefore, includes improvements to the Goddard Earth Observing System model (Randles et al., 2017).

Table 2.1: Summary of datasets used in this chapter.

Dataset	Source	Coverage	Frequency	Period	Resolution (lat and lon)	Reference
NCEP2	NOAA	Global	Monthly	1979-present	2.5° × 2.5°	(Kanamitsu et al., 2002)
ERA5	ECMWF	Global	Monthly	1979-present	0.25° × 0.25 °	(Hersbach et al., 2020)
MERRA2	NASA/GMAO	Global	Monthly	1980-present	0.5° × 0.625°	(Randles et al., 2017)
JRA55	JMA	Global	Monthly	1958-2012	1.25° × 1.25°	(Kobayashi et al., 2015)
GPCC	GPCC	Global	Monthly	1901-present	0.5° × 0.5°	(Schneider et al., 2014)
OISST	NOAA	Globally	Monthly	1982-present	1.0° × 1.0°	(Reynolds and Banzon, 2008)

MERRA-2 assimilates observation types and provides a reliable ongoing climate analysis beyond its terminus (Gelaro et al., 2017). The Japanese 55-year Reanalysis (JRA55, (Kobayashi et al., 2015) is a 55-years longest third generation reanalysis and the first to apply four-dimensional variational analysis. JRA5 was developed by the

Japan Meteorological Agency (JMA) to address issues found in JRA-25 (Onogi et al., 2005) and to further produce a comprehensive atmospheric dataset suitable for studying multidecadal variability and climate change (Kobayashi et al., 2015). Finally, the National Centre for Environmental Prediction (NCEP) - Atmospheric Model Intercomparison Project (AMIP- II) reanalysis (NCEP2, Kanamitsu et al., 2002)dataset is the most used reanalysis in southern African climate studies. Therefore, it is worthwhile to compare it with other reanalyses. Although, it has lower resolutions compared to the three above, NCEP2 is still adequate for resolving large-scale atmospheric phenomenon and teleconnections over southern Africa. The impact of rainfall will be assessed through the Global Precipitation Climatology Centre version 7 (GPCC v7) dataset (Schneider et al., 2014). It is based on statistically interpolated in situ rain measurements. The GPCC is highly recommended for global and regional water balance studies, verification of numerical models and validations of remote sensing-based rainfall estimates. Finally, Optimum Interpolation Sea Surface Temperature (OISST version 2) provides global fields of SST that are based on the combined ocean temperature estimates from satellites and in-situ platforms such as ships and buoys. The monthly fields of OISST are derived through linear interpolation of daily fields. The ability of OISST to resolve SST over coastal zones in South Africa is highlighted by Rouault et al. (2010) . The 1982 – 2020 period is considered for this study, unless stated otherwise and all datasets have been interpolated to the 0.5° × 0.5 ° horizontal resolution.

2.2.2. Methodology

As in Lavaysse et al. (2009,2010), we identified the Kalahari thermal low by determining the geopotential thickness between 850 and 600 hPa due to high topography in southern Africa. This mid-lower atmospheric thickness is a better approximation of mid -lower atmospheric layer temperature as defined below:

$$\Delta z = \frac{R}{g} \int_{p1}^{p2} Td\,(\ln(p)) \qquad (2.1)$$

Where Δz is the geopotential thickness, R is the gas constant of air, g is gravitational acceleration, T is mean temperature of the atmospheric thickness, and p is pressure. p_1 and p_2 represent the 850 hPa and 600 hPa pressure levels, respectively.

The equation (1) can also be written as

$$\Delta z = \alpha\, T \qquad (2.2)$$

Where :

$$\alpha = \frac{R}{g}\, In\, (\frac{p_1}{p_2}) = 10.2 \text{ m K-1}$$

Many definitions have been proposed to characterise the Angola low, with the geopotential height (z_{850}) at 850 hPa (Howard and Washington, 2018, Munday and Washington, 2017) or the relative vorticity at 700 hPa (Howard et al., 2019, Pascale et al., 2019, Crétat et al., 2019). To consider how the geopotential height at 850 hPa (z_{850}) is sensitive to the surface heating, we loosely consider the Angola low, $z_{850} \leq$ 1500 m in summer (DJF). Likewise, the Botswana high is the high-pressure system at 500-hPa that occurs over southern Africa (Driver and Reason, 2017, Reason, 2016). However, we define the Botswana high as $z_{600} \geq$ 4420m. Additionally, we used the mid-tropospheric (700–600 hPa) relative vorticity ($\zeta = \nabla \times \vec{v}$) to discriminate the Angola Low from the Botswana high, with the former being associated with the cyclonic circulation and the latter with the anticyclonic circulation respectively.

We performed the empirical orthogonal functions (EOF) analysis to reveal the leading modes of variability of the thermal low. The impacts of the southern African thermal low on the regional rainfall will be investigated by considering the evolution of the regional-scale circulation, moisture transport dynamics and convection patterns as a function of the thermal low intensity using composite analysis.

Table 2.2: Coefficients of determination for linear (r^2) and cubit (R^2) fits between z_{600} and z_{850} area-averaged between 10º–25ºE; 15º–30ºS and 8º–25ºE, 10º–25ºS (see black boxes in Figure 2.6 a; e) for all months from January 1982 to December 2020. The constants a, b, c d are coefficients of the equation 3.

	ERA5	NCEP2	MERRA2	JRA55
r^2 (linear fit)	0.02	0.07	0.14	0.07

R^2 (cubic fit)	0.85	0.88	0.94	0.89
a ($\times 10^{-3}$ m^{-2})	0.30	042	0.12	0.35
b (m^{-1})	− 1.4	− 1.9	− 0.57	− 1.62
c ($\times 10^{2}$)	21	29	0.88	25
d ($\times 10^{6}$ m)	− 1.07	− 1.52	− 4.47	− 1.26

2.3 Results and discussion

2.3.1 Seasonality and interannual variability of the Kalahari thermal low

2.3.1.1 Link between Botswana high and Angola low pressure systems

To find out how the Botswana high varies with the Angola low, we first binned the 850-hPa geopotential height (z_{850}) and then selected its corresponding 600-hPa geopotential height (z_{600}). We finally smoothed the resulting 600-hPa geopotential height with the running mean and plotted it in Figure 2.1. A strong nonlinear mechanism links the Botswana high (z_{600}) to the Angola low (z_{850}) (Figure 2.1), such that as z_{850} increases, the rate of increase of z_{600} tends to decrease to eventually reach a value at which it cannot longer change. This relationship is of cubic form and can be written as follow:

$$z_{600} = a * z_{850}^3 - b * z_{850}^2 + c * z_{850} + d \qquad (2.3)$$

where *a*, *b*, *c,* and *d,* are constants depending on the reanalysis products (see Table 2.2). However, z_{600} and z_{850} have distinct responses to the mid-lower temperature (Δz) (Figure 2.1) – increased temperature deepens the near surface low-pressure system (z_{850}) and strengthens the mid-tropospheric high-pressure system (z_{600}). For any increase of 1K in the mid-tropospheric temperature, the Angola low strengthens by 7.14 m in NCEP2 and 8.57 m in MERRA2 (Figure 2.1). At the same time, the Botswana high increases between 2.14 m in ERA5 and 3.06 m in NCEP2. This means that at seasonal timescale, the Angola low forms as a baroclinic response to the surface warming, indicative of a thermal low, in agreement with (Howard and Washington, 2018). But the Botswana high is linearly induced by the mid-tropospheric heating. Note

that the high rainfall occurs when the convective system is fed by large heat content air (Figure 2.1). But in summer, owed by intense surface warming, the relationship between z_{600} and z_{850} becomes linear such that a strong Angola low decreases the Botswana high and vice versa (Figure 2.2). This means that these two atmospheric features are intimately related so that they depend on each other. But this response is weaker in MERRA2 than in ERA5, NCEP2 and JRA55 (Figure 2.2).

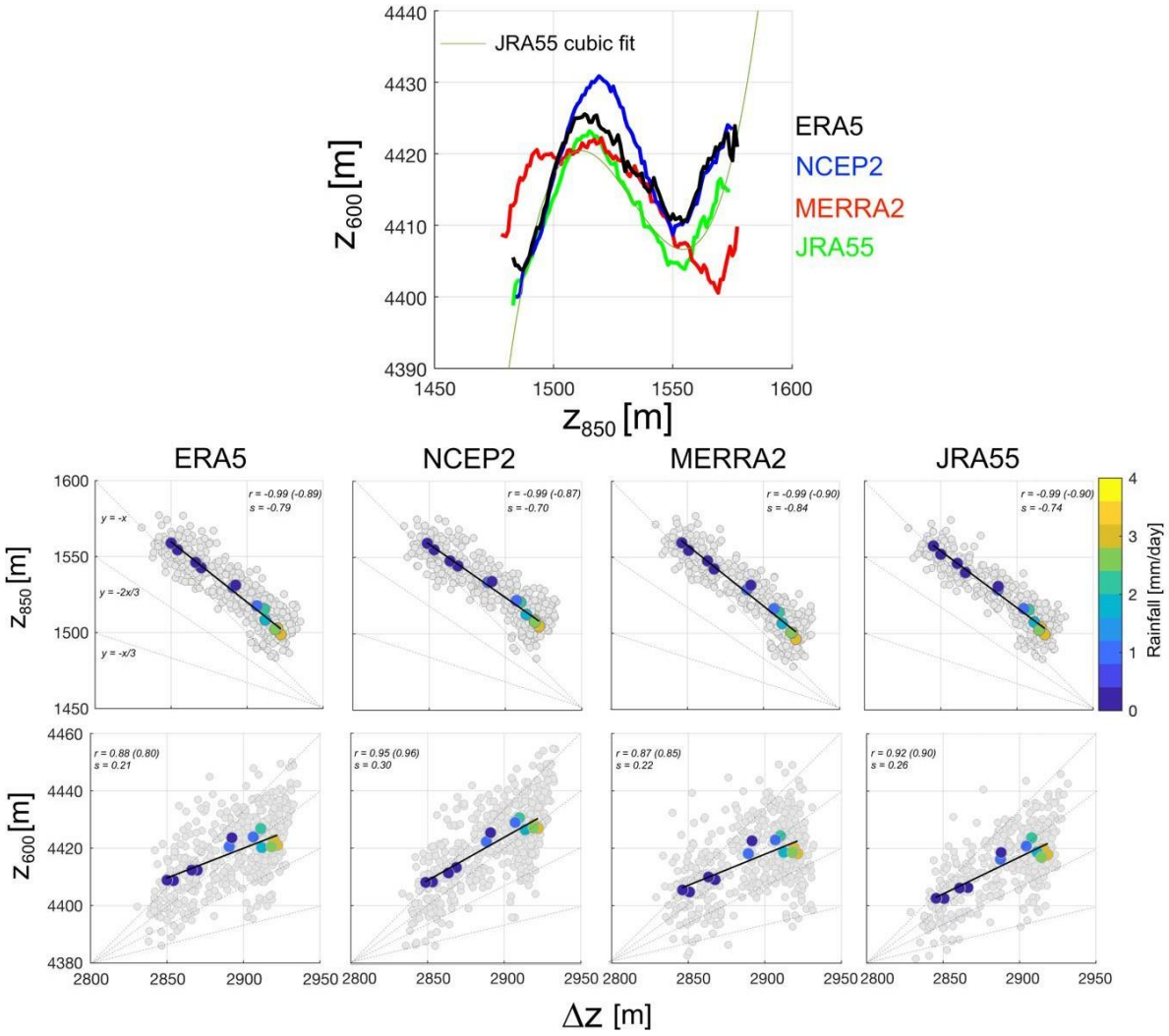

Figure 2.1: (Top panel) Geopotential height index at 600- hPa (z_{600}) as function of the geopotential height at 850- hPa (z_{850}) area-averaged between 10º–25ºE, 15º–30ºS and 8º–25ºE, 10º–25ºS respectively (see black boxes in **Figure 2.5a; e**) for ERA5 (black), NCEP2 (blue), MERRA2 (red) and JRA55 (green). The cubic fit curve for JRA55 is also shown. (Middle panels) Relationship between the atmospheric thickness (Δz) area-averaged between 10º–25ºE, 15º–30ºS and z_{850}. Grey dots represent all months for the study period and shaded dots are for calendar months (i.e., January to December). The shading colour is the southern African rainfall index which is obtained by area-averaging over land south of 15ºS in the GPCC dataset. In each panel, *r* and *s* are the correlation and the slope coefficients respectively. (Bottom panels) As the middle panels, but for z_{600}.

More interestingly, the reversal of the relationship between the Angola low and the

mid-lower temperature indicates that the Angola low is barotropic in summer at the interannual timescale, with some contribution of ENSO (Figure 2.2).

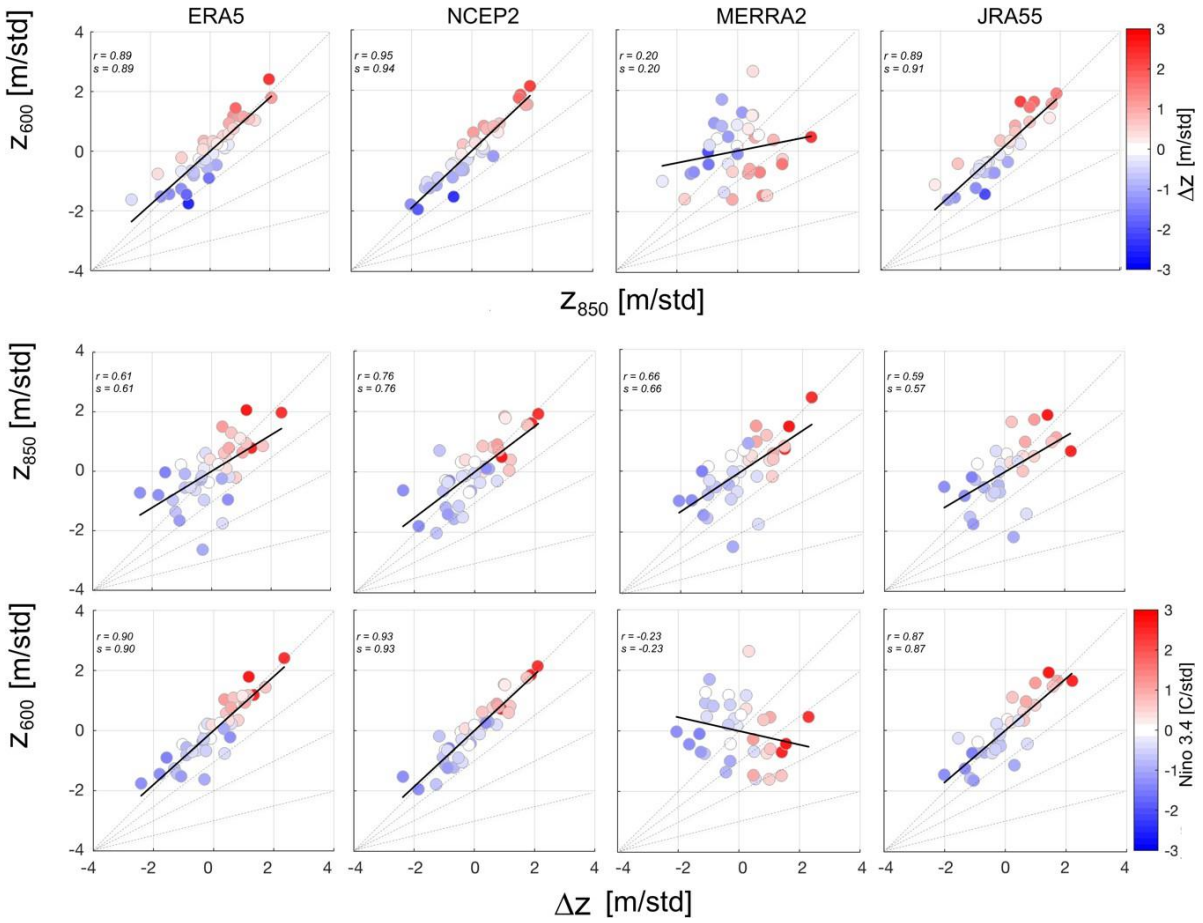

Figure 2.2: (Top panels) Relationship between the geopotential height index at 850- hPa (z_{850}) area-averaged between 8º–25ºE, 10º–25ºS and the geopotential height index at 600- hPa (z_{600}) area-averaged between 10º–25ºE, 15º–30ºS in summer. Shading colours are the Kalahari low (defined as the normalized anomalies of the geopotential thickness (Δz) averaged over 10º–25ºE, 15º–30ºS). (Middle panels) As in top panels, but for the atmospheric thickness (Δz) area-averaged over 10º–25ºE, 15º–30ºS) and z_{850}. (Bottom panels) As in middle panels, but for z_{600}. All indices are normalized anomalies. In the middle and bottom panels, the shading colour is the Kalahari low index (Δz) and the Nino3.4 index is the SST normalized anomalies over central Pacific (120º–170ºW; 5ºN–5ºN) respectively. In each panel, *r* and *s* are the correlation and the slope coefficients respectively.

In other words, the rainfall increases with the increase of the mid-tropospheric high pressure and the deepening of the low-pressure system at low levels (Figure 2.1). In the mid-troposphere, the Botswana high shows a positive response to the increase of the mid-tropospheric temperature, except in MERRA2 (Figure 2.2). In this reanalysis, the Botswana high weakens with the increase of the mid-tropospheric temperature (Figure 2.2).

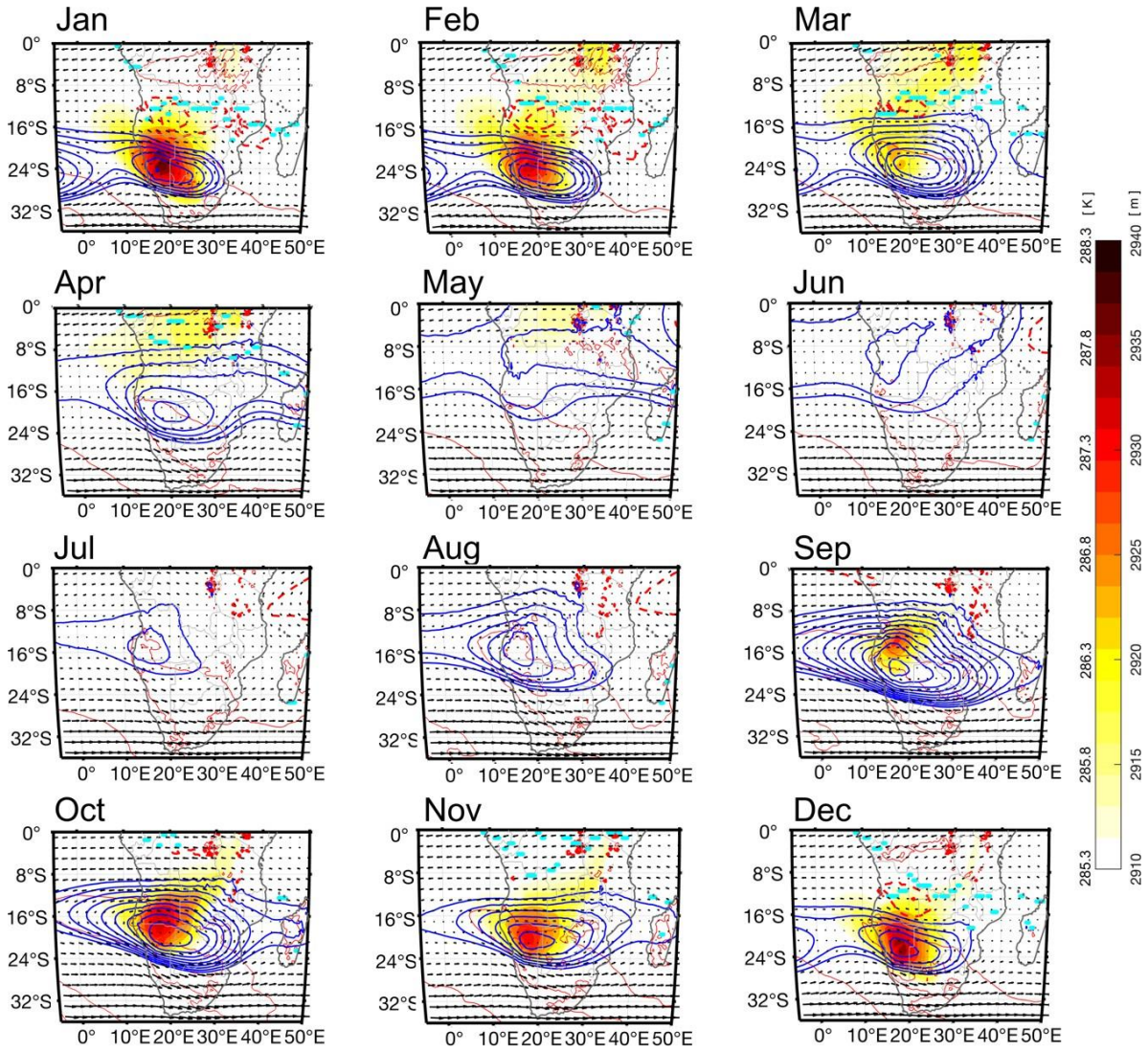

Figure 2.3: Annual cycle of the atmospheric thickness (Δz) between 850 and 600- hPa (shading, m), the 600-hPa geopotential height(blue contours, m), the mid-tropospheric circulation (700–500- hPa, black arrows, m/s) and its associated relative vorticity (ζ, magenta contours, $\times 10^{-6}$ s^{-1}). The rainfall maximum is shown by the cyan line. Only shown $z_{600} \geq 4420$ m with a contour interval of 2 m and ζ at a contour interval of -0.5×10^{-5} s^{-1} and 0.75×10^{-5} s^{-1} respectively. Data are ERA5 and GPCC. Based on equation (2), the unit of Δz can be m or K.

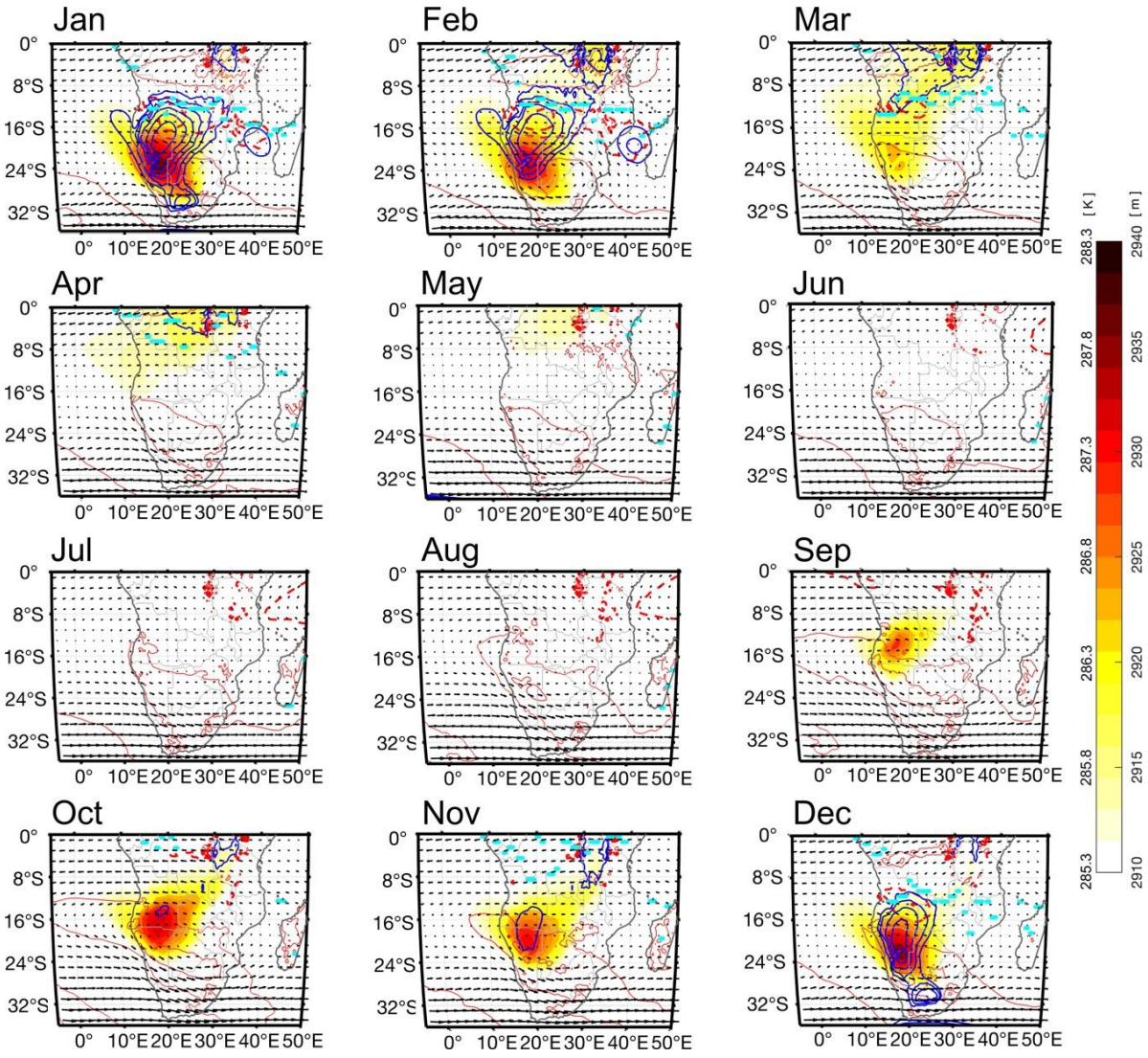

Figure 2.4: Annual cycle of the Kalahari thermal low (Δz, shading, m), the 850-hPa geopotential height (z_{850}, blue contours, m) and the mid-tropospheric circulation (700–500- hPa, black arrows, m/s) and its associated relative vorticity (ζ, magenta contours, $\times 10^{-6}$ s^{-1}). The cyan contour is the rainfall maximum. $z_{850} \leq 1500$ and the negative relative vorticity are shown with a contour interval of 2 m and -0.5×10^{-6} s^{-1} respectively. Data are ERA5 and GPCC. Based on equation (2), the geopotential thickness unit can be m or K.

2.3.1.2 Annual cycle of the southern African thermal low and the regional -scale circulation

The annual cycle of the atmospheric thickness, the mid-tropospheric (700–600- hPa) circulation and its associated relative vorticity are shown in Figure 2.3 and Figure 2.4. All reanalysis products represent similar results, but with small differences. For simplicity, we only showed that of ERA5.

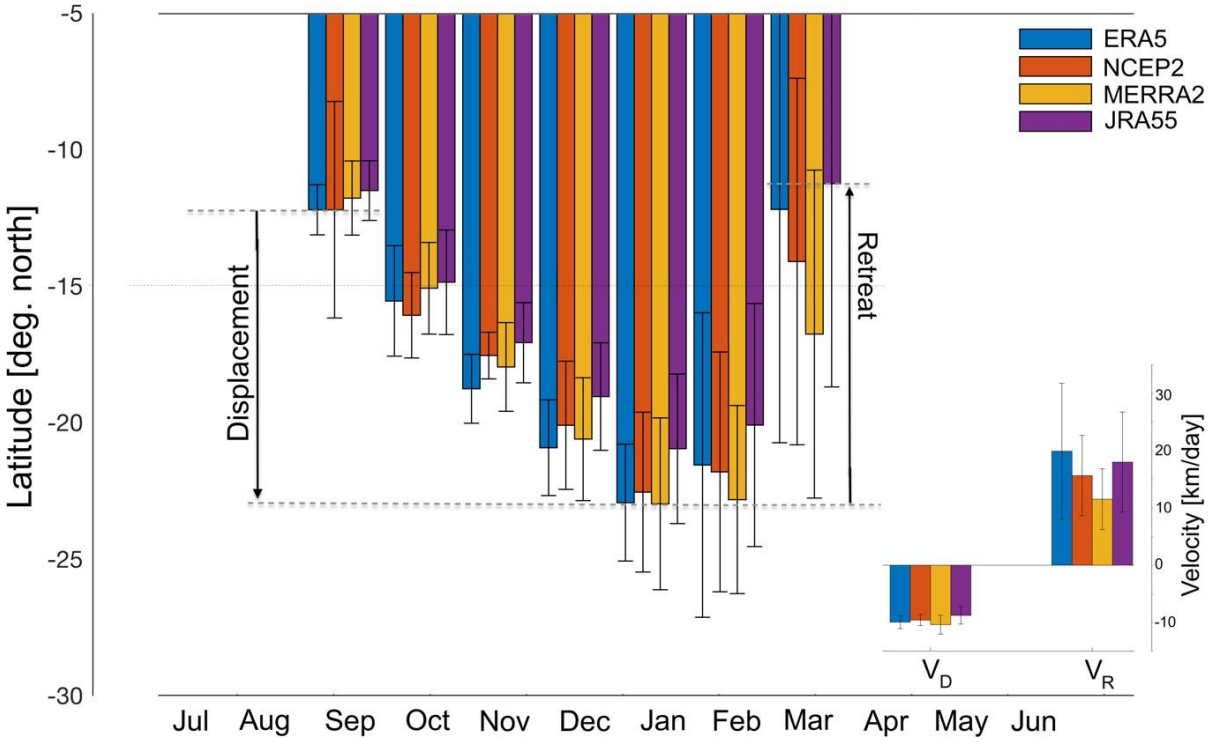

Figure 2.5: Seasonality of the position of the Kalahari thermal low (Δz_{MAX}) in reanalyses – ERA5 (blue), NCEP2 (red), MERRA2 (orange) and JRA55 (violet). The vertical bar indicates the standard deviation. Only shown position of $\Delta Z_{MAX} \geq 2920$ m. Also shown the velocities of displacement (V_D) and retreat (V_R). V_D is the velocity of the KTL from its initiation position until its maturity position and V_R is the velocity from its maturity position until its decay position. The annual cycle starts in July.

The thermal low develops in September over Angola (~12°S) and intensifies in the subsequent months while moving poleward to reach its maximum in January over the Kalahari region in Namibia (Figure 2.4). One month early, the Botswana high starts to strengthen in the mid-troposphere, while the Angola low is almost absent (Figure 2.3). In October, a low-pressure system forms where the tropospheric heating was intense a month earlier over Angola. In summer, the Botswana high slightly decreases, while the Angola low matures, with its tail extending southwards up to south Africa (Figure 2.3 and Figure 2.4). As time evolves, the Botswana high moves poleward towards the Kalahari region and the Angola low further deepens, particularly in DJF, consistent with the seasonal migration of the insolation (Figure 2.3). Note that the regional circulation over southern Africa is geostrophic and driven by the Botswana high (Figure 2.3). As the Botswana high migrates southward, the mid-tropospheric circulation is balanced by the development of a mid-tropospheric cyclonic circulation in its northern margin due to vorticity continuity equation. In December, the KTL further warms and strengthens further the Botswana high (Figure 2.3 and Figure 2.4), which in turn, produces a mid-tropospheric

easterly flow that shifts equatorward to balance its vorticity (Figure 2.3). As consequence, two vortices of opposite sign are found on the northern and southern flanks of the heating zone respectively (Figure 2.3 and Figure 2.4). The Botswana high and the KTL are associated with the mid-tropospheric anticyclonic circulation and the Angola low is associated with cyclonic circulation (Figure 2.3). This is consistent with Mulenga (1999) who showed in a quasi-geostrophic model that the Angola low forms as a result of Matsuno-Gill response to surface heating. In April, the thermal low moved equatorward to disappear in the vicinity of where it originates (Figure 2.5) due to the weakening of both Angola low and Botswana high (Figure 2.3). This retreat of the KTL is faster than during its displacement at 10 km/day in early summer (i.e., from September until January, Figure 2.5). This suggests an asymmetrical seasonal motion of the KTL from its initiation in September until its demise in March despite being almost stationary at the core of the summer season (DJF, Figure 4.5).

Although distinct, the Botswana high and the Angola low are superimposed from October and February (Figure 2.3), making them intrinsically connected in the formation of the KTL (see equation 2.2 and Figure 2.1). At the same time, southern Africa receives around 60% of its rainfall total in summer despite the intense rainfall occurs over the tropical region (between 10°–15° S), i.e., out of our region of interest as shown by the position of rainfall maximum (Figure 2.3). We therefore presume that the KTL may play a crucial role in modulating the southern African rainfall via atmospheric mechanisms. It is also important to note that from April to September, the mid-troposphere over southern Africa is dominated by the westerly jet related to the formation of Angola low (Figure 2. 3).

2.3.1.3 Mean-state structure of the KTL and its associated circulation in summer.

In Figure 2.6, we plotted the seasonal DJF mean of the atmospheric thickness (Δz), the horizontal mid-tropospheric circulation and its associated relative vorticity and the Botswana high in summer. One can note that the KTL is the only source of heat in the mid-lower troposphere over southern African subcontinent. With its oval shape, oriented in the southeast and northwest direction, the KTL is well-represented in all datasets (Figure 2.6).

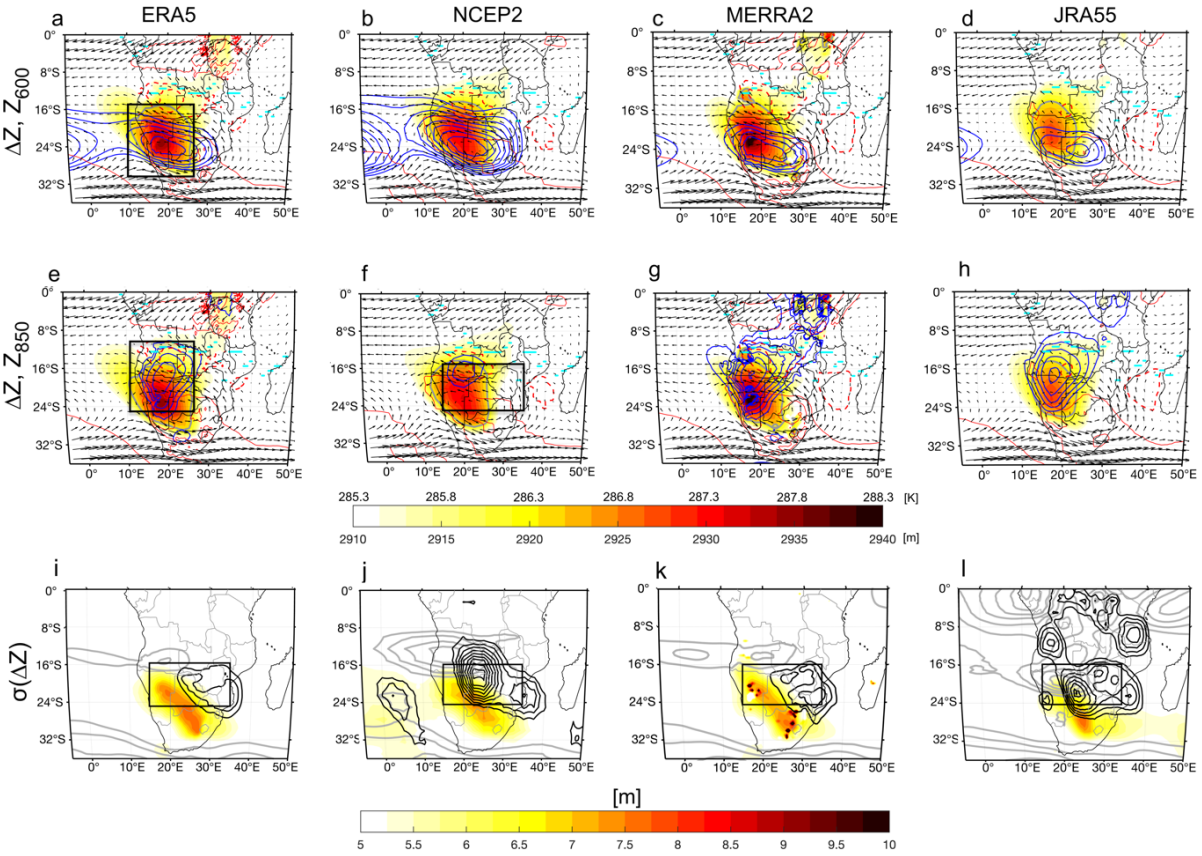

Figure 2.6: (Top panel) Seasonal-mean atmospheric thickness (Δz) between 600- and 850- hPa, shading, m), the mid-tropospheric (700–600- hPa) circulation (black arrows, m/s) and its associated relative vorticity (red contours, $\times 10^{-5}$ s^{-1}) and the geopotential height at 600- hPa (z_{600}, blue contours, m) in summer. (Middle panel) As top panel, but for the geopotential height at 850- hPa (z_{850}, blue contours, m). (Bottom panel) Standard deviation of the atmospheric thickness (Δz, shading, m), the mid-tropospheric zonal (gray contours, m/s) and meridional (black contours, m/s) winds. In the top and middle panels, the solid and dashed red contours represent anticyclonic and cyclonic circulations respectively, while the cyan and gray contours are the rainfall maximum and the 2920 m isoline respectively. Data are ERA5 and GPCC. Based on equation (2), the unit of Δz can be m or K.

The intensity of KTL varies very slowly, but the KTL can migrate diagonally either equatorward towards Namibia or poleward towards Free state, southern Africa and Lesotho (Figure 2.6). This displacement of KTL has a huge impact on rainfall distribution over southern Africa (Pascale et al., 2019). A large variation of the mid-tropospheric meridional and zonal wind components is associated with a weak variability of KTL (Figure 2.6), with the former being greater than the latter in all reanalyses. However, these variations are higher in NCEP2 and JRA55 than in ERA5 and MERRA2 (Figure 2.6).

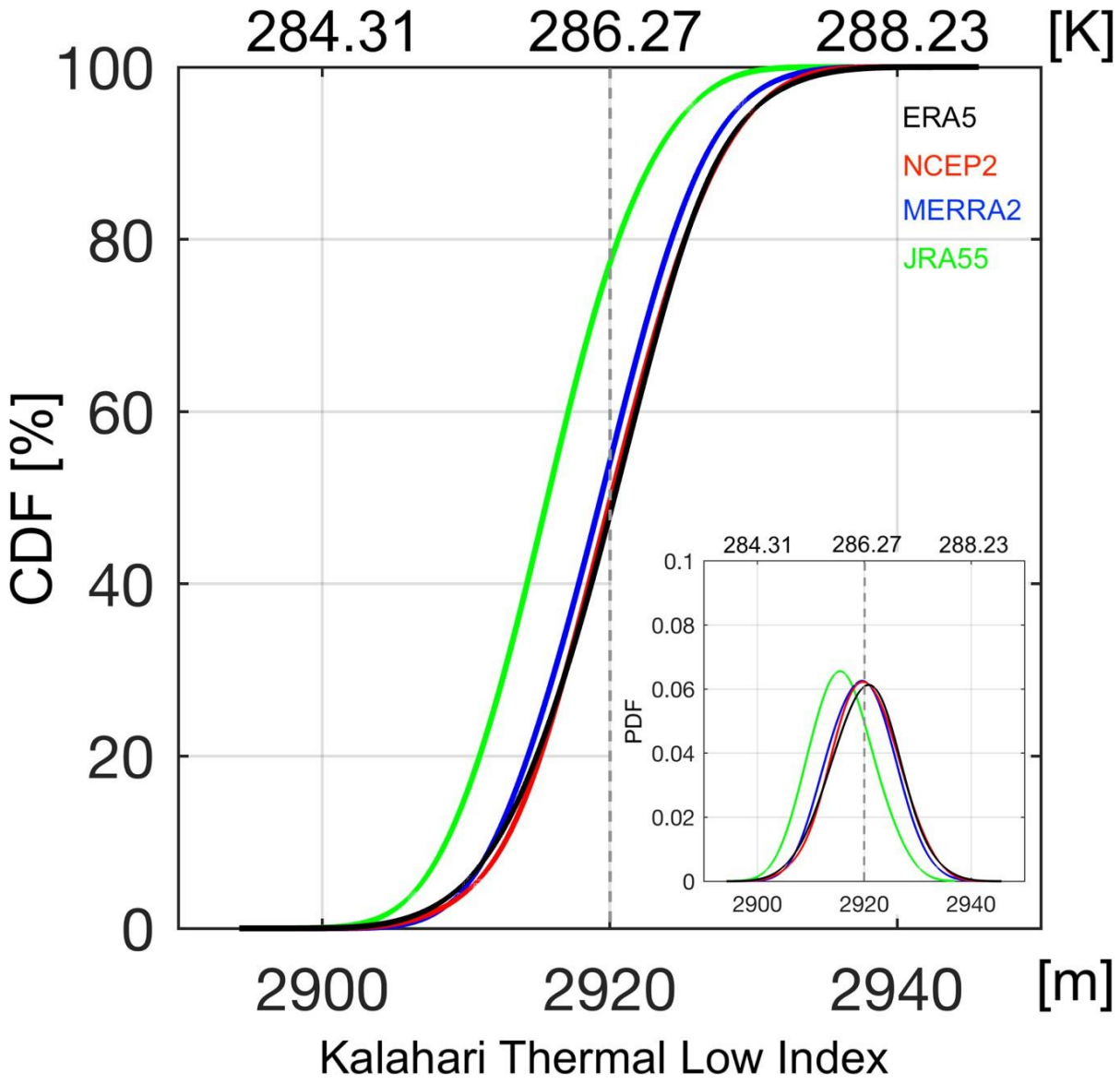

Figure 2.7: Distribution of the Kalahari low in reanalysis products: ERA5 (black); NCEP2 (red); MERRA2 (blue) and JRA55 (green). The vertical dotted grey line marks the ~50%-percentile threshold of the Kalahari low index (10°–25°E, 15°–30°S). Based on equation (2), the unit of the Kalahari low (Δz) index can be m or K.

More strikingly, the cores of KTL and Botswana high are not collocated: the core of the Angola low is more equatorward and situated around 6° north of the KTL maximum, while the ridge of the Botswana high is located in its vicinity, except in JRA55, in which it is at its eastern flank (Figure 2.6). The position of KTL is more determined by the ridge of the Botswana high rather than by the trough of the Angola low (Figure 2.3).

We also compared the KTL in reanalyses through its distribution (Figure 2.7). The warm region that exceeds the 50% percentile of the KTL intensity – which is 2920 m

– is set as a threshold (Figure 2.7). The KTL is strong in ERA5, NCEP2 and MERRA2, but weaker in JRA55 in which it increases rapidly around cold (low) values (Figure 2. 6–7).

The regional mid-tropospheric circulation over southern Africa is geostrophic and is dominated by a strong anticyclonic vortex associated with the Botswana high (Figure 2.6). In its northern flank, there is a small vortex of opposite sign that forms as a Matsuno-Gill-like response to the off-equatorial diabatic heating related to the KTL (Gill, 1980), indicative of the Angola low. The diabatic heating associated with KTL produces a mid-tropospheric easterly flow that shifts equatorward although it is embedded within the Botswana high (Figure 2.6). However, Adebiyi and Zuidema (2016) argued that this southern branch of the African easterly jet (AEJ–S) is diabatically driven by the temperature–moisture gradient between the poleward hot–dry convection related to the thermal low and the equatorward cool–moist convection associated with intense rainfall. On the southern margin of the heating region, a return flow consisting of a weak mid-lower easterly jet, which is part to the regional–scale mid-tropospheric anticyclonic vortex associated with the KTL ($\zeta > 0$), can also be spotted (Figure 2.6). An additional return flow is found at the northern margin of the heating area, where the north-easterly flow coming from equator circumvents into a weak north-westerly flow, indicative of the cyclonic circulation ($\zeta < 0$) related to the Angola low (Figure 2.6). This means that the Botswana high cannot be generated as a response to the latent heat release associated with the precipitating convection that occurs exclusively in the tropical central Africa, as shown by the position of intense rainfall (Figure 2.3;6) as previously reported by (Reason, 2016).

2.3.2 Vertical structure of the atmosphere associated with the KTL.

The vertical structure consists of a shallow meridional circulation (SMC), driven by the divergent flow, with its lower branch formed by the low-level southerly jet (LLSJ), particularly between 35^{o}–15^{o}S and its upper branch is constituted by the mid-tropospheric northerly jet (MTNJ) that advects the moist air from the convective region where the rainfall maximum occurs towards the southern Africa (Figure 2.8). This is consistent with (Zhang et al., 2008) who argued that a thermal low may induce a SMC in the mid-lower troposphere. Over southern Africa, the thermally-induced SMC generates a contrasted wind divergence in the mid-lower troposphere – a weak low-

level convergence and a strong mid-tropospheric divergence (Figure 2.8). The SMC is missing in ERA5 (Figure 2.8). On the other hand, the meridional component of the rotational wind, that dominates the total meridional wind, also shows an opposite circulation in the mid-lower troposphere, with a southerly wind in the mid-troposphere and the northerly wind at low levels (Figure 2.8). This weak mid-tropospheric subtropical southerly jet (STSJ) forms when the north-westerlies veer around the KTL to become south-easterlies at ~25°–15°S (Figure 2.9). This STSJ – with its core located ~600- hPa, 20ºS – connects the dry south-southern Africa (i.e., between 35°–25°S) to the wet north-southern Africa (i.e., between 25°–15°S). However, the north-southern Africa is wetter in ERA5 and MERRA2 than in NCEP2 and JRA55 (Figure 2.9). For NCEP2, the negative bias of the specific humidity may be due to its derivation from the relative humidity. For JRA55, high specific humidity is localized in southern Africa because it is intimately related to the high temperature due to the presence of the KTL (Figure 2.9).

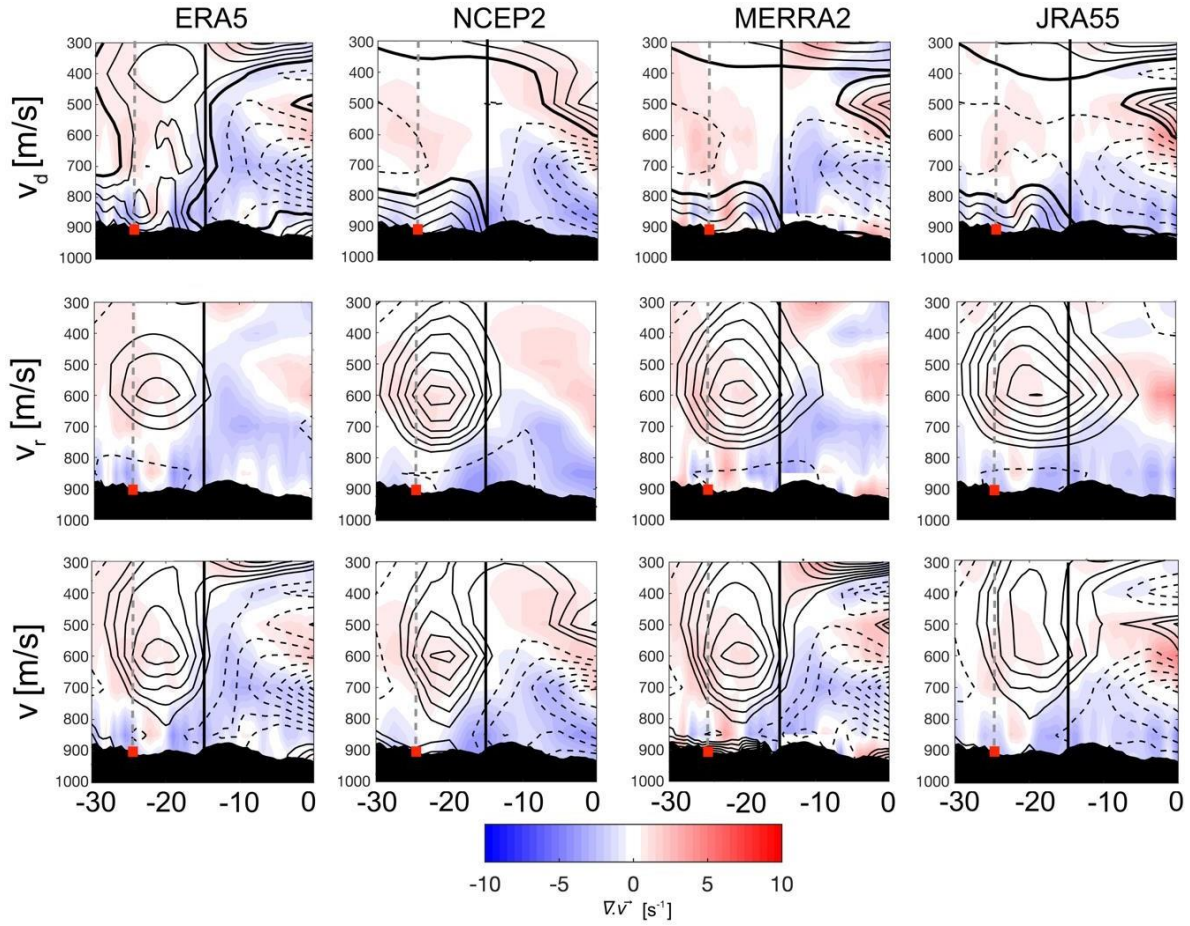

Figure 2.8: Latitude - pressure cross-section of the wind divergence (shading, s^{-1}) and (top panels) meridional component of the divergent wind (v_d, contours, m/s). (Middle panels) same as top panels, but for the meridional component of the rotational wind (v_r, contours, m/s). (Bottom panels) same as top panels but for (total) meridional wind (v, contours, m/s). The contour interval is 0.25 m/s for positive value and 0.5 m/s for negative value respectively, with solid and dashed contours representing positive and negative values. The bold black line in the middle panels shows the zero contour. In each panel, the vertical black and dotted grey lines mark 15ºS and 25ºS respectively. The red box indicates the (warmest) position of the KTL.

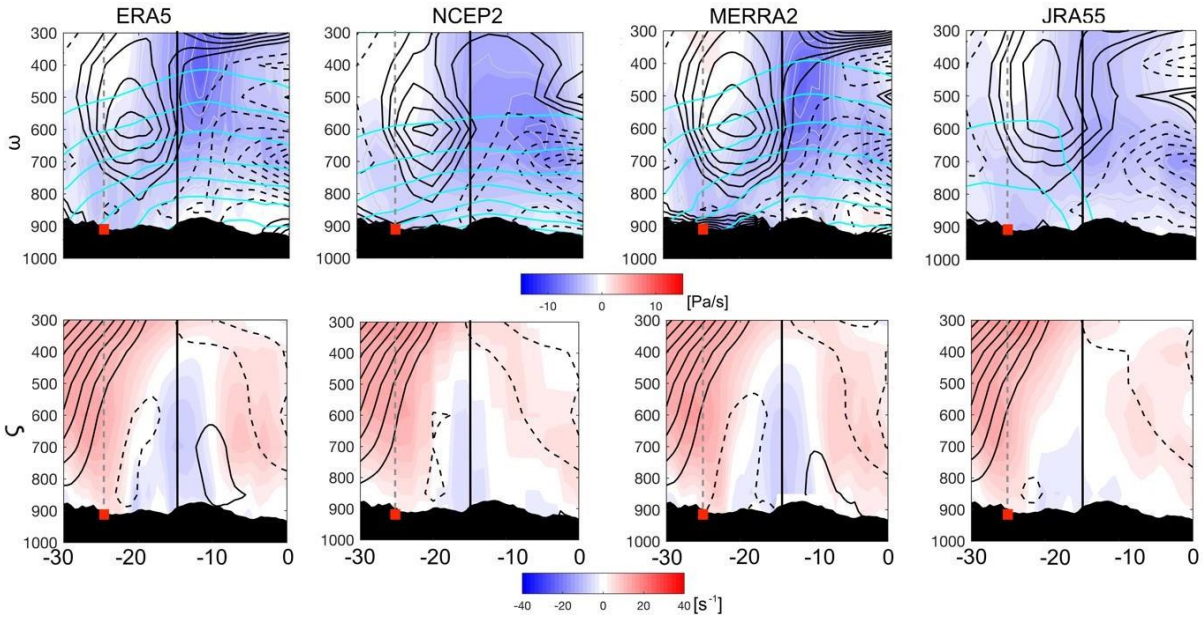

Figure 2.9: Latitude - pressure cross-section of (top panels) vertical velocity (shading, $\times 10^{-2}$ Pa/s), meridional wind (black contours, m/s) and specific humidity (cyan contours, kg/kg at 2 kg/kg contour interval). The contour interval is 0.25 m/s for positive value and 0.5 m/s for negative value respectively. (Bottom panels) relative vorticity (shading, $\times 10^{-6}$ s^{-1}) and zonal wind (contours, m/s). Only shown $u \geq 1$ m/s at 2 m/s contour interval and $u \leq -3$ m/s at 3 m/s contour interval respectively. In each panel, solid and dashed contours represent positive and negative values respectively. The vertical black and dotted grey lines mark 15°S and 25°S respectively, while the red box indicates the (warmest) position of the KTL.

Moreover, the STSJ does not advects the mid-tropospheric dry air into the convective region where the rainfall is maximum (Figure 2.3 & 6), in disagreement with previous works (Hurley and Boos, 2015, Zhai and Boos, 2017). This STSJ is stronger in MERRA2 than in ERA5, NCEP2 and JRA55 (Figure 2.8). However, because the divergent wind contributes to the vertical motion (due to continuity equation), which in turn, is related to the Hadley circulation, this recirculation associated with the rotational flow has been mistaken as the SMC in previous studies ((Zhai and Boos, 2017, Nie et al., 2010, Hurley and Boos, 2013). Further investigation about the accurate representation of the vertical structure of the SMC (Nguyen et al., 2018) is needed but it is beyond the scope of this study.

Over southern Africa, the low-level convergence triggers a weak vertical motion, particularly at ~25°S where the KTL is the warmest (Figures 2.8–9). This ascent of warm air is capped by the mid-troposphere divergence associated with the subsidence (Figures 2.8–9). This results in a formation of the bottom-heavy structure of the vertical profile of the vertical velocity over south-southern Africa, suggestive of a shallow

convection (Figure 2.9). When moving equatorward, the strong mid-lower wind convergence triggers a strong ascent of moist air over south-central Africa, with its maximum at 10°S, 400 hPa (Figures. 2.8–9). In NCEP2 and JRA55, this vertical velocity maximum occurs in the mid-troposphere (~600 hPa, Figure 2.8). Hence, over the north–southern Africa, the top-heavy structure of the vertical profile of the vertical velocity is predominant, indicative of a deep convection conducive to the intense rainfall, consistent with the position of rainfall maximum (Figure 2.6). Moreover, the Angola low which is characterized as the cyclonic circulation ($\zeta < 0$) separates the anticyclonic circulation ($\zeta > 0$) in two parts, with a strong vortex over southern Africa, indicative of the KTL and an additional weaker one over central Africa (Figure 2.9). Thus, the mid-lower westerly jet and the AEJ-S appear to be rotational flows as they are both controlled by the vorticity. The relative vorticity is weaker in NCEP2 and JRA55 than in ERA5 and MERRA2 (Figure 2.9). The same goes for the two rotational flows (Figure 2.9). Overall, the difference in the atmospheric condition over southern Africa region discriminates two parts – the subtropical southern Africa (SSA) between 35º–25ºS, where the atmosphere is dry, baroclinic and anticyclonic ($\zeta > 0$); and the tropical southern Africa (TSA) between 25º–15ºS where the atmosphere is wet, barotropic and cyclonic ($\zeta < 0$).

Furthermore, a warm KTL strengthens the STSJ, which in turn, is associated with decreased rainfall over southern Africa (Figure 2.10). On the other hand, a relatively cold KTL weakens the SMC which is associated with increased rainfall over southern Africa (Figure 2.10). This is consistent with Hurley and Boos (2013). For the mid-tropospheric zonal wind, a warm KTL increases the AEJ-S and reduces the rainfall over southern Africa (Figure 2.10). Likewise, a cold KTL weakens the AEJ-S and enhances rainfall over southern Africa (Figure 2.10). These results are consistent in all reanalyses, except in NCEP2 in which the AEJ-S seems to be independent to the KTL (Figure 2.10).

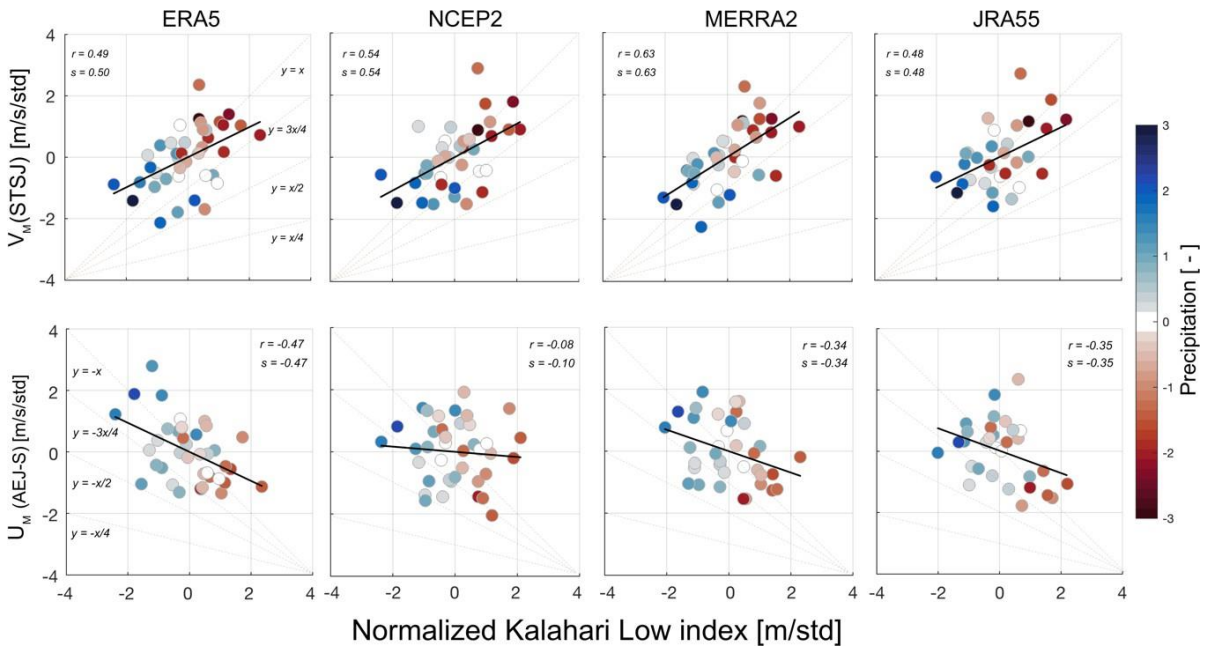

Figure 2.10: Scatterplot of KTL vs meridional (V_M) and zonal (U_M) components of the mid-tropospheric wind (i.e., STSJ and AEJ-S respectively) in different reanalysis products and area-averaged over 15º–35ºE, 15º–25ºS . The colour of each dot is the normalised southern Africa rainfall anomaly. The regression line is represented by the black line and in each panel, *r* and *s* are the correlation and slope regression coefficients respectively. All variables are normalized by their respective standard deviation.

2.3.3 Interannual variability of the KTL

Before we investigate the interannual variability of the KTL, we first plotted the correlation between the KTL index and the rainfall in Figure 2.11. A strong negative correlation linked the KTL intensity to rainfall in all reanalysis products (Figure 2.11), suggesting that a warmer KTL leads to drought conditions over southern Africa. A colder KTL would lead to above normal conditions (see also Figure 2.10). This is consistent with studies on the relationship between SMC and precipitation in other regions. Over West Africa, it is understood that the enhanced rainfall is caused by a stronger SMC over the Sahara (Haarsma et al., 2005; Zhang et al., 2008; Biasutti et al., 2009), suggesting a positive correlation between the Sahara heat low and the rainfall.

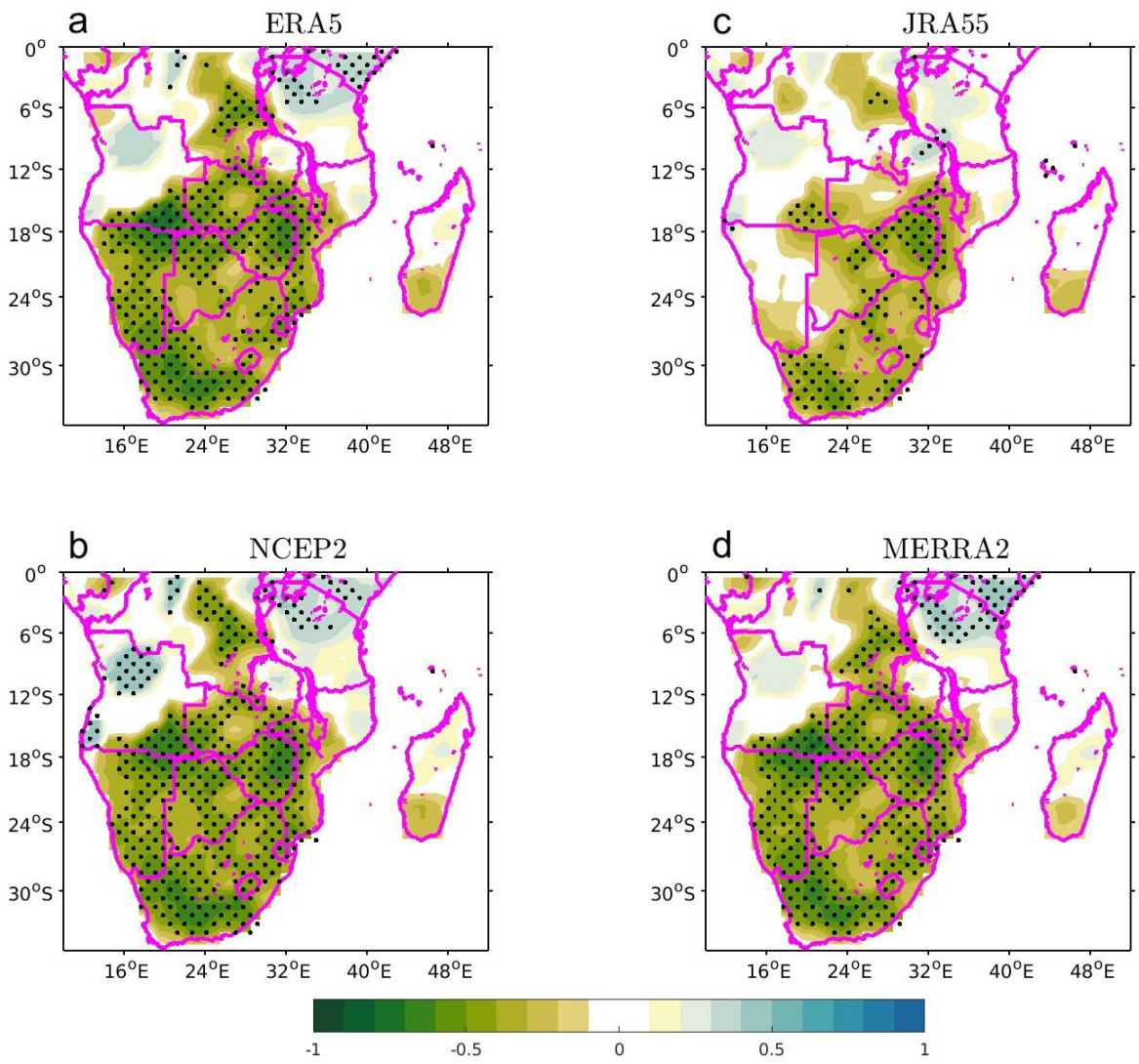

Figure 2.11**:** Correlation between normalized Kalahari Low index and normalized rainfall anomalies for (a) ERA5; (b) NCEP2; (c) JRA55 and (d) MERRA2. The stipple indicates correlation that is significant at $p < 0.05$ (t-student test).

However, Zhai and Boos (2017) found a negative correlation between the SMC and rainfall over southern Africa and argued that a strong SMC inhibits the monsoon precipitation by advecting the mid-tropospheric warm and dry air into the convective region. In Figure 2.12, we depict the leading mode of variability (EOF #1) of the KTL in all the reanalyses. This robust feature reflects a zonally elongated pattern of high atmospheric thickness centred around the Kalahari region and surrounded by cold regions in the northern and southern edges respectively (Figure 2.12). In each dataset, this mode explains ~40% of variance (Figure 2.12a). The impacts of this leading mode variability on the southern Africa rainfall and circulation have never been investigated.

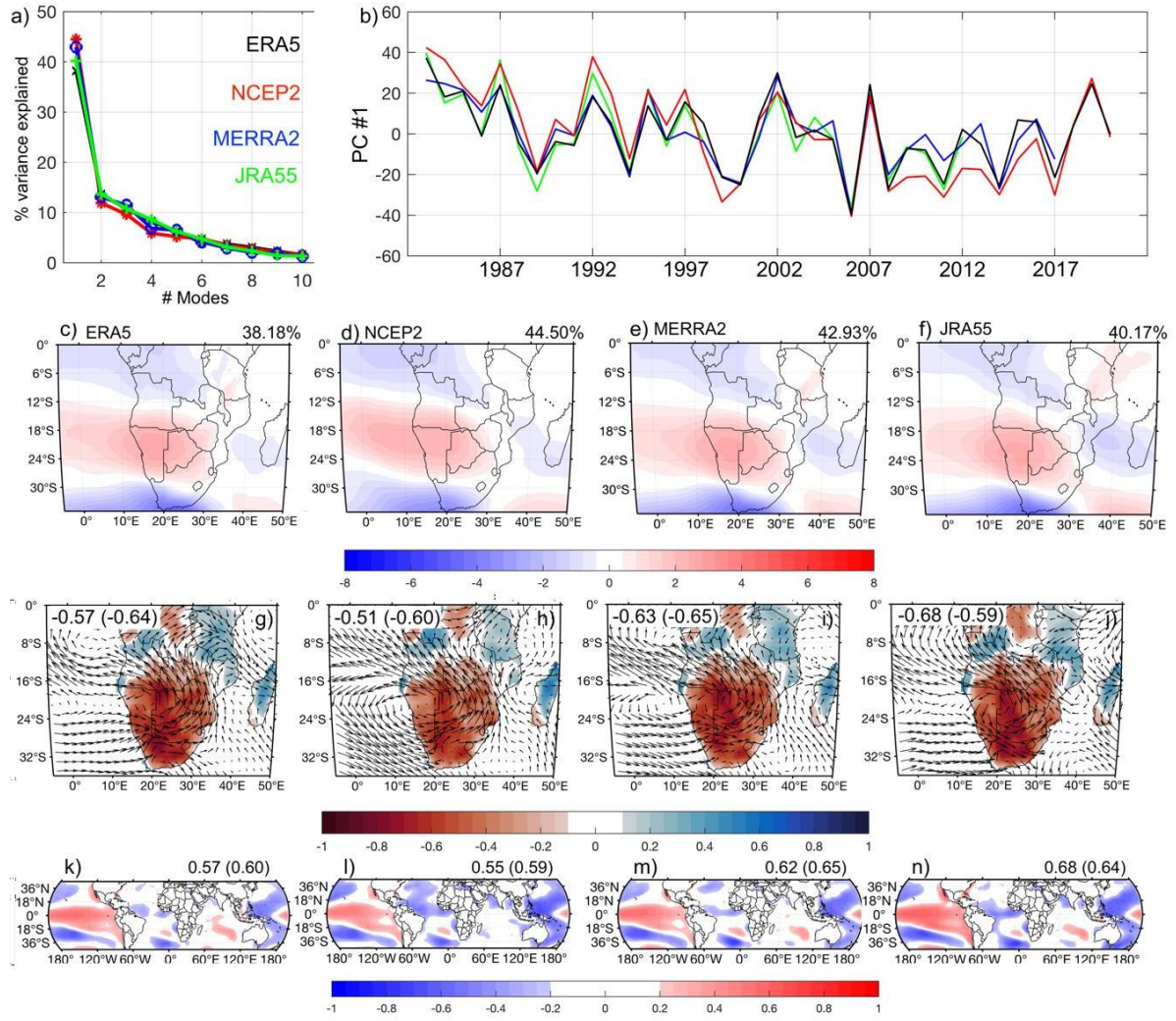

Figure 2.12: (a) Percentage of explained variance for the 10 first EOFs of detrended geopotential thickness. (b) The leading principal component (PC#1) for ERA5 (black); NCEP2 (red); MERRA2 (blue) and JRA55 (green). The leading mode of the geopotential thickness for each reanalysis and its associated correlation map (i.e., between the PC#1 and normalised rainfall (SST anomalies) for (c, g, k) ERA5; (d, h, l) NCEP2; (e, i, m) MERRA2; (f, j, n) JRA55. Dataset of SST is OISST. In (a – f) the number in the upper corner is the percentage of the variance explained for each reanalysis. In (g – n), correlation coefficient is shown in the right (left) upper corner. The one in the paratheses is for the detrended anomalies. The arrows indicate the mid-tropospheric 700–600- hPa) circulation (black arrows, m/s).

Figure 2.12 also shows the correlation between the PC #1 and summer rainfall anomalies and the overlying mid-tropospheric circulation for each reanalysis. When the central Pacific is also warmer than normal, the rainfall pattern over southern Africa is drier when the KTL is warmer than average, with a dominant anomalous anticyclonic vortex (Figure 2.12), suggesting a strong influence of the Botswana high. This pattern is reminiscent of the correlation between the KTL and the regional rainfall.

2.3.4 Control of the KTL on moisture transport dynamics and regional rainfall

Our results showed that over southern Africa, decreased rainfall is caused by a stronger SMC (Figure 2.10). the upper branch of this SMC does not transport the mid-tropospheric dry air into the tropical convective region to prevent the convection to deepen and thus reduce the precipitation (Figures 2.8-9). This raises a question; how does the KTL control the regional rainfall and what are its associated moisture transport dynamics over southern Africa?

To answer to this question, we first plot the composite of the KTL and the mid-tropospheric circulation and its associated relative vorticity during its warm and cold phases respectively in Figure 2.13. The composites maps were plotted by averaging all the summers (DJF) when the KTL was either higher or lower than normal over the climatological period (Starting from the DJF of 1982/83 until the DJF of 2018/19). The warm phase is characterised by the summers when the KTL intensity was higher-than-normal. The cold phase is characterised by summers (DJF) when the KTL intensity is lower than normal. During the warm phase, the KTL is well-developed in the southern African landmass, occupying more than half of its area (Figure 2.13). This strong diabatic heating widens the Botswana high, which in turn, deviates equatorward the dominant mid-tropospheric moisture transport that zonally crosses the southern Africa subcontinent from the Indian ocean by the strengthening the SMC (Figure 2.13). To balance its vorticity, this northward displacement of a strengthened AEJ-S is accompanied with the equatorward shifting of the cyclonic circulation (Angola low), and spatially reduced its extension (Figure 2.13). This confirms the linear response of the Botswana high to the KTL and the Angola low respectively (Figure 2. 2). This can also be observed when using the geopotential height at 600- and 850- hPa (Figures 2.14 and 2.15). This strong north-westward advection of moisture is stronger in MERRA2, ERA5 and NCEP2 than in JRA55 in which it barely crosses the landmass (Figure 2.13). This reduces the strength of the SMC and weakens the AEJ- S that moves poleward (Figure 2.13). Consequently, the Angola low (cyclonic circulation) widens and moves poleward due to its vorticity (Figure 2.13).

The composite difference between these two phases suggests that anomalous surface warming due to KTL induces a tropospheric subsidence over southern Africa and centred at its core (Figure 2.14). During the cold phase, the KTL shrinks around its

core and allows the anticyclonic circulation (Botswana high) to weaken and move poleward (Figure 2.14). The surrounding warm air expands upwards but is capped aloft by a strong subsidence (Figure 2.14). But the strengthening of this subsidence forms a dome that prevents warm air to escape from the mid-lower troposphere, forcing it back to the ground, as shown by the vertical vorticity (Figure 2.16). As it sinks, the warm air is compressed and releases more heat (Figure 2.16).

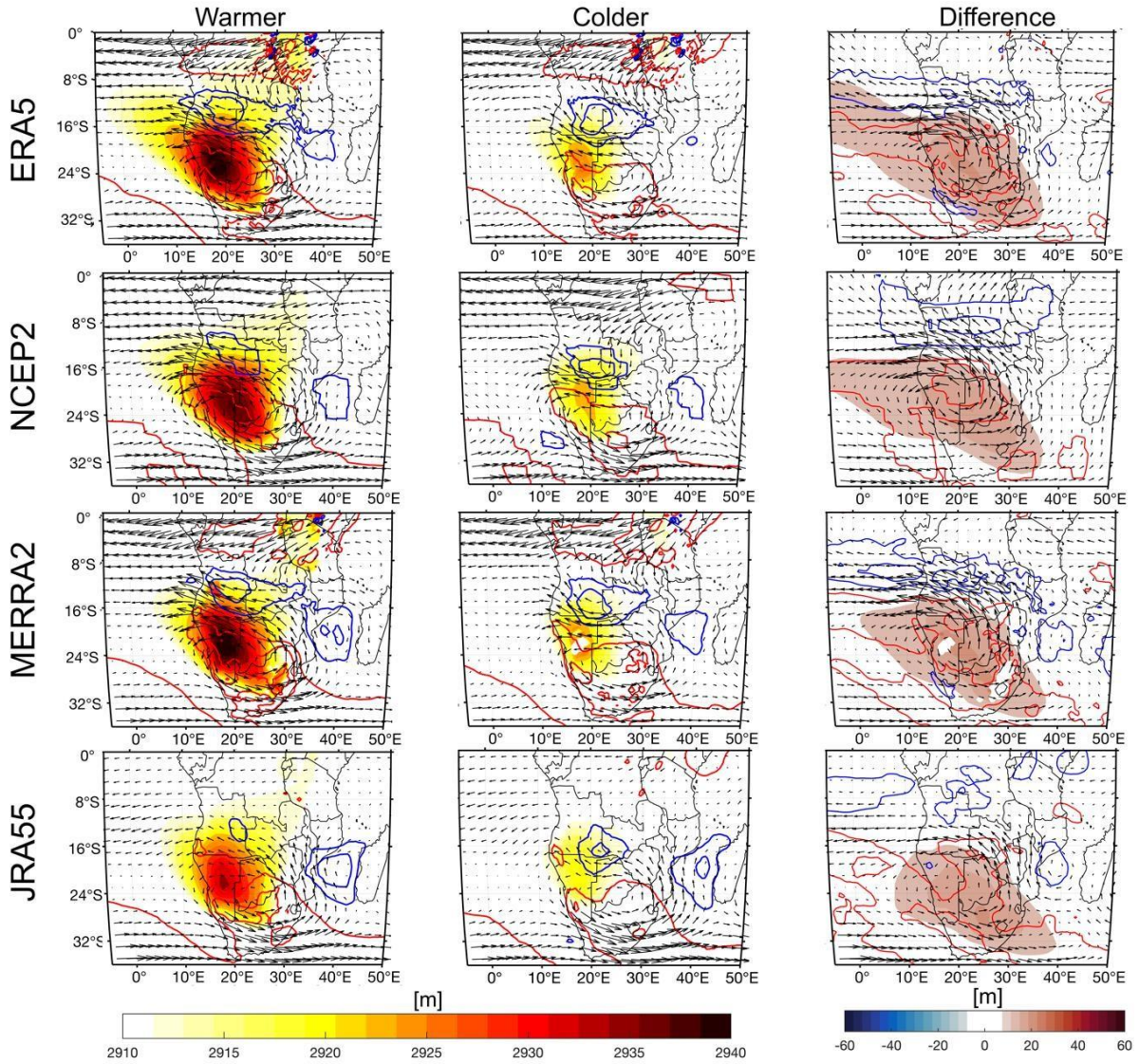

Figure 2.13: Composite of the atmospheric thickness (shading, m), vertically integrated moisture flux ($< q\vec{v} >$, black arrows, m/s) in the mid-troposphere (700–600- hPa) and its associated relative vorticity (contours, $\times 10^{-6} s^{-1}$) for (left panels) warm, (middle panels) cold phases of KTL. (right panels) Difference between these two phases. Red and blue contours indicate the positive and the negative values. The contour interval is $-0.5 \times 10^{-6} s^{-1}$ for the negative and $0.75 \times 10^{-6} s^{-1} m$ for positive values respectively. For the difference the contour interval is $0.25 \times 10^{-6} s^{-1} m$. $<.>$ the mass- weighted vertical integral (i.e., $\int \frac{dp}{g}$) from 700–600 hPa and g, the gravitational constant.

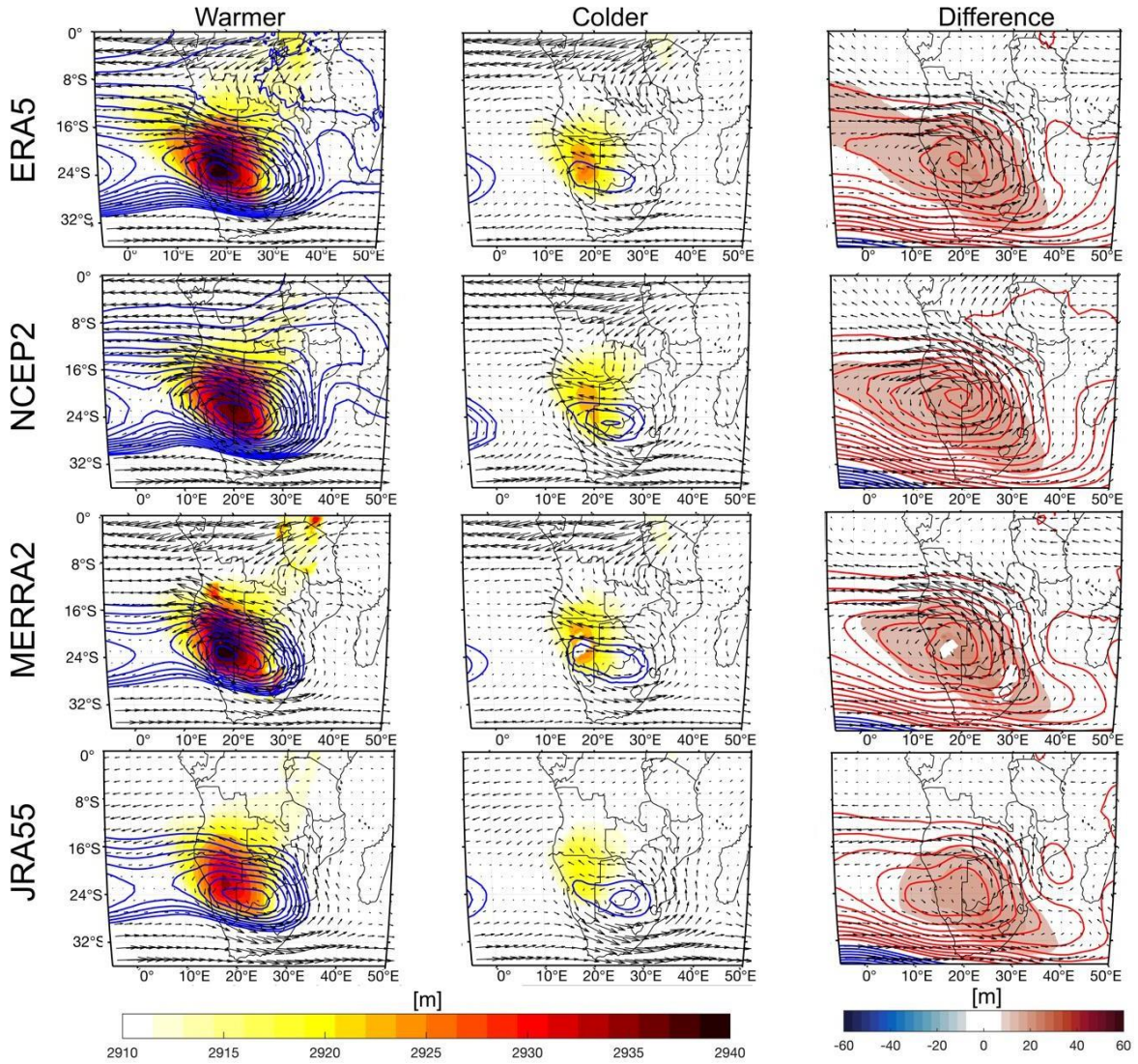

Figure 2.14: Composite of the Kalahari thermal low (Δz, shading, m), Botswana high (z_{600}, blue contours, m) and the mid-tropospheric circulation (black arrows, m/s) during (left panels) warm, (middle panels) cold phases of KTL. The difference between these two phases is on the right panel. The contour interval is 2m for the two first panels for $z_{600} \geq 4420$m and 3 m for the last panel.

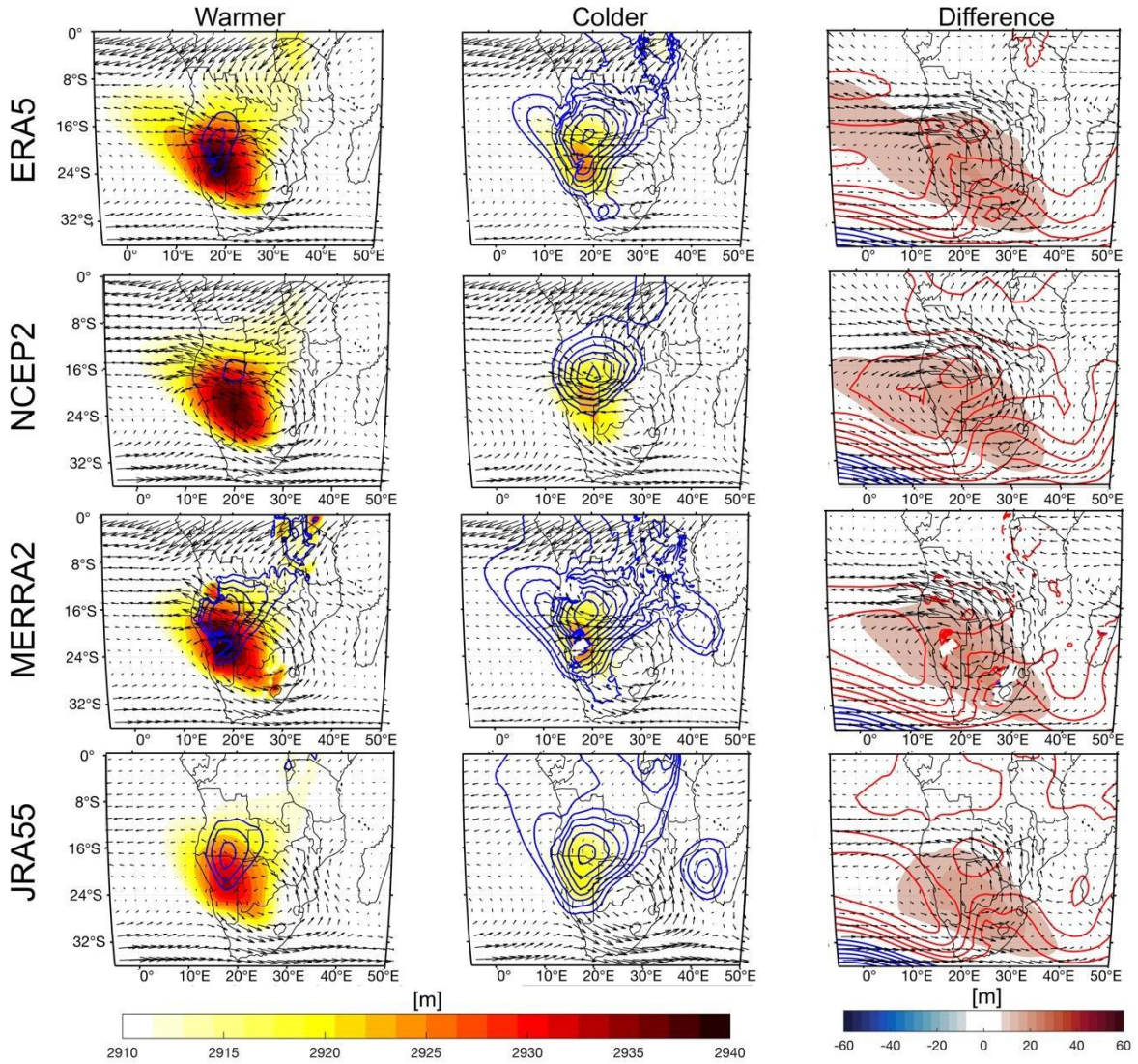

Figure 2.15: As for Figure 2.14. but for Angola low (z_{850}, contours, m), with $z_{850} \leq$ 1500 m.

The heat causes the surface to lose more moisture through evaporation, creating further warming in the region (Figure 2.16). Above15ºS (i.e., over central Africa), the lower atmosphere is anomalously wet (Figure 2.16), indicative of dryline (Taljaard, 1958, Howard et al., 2019). In other words, the variability of the KTL plays a significant role in the formation of drylines over southern Africa, consistent with van Schalkwyk et al. (2022). Unexpectedly, this mechanism is missing in JRA55, in which the mass air is wetter (Figure 2.16).

The heat dome is associated with a strong anomalous anticyclonic circulation over southern Africa, which displaces equatorward the anomalous cyclonic circulation and reinforced both the SMC and the AEJ-S (Figure 2.16). The strong anomalous south-

easterly that crosses the southern Africa subcontinent in the east-west direction veers around the reduced anomalous cyclonic circulation (Figures 2.13 & 2.16).

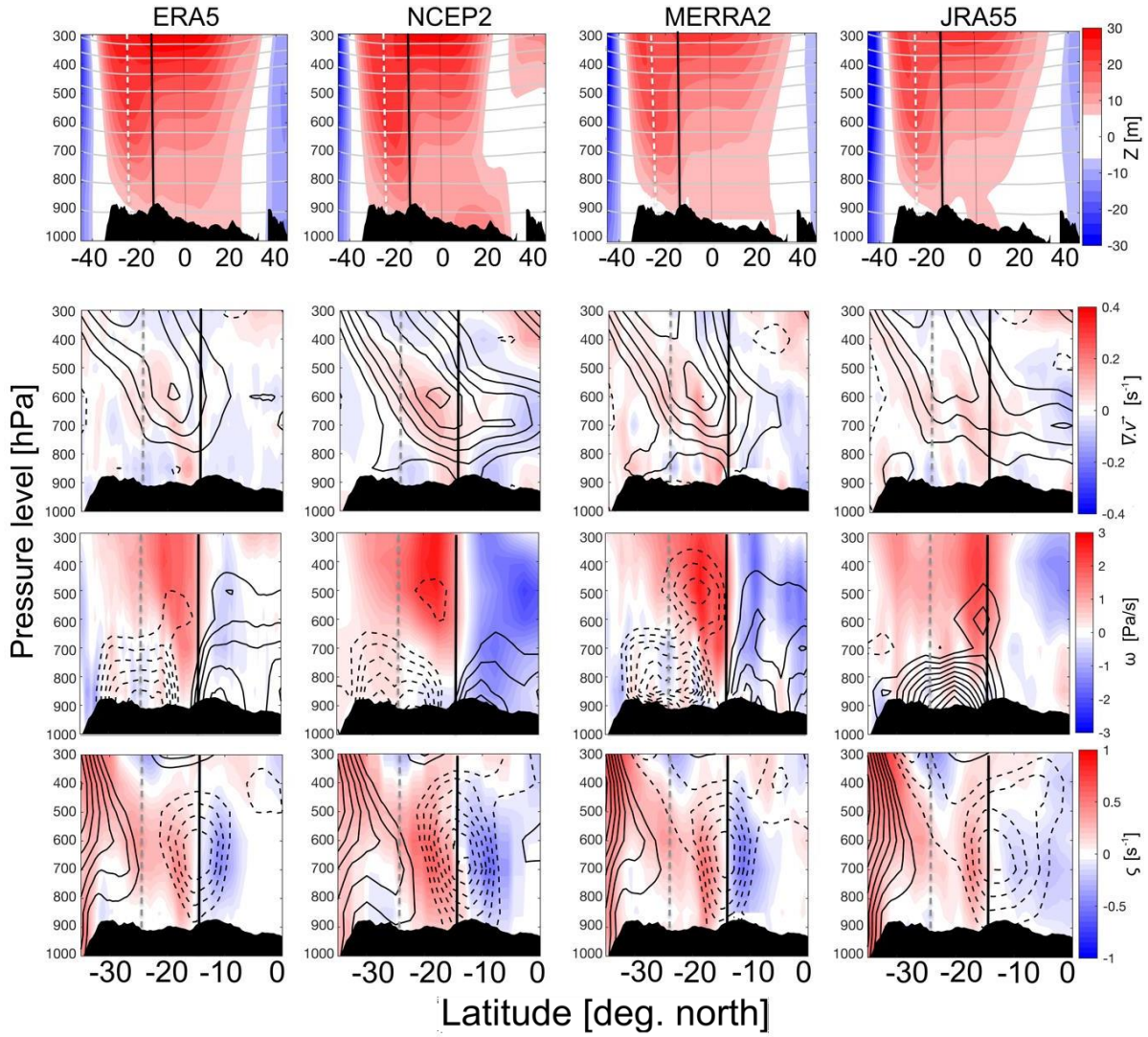

Figure 2.16: Cross-section latitude–pressure of the difference between warm and cold phases of KTL for the (a–d) geopotential height (shading, m). The grey contour is for the seasonal-mean geopotential at 1000 m interval. (e–h) wind divergence (shading, s^{-1}) and meridional wind (contours, m/s) at 0.25 m/s interval. (i–l) vertical velocity (shading, Pa/s) and specific humidity (contours, g/kg) at 1 g/kg. (m–p) relative vorticity (shading, s^{-1}) and zonal wind (contours, m/s) at 0.4 m/s. Only shown |v| > .25 m/s at 0.25 m/s interval and u < -3 m/s at 1m/s contour interval. The solid and dashed contours represent positive and negative values respectively. In each panel, the vertical black and dotted grey lines mark 15ºS and 25ºS respectively. The longitude selected are from 10° – 25 °E.

This accelerates the anomalous SMC that carries the anomalous dry air into the convective region, as shown by the anomalous convergence (Figure 2.16). This confirms that over southern Africa, the cross-equatorial moisture advection is produced by transient components (Zhai and Boos, 2017). This anomalous SMC is

stronger in NCEP2 and JRA55 than in ERA5 and MERRA2 (Figure 2.17). As a consequence, the predominance of subsidence associated with high-pressure systems suppress the deep convection and leads to drought conditions over southern Africa (Figure 2.17). This result is consistent with previous works (Reason, 2016, Pascale et al., 2019) that investigated the impacts of the Botswana high variability or the meridional displacement of and Angola low on southern African rainfall.

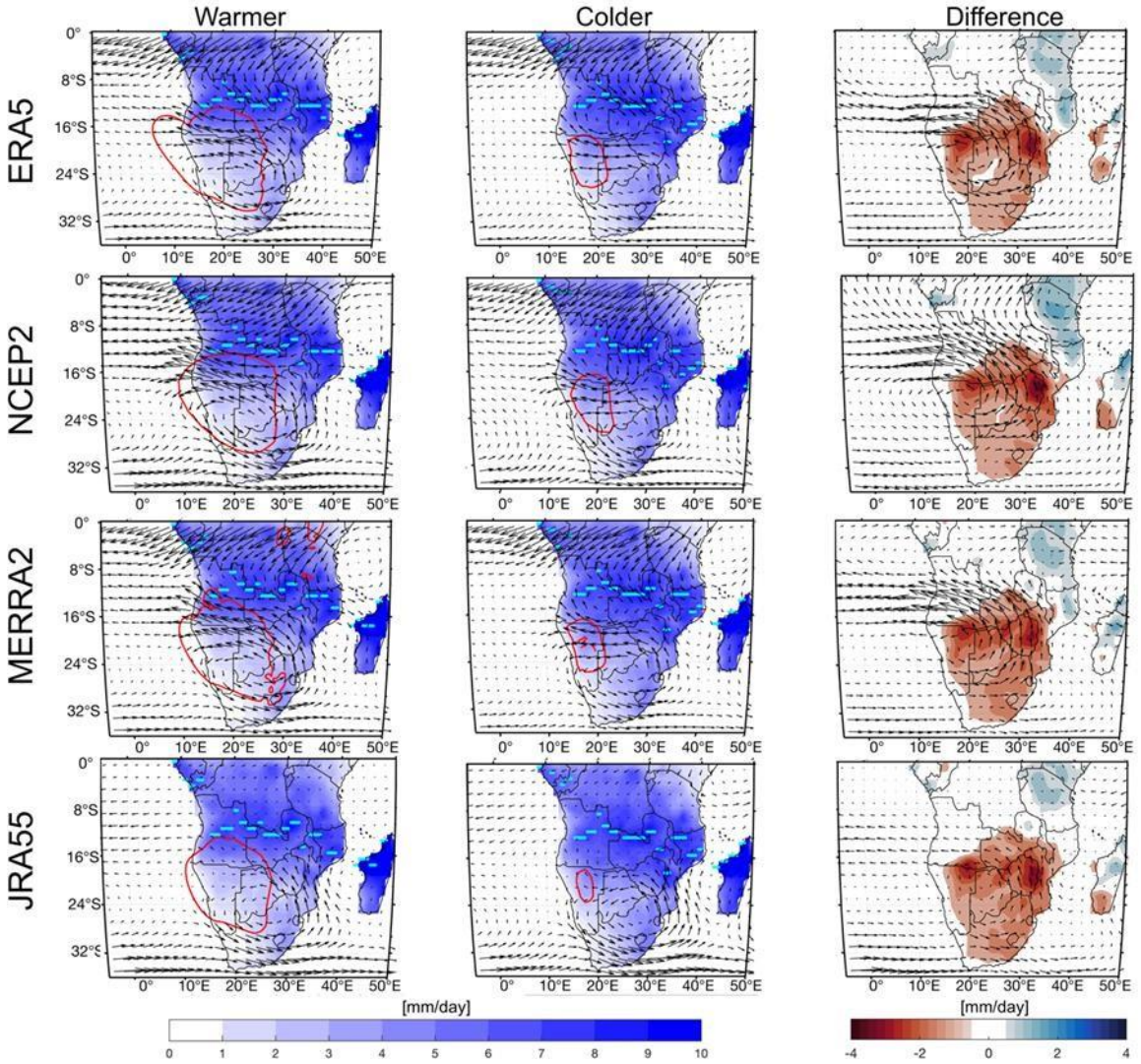

Figure 2.17: Same as Fig 2.15 but for rainfall (shading, mm/day). The red contour is the 2920 m isoline that represents the KTL.

2.4 Conclusion and discussion

The main objective of this paper was to document the Kalahari Thermal Low by highlighting its potential roles on the regional hydroclimate. Firstly, we found that in summer (DJF), the Botswana high and the Angola tropical low are highly dependent on each other

such that a deepened z_{850} reduces z_{600} (Figure 2.2). We therefore connected these two most important features of the southern Africa's climate as part of a same robust atmospheric feature, the KTL. The KTL is a semi-permanent heating source in the southern Africa. It displaces poleward at 10 km/day from its initiation in September until its maturation in January before receding rapidly and disappearing in March at the vicinity of where it originated. The link between the KTL and Angola low shows two distinct behaviours at different timescales. At a seasonal cycle timescale (annual cycle), the Angola low, driven by the KTL, responds as a thermal low. At the interannual timescale, the reversal of the relationship in summer suggests that the Angola low behaves as a tropical low and forms a Matsuno-Gill-like response to diabatic heating related to KTL, consistent with Mulenga (1999).

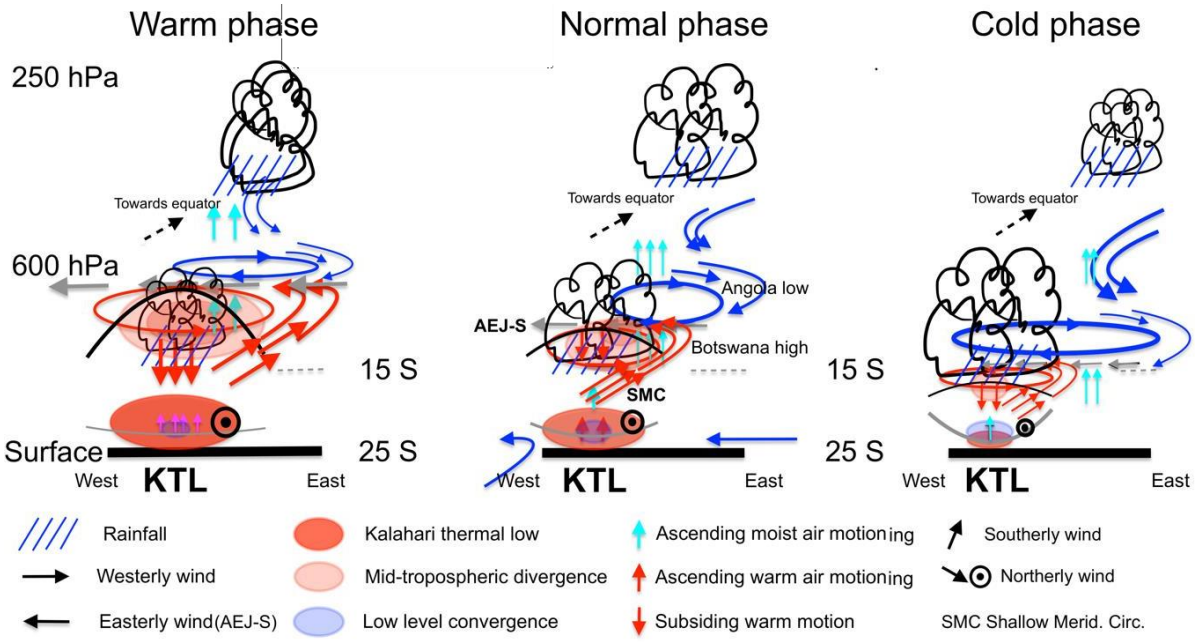

Figure 2.18: Schematic diagram showing the driving mechanisms through which the Kalahari thermal low (KTL) controls the regional precipitation.

The KTL shows a strong negative correlation with southern African rainfall in summer implying that warm KTL reduces rainfall. This teleconnection is explained by the leading mode of variability of KTL, with some contribution of El Nino Southern Oscillation. This teleconnection is controlled essentially by the formation of the heat dome rather than by the anomalous advection of mid-tropospheric of dry air into convective region as previously suggested by Zhai and Boos (2017). We summarized this mechanism in the schematic diagram in Figure 2.18. Indeed, during the warm phase, the anomalous surface heating induced a strong anomalous tropospheric

subsidence centred at the core of the KTL (Figures 2.16 & 2.18). The surrounding anomalous warm air mass ascends to be capped later by the anomalous subsidence aloft. This strengthened subsidence forces the warm air to sink, compress and releases more heat (Figure 2.18). This latent heat release heats the area, while losing more moisture through the evaporation. The heat dome is associated with a strong anomalous anticyclonic vortex over southern Africa, which displaces equatorward the anomalous cyclonic circulation and reinforced both the SMC and the AEJ-S (Figure 2.18).

More interestingly, the equatorward position of the Angola low circumvents and accelerates the anomalous SMC that carries the anomalous dry air into the convective region (Figure 2.16). In partial agreement with Zhai and Boos (2017), we found that it is the anomalous strong subsidence that suppress the deep convection rather than the mid-tropospheric dry air carried by transient components that reduces the regional rainfall (Figure 2.18). This finding agrees with Pascale et al.(2019) and completes it by providing the causal effect of the meridional displacement of the Angola low. On the other hand, during the cold phase of KTL, the induced mid-tropospheric divergence is reduced, favouring the formation of the moisture convergence that triggers the deep convection and leads to above normal rainfall condition (Figure 2.18). This is suggestive of a prominent role of the Angola low as widely reported by previous works (Pascale et al., 2019, Crétat et al., 2019, Howard and Washington, 2018, Munday and Washington, 2017).

This observational study of the KTL sheds more light on the mechanisms responsible of the dry climate over southern Africa, by linking the two most important features of the regional climate – the Angola low at its bottom and Botswana high aloft. Due to global warming, southern Africa will experience the increase of heatwave related to the occurrence of more heat domes in the future, which will likely lead to drought condition. Our results shed light on the formation of the heat dome-like atmospheric circulations due to the KTL in southern Africa. Further investigations on these driving mechanisms, which are likely to lead to more heatwaves and drought, are needed in the context of global warming. Thus, the KTL, as one of the key drivers of southern Africa's climate, should be monitored and further investigated to help decision-makers with mitigative policies that can help people cope with the effects of climate change.

3 Observational Study of the Shallow Meridional Circulation and its Contribution to the Regional Moisture Budget over Southern Africa

3.1. Introduction

Many studies (Trenberth et al., 2000, Nolan et al., 2007, Zhang et al., 2008, Nie et al., 2010, Zhai and Boos, 2017) reported that in the monsoonal regions, the shallow meridional circulation (SMC) superimposes on a deep and moist Hadley Circulation that produce rainfall during local summer. The SMC is a vertical meridional overturning circulation that has its maximum wind and return flow in the middle troposphere, where it transports the dry air into the deep tropical convective region (Zhang et al., 2008; Nie et al., 2010; Zhai and Boos, 2017). Nie et al. (2010) highlighted the existence of the SMCs on both sides of the equator during local summer (Figure 3.1). Both SMCs feed into the deep convection but produce little cross-equatorial flow in the mid-troposphere (Nie et al., 2010). Zhai and Boos (2017) investigated the relationship between the horizontal moisture advection produced by SMCs and the monsoon precipitation. They found a negative relationship between them, meaning that the upper branch of the SMC dries up the mid-troposphere by advecting dry air into the convective region. This inhibits the monsoon precipitation and modulates interannual rainfall variability. This finding is consistent with what we found in the previous chapter that a warm phase of Kalahari Thermal Low (KTL) induces a strong mid-tropospheric meridional circulation, which, in turn, is associated with reduced precipitation over southern Africa (Figure 2.14 and 2.17). However, during the cold phase of KTL, a weakened mid-tropospheric meridional circulation is associated with enhanced rainfall (Figure. 2.15 and 2.17). Yet, it remains unclear how this thermally driven SMC contributes to the regional moisture budget.

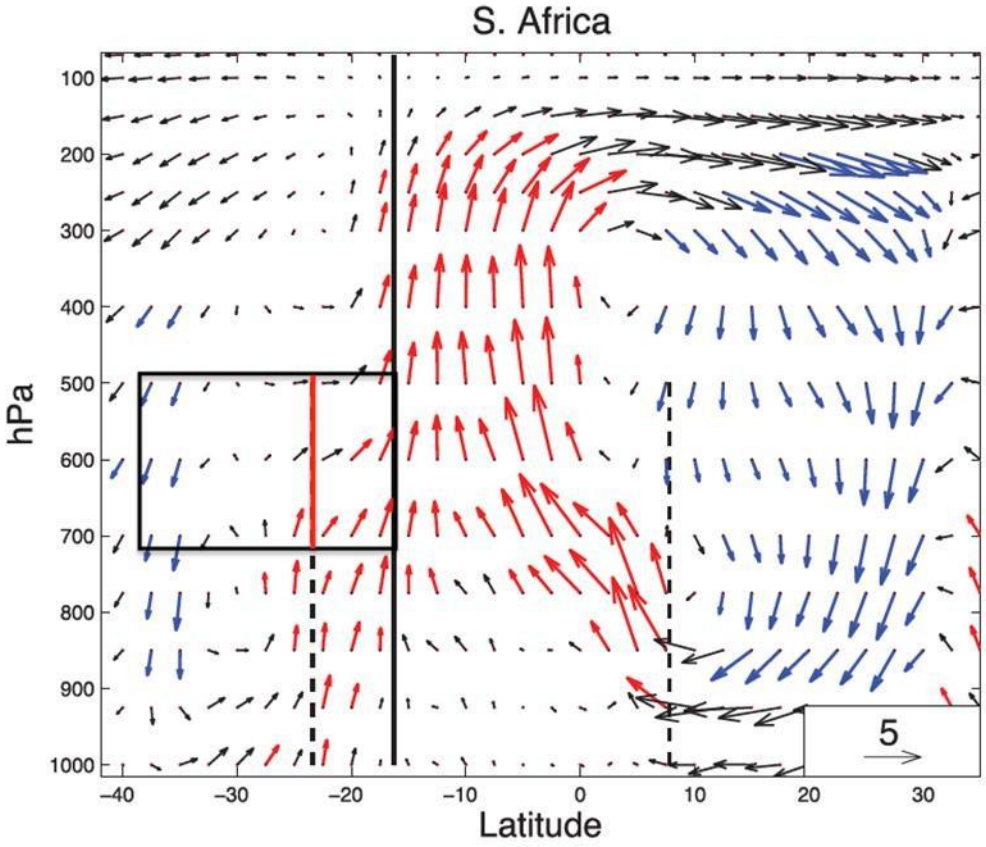

Figure 3.1: January latitude–vertical cross section of the wind vectors of African monsoons. Vectors with upward (downward) motion stronger than -0.02 Pa/s (0.02 Pa/s) are red (blue); other vectors are black. The vertical black solid (dotted) line indicates the latitude of the θ_{eb} (θ_b) peak. The vertical velocity is amplified 80 times for better illustration. The black box highlights the upper branch (return flow) of the shallow meridional circulation in southern Africa, with the red vertical line separating the region in the north-southern Africa and south-southern Africa respectively (Figure adapted from Nie et al., 2010, Figure 8).

In the previous chapter, the partitioning of the horizontal wind into its divergent and rotational components highlighted two contrasting vertical structures of the atmospheric circulation over southern Africa (see Figure 2.8). The meridional component of the rotational wind that dominates the total meridional wind shows a recirculation in the mid-lower troposphere (Figure 2.8). Its upper branch is constituted by the subtropical southerly jet (STSJ) that transports the mid-tropospheric dry air into the convective region (Figure 2.8). The STSJ forms over the tropical southern Africa (i.e., 25°–15°S) when north-westerlies turn to become south-easterlies. Its lower branch is formed by a weak low-level northerly jet that carries the moist air from tropics to subtropical regions of southern Africa (Figure 2.8). This is the vertical structure that is widely discussed in the literature (Zhai and Boos, 2017, Nie et al., 2010, Hurley and Boos, 2013).

On the other hand, because the divergent flow contributes to the vertical motion (Dutton, 2002), it shows a tropospheric circulation opposite to that of the rotational wind (Figure 2.8). This comprises a SMC, with the mid-tropospheric northerly jet (MTNJ) as its upper branch and the low-level southerly jet as its lower branch (Figure 2.8). To settle out this controversy, further investigation is needed.

Additionally, Schwendike et al. (2014) identified – over the western side of southern Africa landmass – a local Walker cell that develops in summer. This local Walker-like cell is associated with ascent motion over landmass and subsidence over surrounding oceans (Schwendike et al., 2014). However, over the subtropics, the vertical structure of this local Walker-like circulation is not fully documented because many studies (Yu and Zwiers, 2010, Yu et al., 2012, Bayr et al., 2014) focused primarily on the equatorial circulation.

In this chapter, we address the following questions:

(i) What are the vertical structures of the SMC and its counterpart zonal circulation over the subtropical region of southern Africa?

(ii) How does the mid-tropospheric moisture advection ($\vec{v}.\nabla q$) relate to the upper branch of the SMC and interact with the southern African monsoon and its associated convection?

(iii) What is the contribution of the SMC to the regional moisture budget over southern Africa?

3.2. Data and Methodology

3.2.1. Dataset

In the previous chapter, the satellite-era reanalysis products reproduced quite well the KTL and its induced mid-tropospheric circulation. Unless stated otherwise, we used three monthly reanalyses. The National Centre for Environmental Prediction (NCEP) – Atmospheric Model Intercomparison Project (AMIP-II) reanalysis (NCEP2, (Kanamitsu et al., 2002)) dataset, which is the most used reanalysis in the climate studies over southern Africa, despite its resolution limitation. The European Centre for Medium-Range Weather Forecasts (ECMWF) ERA5 (Hersbach et al., 2020) is the enhanced version of ERA-Interim. It is the fifth generation of atmospheric reanalysis

produced and provides hourly estimates of large-scale numerous atmospheric, land and oceanic variables. ERA5 is based on the Integrated Forecasting System and therefore benefits from a decade of developments in core dynamics, model physics and data assimilation (Hersbach et al., 2020). ERA5 has an enhanced horizontal resolution of 31 km compared to 80 km for ERA-interim and resolves the atmosphere into 137 levels from the surface up to 80 km. The Japanese 55-year Reanalysis (JRA55, Kobayashi et al., 2015) is a 55-years longest third generation reanalysis and the first to apply four-dimensional variational analysis. JRA5 was developed by the Japan Meteorological Agency (JMA) to address issues found in JRA-25 (Onogi et al., 2005) and to further produce a comprehensive atmospheric dataset suitable for studying multidecadal variability and climate change (Kobayashi et al., 2015). The variables used are the horizontal wind with its zonal (*u*), meridional (*v*) components; the vertical velocity (ω), geopotential height (*z*), and specific humidity (*q*), which was obtained from the relative humidity.

For rainfall, we used the Global Precipitation Climatology Centre version 7 (GPCC v7) dataset (Schneider et al., 2014) to assess the influence of the SMC. GPCC is based on statistically interpolated in situ rain measurements covering all land areas (0.5° × 0.5° horizontal resolution) at monthly temporal resolution. All selected variables have been interpolated to a 0.5° × 0.5 ° grid and span from DJF 1982/83 to DJF 2020/21.

3.2.2. Methodology

The governing equations of the atmospheric moisture budget and continuity (Peixoto and Oort, 1992, Seager and Henderson, 2013) are written as follows:

$$\frac{\partial_t < q > + < \nabla . (q \vec{V}) >}{\rho} = E - P \qquad (3.1)$$

$$\Delta\omega = -g < \nabla . v^{\rightarrow} > \qquad (3.2)$$

with $<.>$ the mass-weighted vertical integral (i.e., $\int \frac{dp}{g}$) from the low-level pressure p_l to the upper-level pressure p_u; g, the gravitational constant; ρ, the density of water; q, the specific humidity; $\vec{V} = (v^{\rightarrow}, \omega)$, the wind, where $v^{\rightarrow}$ and ω are horizontal wind and vertical velocity respectively; $\Delta\omega = \omega(p_l) - \omega(p_u)$; P, the rainfall and E, the evaporation. Since, our data are at a monthly resolution, the calculated moisture

budget components do not include the contributions from the sub-monthly transient eddies as highlighted in previous work (Zhai and Boos, 2017).

To separate the horizontal wind $\vec{v} = (u, v)$ into its rotational $\vec{v}_r$ (divergent-free) and divergent $\vec{v}_d$ (vorticity-free) components, we use the Helmholtz decomposition (Hammond and Lewis, 2021):

$$\vec{v} = \vec{v}_r + \vec{v}_d \tag{3.3}$$

$$= -\nabla\chi + k \times \nabla\varphi \tag{3.4}$$

With φ is the streamfunction and χ is the velocity potential that are obtained from

$$\nabla^2\chi = \delta \tag{3.5}$$

$$\nabla^2 \varphi = \zeta \tag{3.6}$$

Where δ is the divergence and ζ is the vorticity.

Because rainfall is strongly correlated with vertical motion (Parker et al., 2016, Zhai and Boos, 2017), we computed the mass-weighted stream functions (ψ_m, ψ_z) with either the meridional (v_d) or the zonal (u_d) component of the divergent wind (Innes and Pierrehumbert, 2022, Nguyen et al., 2018, Yu and Zwiers, 2010, Yu et al., 2012, Bayr et al., 2014) to accurately represent the vertical structure as follow:

$$\psi_m = 2\pi r sin(\theta) < [v_d] > \tag{3.7}$$

$$\psi_z = 2\pi r < [u_d] > \tag{3.8}$$

r is the earth's radius, θ is the latitude and the brackets ($[A]$) denote the zonal or the meridional average of a variable *A*. Note that the divergent wind contributes to the vertical motion (Dutton, 2002) and the continuity equation of each partitioned circulation is satisfied independently for the global domain in the zonal and meridional directions because they are in the orthogonal planes.

3.2. Results

3.2.1. Regional circulation over southern Africa

In this subsection, we examine the horizontal wind field and its decomposed divergent and rotational components at lower (850 hPa) and middle troposphere (700–600- hPa) over southern Africa in summer (Figure 3.1). In addition to the wind field at each

atmospheric layer, we also plotted its associated relative vorticity, $\zeta = \nabla \times \vec{v}$. The low-level circulation over the southern Africa subcontinent is cyclonic ($\zeta < 0$), expect over the south–eastern region of south Africa, where the circulation is locally anticyclonic (Figure 3.2d-f). The moisture inflow into southern Africa (15°–25°S) is predominantly zonal, and it compromises low-level north-easterly jet that flows across the KTL (Figure 3.2f). This low-level north-easterly jet is made up of two different wind patterns: the north-easterly flow from east Africa, and the easterly jet from south-western Indian Ocean, reminiscent of a monsoon-like circulation (Figure 3.2f). These two wind patterns are rotational by nature (Figure 3.2e). At the same time, the low-level divergent flow is dominated by the monsoon-like circulation along the Atlantic coastal region (Figure 3.2d). Over the landmass, the weak north-westerly jet flowing from Congo Basin and a weak south-easterly flow meets to form the Congo air boundary (Figure 3.2d), consistent with Howard and Washington (2018).

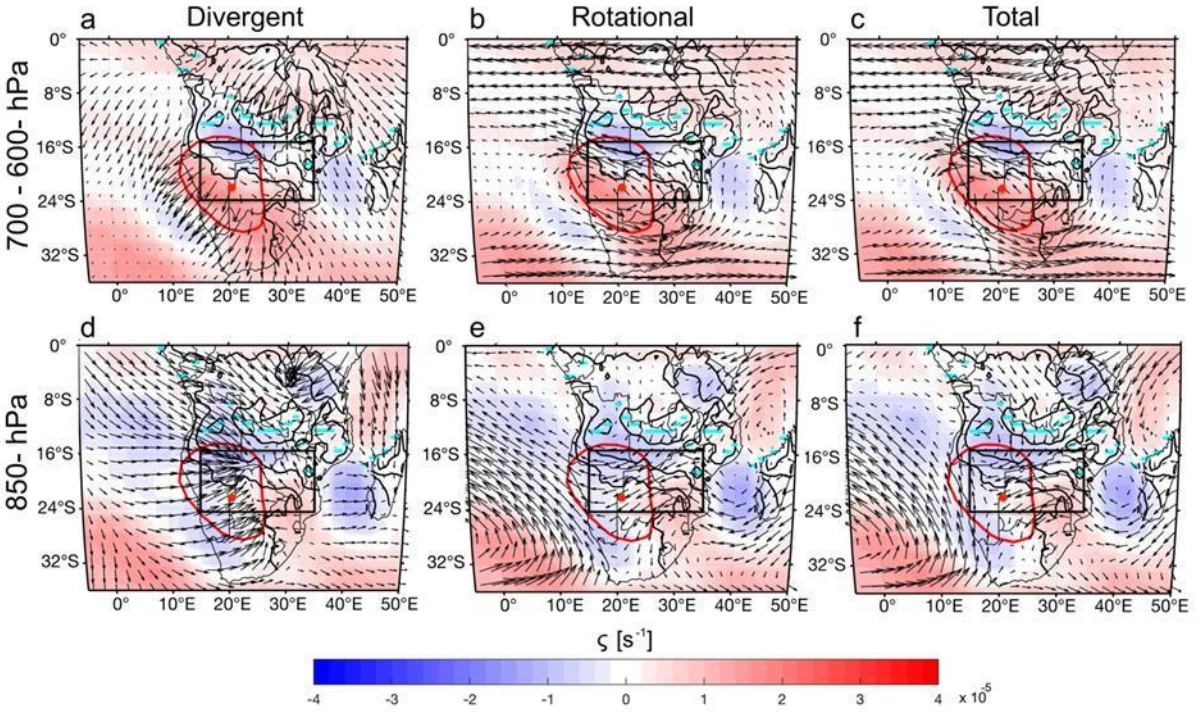

Figure 3.2: Vertical-mean relative vorticity (shaded, s^{-1}) and vertically integrated moisture flux of (left) divergent (arrows, m/s), (middle) rotational (arrows, m/s) and (right) total (arrows, m/s) winds at lower (850-hPa) and middle (700–600-hPa) troposphere respectively in DJF. The cyan contours represent the location of the maximum value of the precipitable water. The red bold contour represents the Kalahari thermal Low (i.e., 2920-m isoline, see chapter 2 for details) and the red dot indicates its maximum.

However, the low-level south-easterly is prevailing over southern Africa (~15°–25°S), while low-level north-westerly jet is a continuation of the monsoon-like circulation from the tropical Atlantic Ocean (at 5^{o}–10^{o}S) into the subcontinent (Figure 3.2d; f). This means that the low-level westerly jet over southern Africa is not controlled by the Angola low as widely reported (Cook et al., 2004, Vigaud et al., 2009, Munday and Washington, 2017, Pascale et al., 2019). Over the south-eastern Atlantic Ocean, the low-level circulation is driven by the SAH (Figure 3.2d-f). At the mid-troposphere, the Angola low that is characterized as the remnant of the low-level cyclonic circulation (see Howard and Washington, 2018; Pascale et al. 2019; Cretat et al. 2019) separates the anticyclonic circulation ($\zeta > 0$) in two parts, with a strong vortex over southern Africa, indicative of the KTL, and an additional weaker one over central Africa (Figure 3.2b-c). At 25°–35°S, the inflow related to the mid-tropospheric vortex is constituted by a rotational wind that veers around the KTL to form a counterclockwise circulation while crossing the northern flank of the KTL (Figure 3.2b-c).

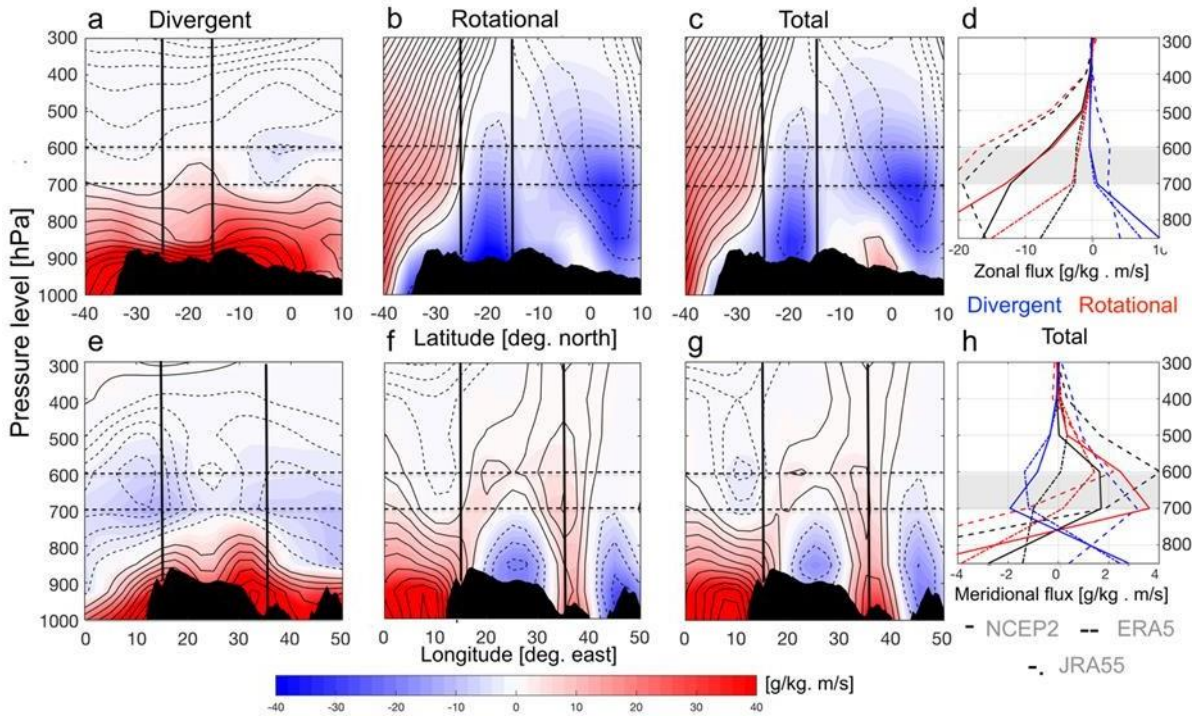

Figure 3.3: (Top) Zonal-mean of the zonal component of (left) divergent (u_d, m/s), (middle), rotational (u_r, m/s) and (right) total wind (*u*, m/s) as function of latitude and pressure level. (Bottom) similar to (top) but for the meridional-mean meridional wind (*v*, m/s) as function of longitude and pressure level. The vertical black lines delineate the zonal boundaries of southern Africa, (15º & 30º E). The horizonal red dashed lines highlights the mid-troposphere (700-500 hPa)

This is reminiscent of the southern branch of the mid-tropospheric (African) easterly jet (AEJ-S). Due to the conservation of its vorticity, the mid-tropospheric airflow curves to the north, assuring a continuation of the inflow into the southern African subcontinent before it becomes a subtropical southerly jet around 15°–25°S (Figure 3.2b-c). As a result, the mid-tropospheric air is transported northward over the southern African landmass rather than coming from the Indian ocean (Figure 3.2b-c). Furthermore, there is a mid-tropospheric divergent flow that is essentially meridional and carries the moisture southward from Congo basin, with the moisture outflow occurring over the coastal areas of the subcontinent (Figure 3.2a, c).

Interestingly, in the meridional direction, the divergent flow shows a recirculation in the mid-lower troposphere – equatorward at low-levels and poleward at mid-levels (Figure 3.2a, d & Figure 3.3a, e). Conversely, the rotational wind shows a recirculation in the

mid–lower troposphere over the landmass – equatorward at mid-levels and poleward at low-levels similar to the meridional wind (Figures 3.2b, e & 3.3b, f). However, the upper branch of this latter recirculation is the dominant component in the meridional wind (Figure 3.3 e-g). All reanalyses capture these contrasted meridional circulations quite well in partitioned components, except in ERA5, in which the vertical structure of the divergent circulation is similar to its rotational component (Figure 3.3h). To elucidate which constitute the upper branch of the SMC between these two meridional recirculations, we compute the meridional overturning circulations over southern Africa in the next subsection.

3.2.2. Vertical structure of the meridional circulation

In summer, the vertical structure over central and southern Africa is characterised by two asymmetric overturning cells (Figure 3.4). At low levels, the circulation is equatorward, with the ascending branch ($\psi_m = 0$) associated with the horizontal convergence occurs in the southern hemisphere, at ~15°S (Figure 3.4). Note that the horizontal convergence is caused by the vertical velocities at the top and bottom boundaries (see equation 3.2 and Figures 3.4 & 3.5). At upper levels, the circulation is poleward, and the subsiding branches occurs over midlatitudes in each hemisphere (Figure 3.4). The northern Hadley cell is deeper, wider, and clockwise (Figure 3.4). Its maximum is located at upper troposphere in ERA5, and in the middle and lower troposphere in NCEP2 and JR55 respectively (Figure 3.4). Similar patterns are also obtained for the northern cell when using the zonal-mean total meridional wind ([v]) (Figure 3.5). On the other hand, the southern Hadley cell is shrunk and counterclockwise (Figure 3.4). Its maximum is located at lower troposphere in NCEP2 and JRA55, except in ERA5, in which it is at upper levels (Figure 3.4). In other words, the southern Hadley cell is shallower than its northern counterpart, except in ERA5 (Figure 3.4). Thus, between 15°–25°S, due to its proximity with the strong ascending branch (related to the northern Hadley cell), the high rainfall that occurs there is associated with deep convection (Figure 3.4).

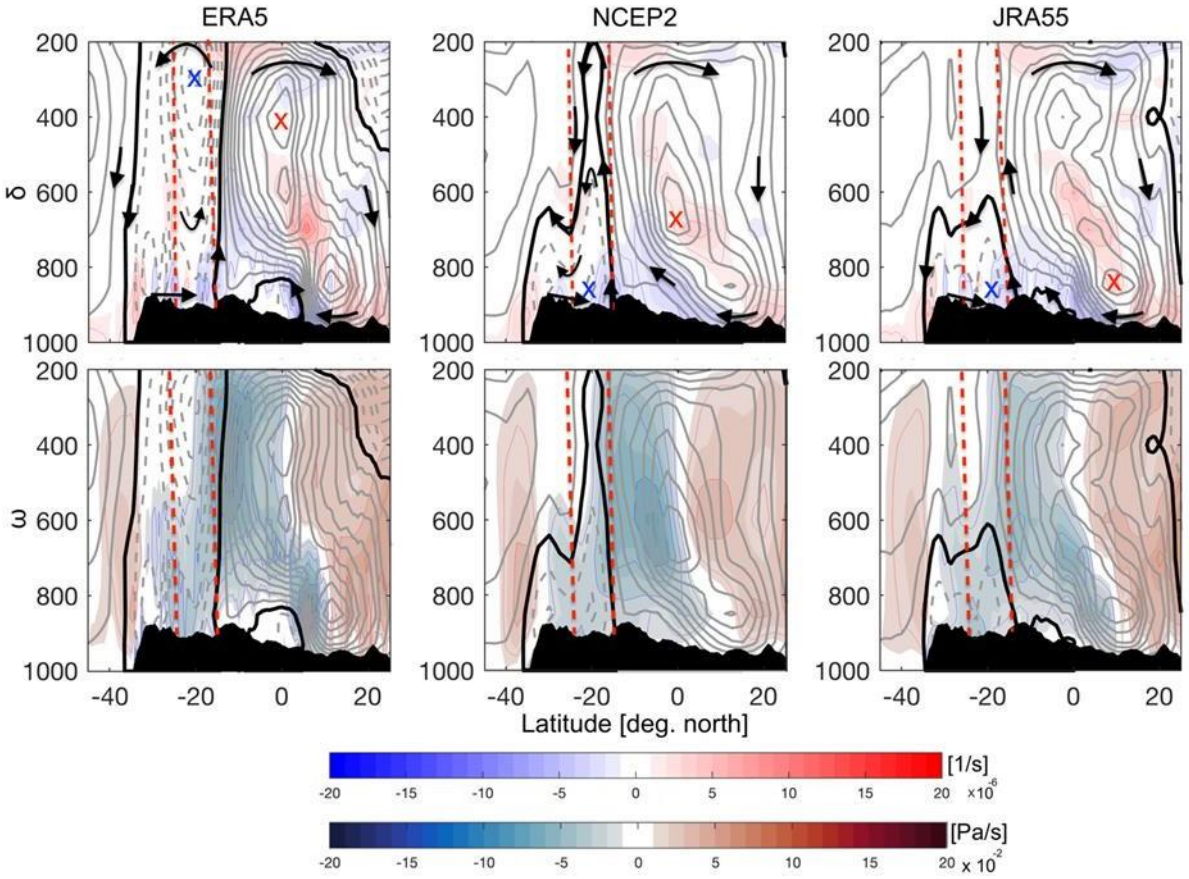

Figure 3.4: (Top) Latitude–pressure (hPa) cross-section (averaged between 15°–30°E) of the meridional mass-weighted streamfunctions (ψ_m, gray contours, $\times 10^9$ kg/s) and divergence (δ, shaded, s^{-1}) in summer for (left) ERA5, (middle) NCEP2 and (right) JRA55 for the zonally-mean meridional component of divergent wind. (Bottom) Similar to top panels, but for the vertical velocity (ω). The thick black contour represents $\psi_m = 0$. The clockwise (positive) and anticlockwise (negative) ψ_m are shown by solid and dashed contours at 30×10^9 kg/s interval. The × symbol marks the maximum value of ψ for either the southern (blue) or northern (red) Hadley cell. The vertical red dashed lines delineate the north-southern Africa (i.e., 15° and 25° S) respectively. In top panels, arrows indicate the flow direction.

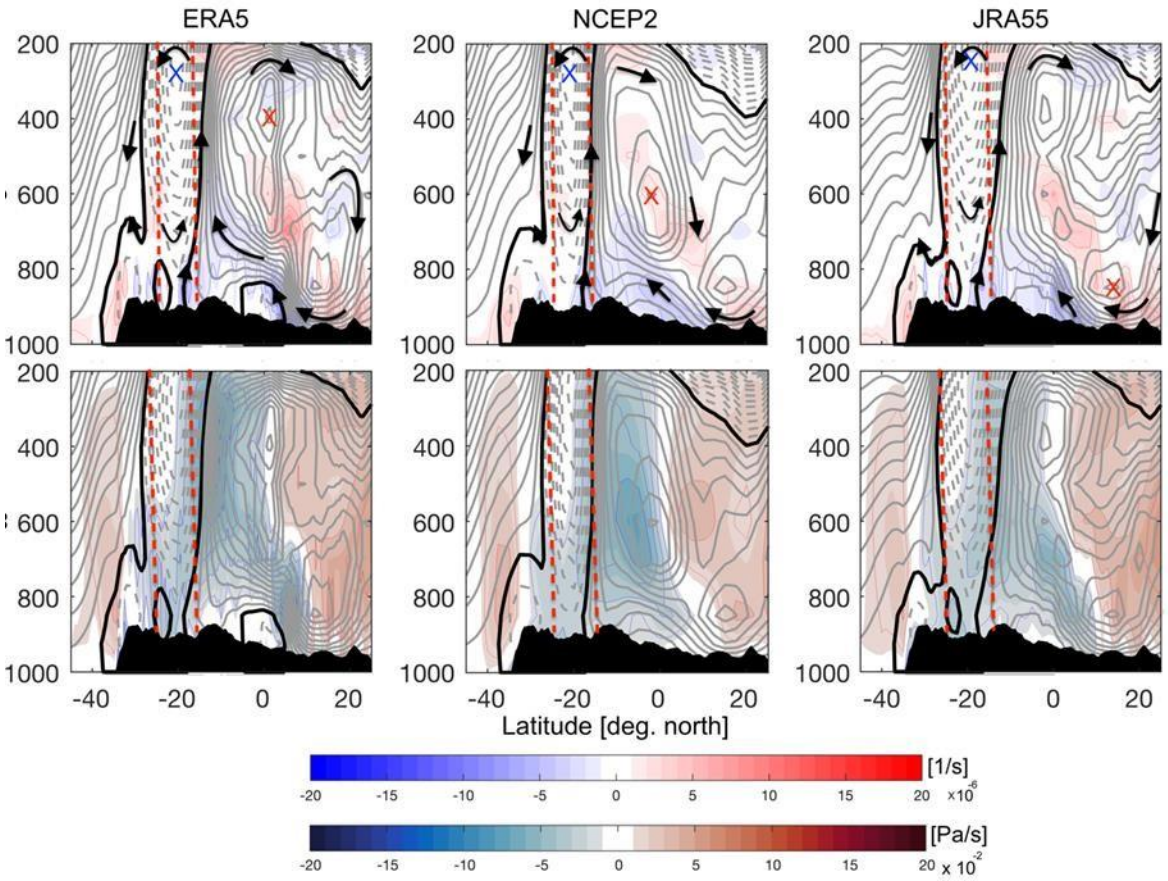

Figure 3.5: As in Figure 3.4, bur for the total meridional wind.

At mid-troposphere of the same region, the circulation is poleward (Figure 3.4). Indeed, owed to the formation of the KTL, the vertical structure of the convergence shows a dipole in the mid-lower troposphere – a low-level convergence associated with a surface warming and a mid-tropospheric divergence, which in turn, is weaker than its northern counterpart related to the Sahel low (Figure 3.4). This former generates mid-upper tropospheric subsidence that caps the shallow convection underneath and distorts the ascending branch of the southern Hadley cell (Figure 3.4). This forms the bottom-heavy structure of the southern Hadley cell, with its upper branch being poleward (Figure 3.4). This means that regionally, when the atmospheric mechanisms are set-up, the southern Hadley cell develops as a thermally driven SMC over southern Africa. When using the zonal-mean total meridional wind ([v]), the circulation is poleward at upper levels for the southern cell in all reanalyses (Figure 3.5). This suggests that the mid-tropospheric dry air advected northward into the convective region is carried by the subtropical southerly jet (STSJ) (Figure. 3.2–3.4). This overall means that the upper branch of the SMC (see Figure 3.1) is misrepresented in the literature (Zhai and Boos, 2017, Nie et al., 2010).

In the northern hemisphere, there is an additional ascending motion at low-levels around 5° N (Figure 3.4). This shallow convection is also capped by a strong subsidence associated with a strong divergence in the mid-troposphere (Figure 3.4). This favours the formation of a return flow in the mid-troposphere (Figure 3.4). Consequently, it distorts the northern Hadley cell to form its bottom–heavy structure (Figure 3.4). This indicates the coexistence of both shallow and deep Hadley circulations in the northern Hemisphere. Similar results have been reported (Nie et al., 2010).

3.2.3. Vertical structure of zonal circulation over southern Africa

Following Schwendike et al. (2014), this subsection intends to qualitatively give more details about the vertical structure of the zonal circulation over subtropical region of Africa. Two separated overturning cells are embedded in one counterclockwise circulation that dominates the atmosphere over southern Africa (Figure 3.6). The first overturning cell has its ascending branch over the western side of the landmass (15°–25°E), where the KTL forms, and its subsiding branch over the Atlantic Ocean where the low-level divergence prevails (Figures 3.6 and 2.3). Due to the surface heating associated with the low-level convergence, the warm and moist air rises to ~ 300 hPa despite the presence of the mid-tropospheric divergence (Figure 3.6). A distortion of the ascending branch due to the mid-troposphere divergence occurs only in ERA5 (Figure 3.6). At upper levels, the circulation is westward (Figure 3.6). The closing branch of the overturning cell is constituted by the low-level monsoon-like circulation that originates from the cold Atlantic Ocean (Figure 3.6). The maximum of the zonal mass-flux is located at the same latitude but at different positions: ~ 850- hPa, 15°E in NCEP2 and JRA55 and ~ 850- hPa, 10°E in ERA5 (Figure 3.6).

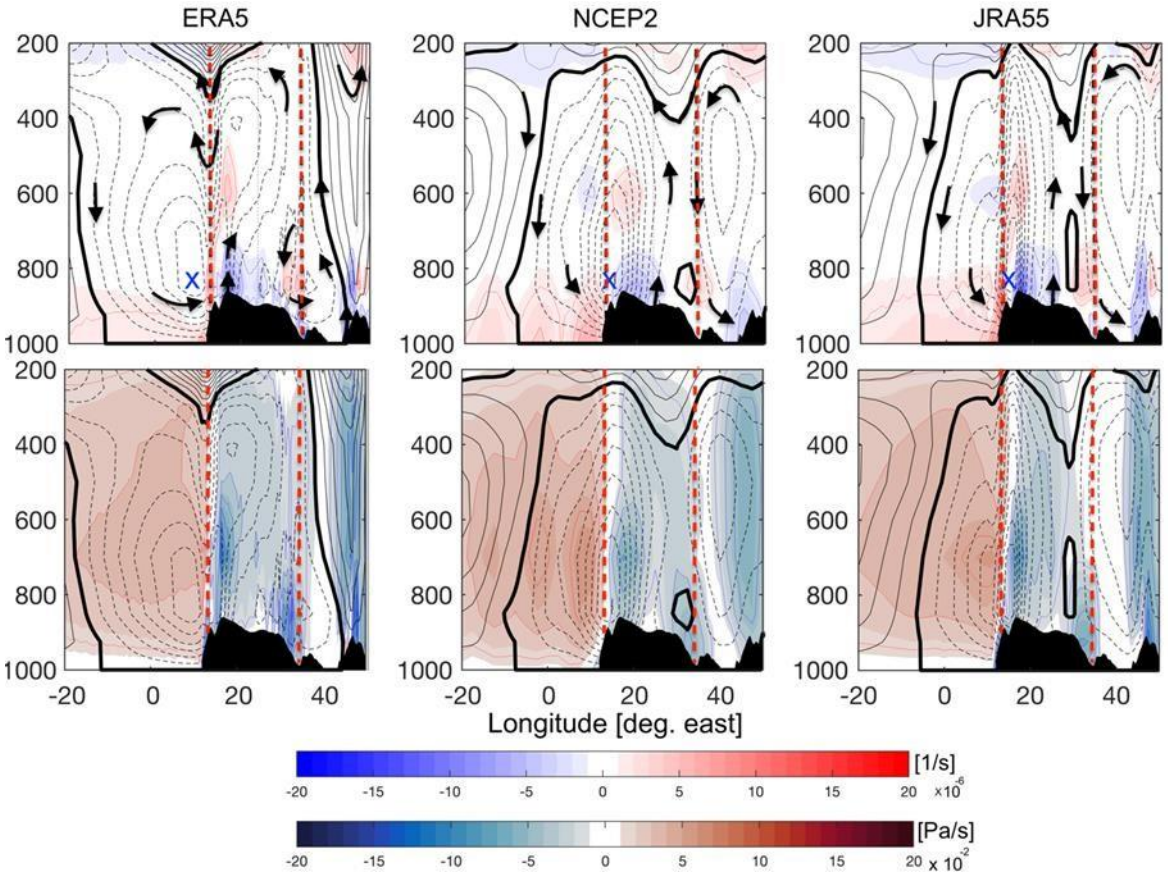

Figure 3.6: Longitude – pressure level (hPa) cross-section (averaged between 15º–30º S) of the zonal mass-weighted streamfunction (ψ_z, gray contours, $\times 10^9$ kg/s) and divergence (δ, shaded, s^{-1}) in summer for (left) ERA5, (middle) NCEP2 and (right) JRA55. The thick black contour represents $\psi_z = 0$. The clockwise (positive) and counterclockwise (negative) ψ_z are shown by solid and dashed contours at 30×10^9 kg/s interval. The × symbol marks the maximum value of ψ_z of the counter-clockwise Walker-like cell (blue). In top panels, arrows indicate the flow direction.

Notably, over the Atlantic Ocean, the mid-tropospheric convergence – that mirrors the mid-tropospheric divergence over landmass – can be seen in NCEP2 and JRA55, but it is absent in ERA5 (Figure 3.6). On the other hand, the second overturning circulation has its descending branch over the eastern side of the subcontinent and Mozambique channel (25°–40°E), suggesting a Walker-like cell over south-western Indian Ocean (Figure 3.6). In ERA5, the second overturning cell is shallow and confined over the Mozambique channel (32°–42°E) between the surface and 700- hPa (Figure 3.6). However, in ERA5, the ascending branch, which is generated by a strong convergence, occurs around the Madagascan escarpment (45°–50°E), indicative of an anabatic effect. At the eastern flank of the Madagascan escarpment, there is a deep

clockwise overturning cell (Figure 3.6). However, in NCEP2 and JRA55, this ascending branch is shallow as it extends up to ~700- hPa (Figure 3.6). Moreover, the descending branch of the Atlantic cell is also visible in the western Atlantic Ocean (Figure 3.6). Overall, these findings are consistent with Schwendike et al. (2014), but qualitatively details the vertical structure of the Walker-like cells over subtropical region of Africa.

3.2.4. Moisture advection of the SMC and its contribution to the moisture budget

3.2.4.1. Moisture advection and its link to rainfall and its associated convection

Previous study Zhai and Boos (2017) argued that the mid-tropospheric moisture advection of the SMC, driven by surface conditions, controls the precipitating convection. To probe this hypothesis, we first represent the spatial pattern of the horizontal mid-tropospheric (700–600 hPa) moisture advection over southern Africa in Figure 3.7. In partial agreement with Zhai and Boos (2017) , we find that the horizontal mid-tropospheric dry air mass is advected equatorward through the subtropical southerly jet (Figure 3.7e) and is strongly correlated with subsistence (Figure 3.8c). This implies that a strong horizontal dry air advection can induce a vertical descending motion over the KTL, conducive to shallow convection and vice versa. We used the vertical velocity ($\Delta\omega$) as a proxy of the convection in the mid-lower troposphere. This is consistent with previous works (Zhai and Boos, 2017, Nie et al., 2010). Furthermore, the zonal component contributes to the overall pattern of dry air advection that dominates over the subcontinent (Figure 3.7b), and its meridional component is associated with poleward moist air inflow into South Africa from the Atlantic coastal region (Figure 3.7a). This meridional moist air advection is balanced by the zonal advection of dry air (Figure 3.7b). A further decomposition of the horizontal moisture advection into its rotational and divergent components ($\vec{v}.\nabla q = \vec{v}_d.\nabla q + \vec{v}_r.\nabla q$) confirms that the zonal component of the rotational wind that depends strongly on the anticyclonic circulation is the main conveyor belt of the mid-tropospheric dry air (Figure 3.7d). This mid-tropospheric easterly jet forms as a thermal wind due to the meridional thermal contrast between the induced poleward anticyclonic circulation related to the warm KTL and the equatorward cyclonic circulation generated by the Angola low (Figure 3.7d). This mechanism is similar to that proposed by Adebiyi and Zuidema (2016), in which the southern branch of the mid-tropospheric easterly jet is diabatically formed by the temperature–moisture

gradient between the poleward hot–dry convection and the equatorward cool–moist convection associated with intense rainfall. More importantly, there is a zonal contrast of moisture advection over South Africa, with inflows drying out the mid-troposphere of the Atlantic coastal regions and the outflows moistening the mid-troposphere of the eastern coast of south Africa and the Angolan coast respectively (Figure 3.7d-e).

Conversely, the divergent wind slightly moistens the mid-troposphere while moving poleward, encouraging vertical ascending motion over the Angola low (Figures 3.7c; 3.8a). This poleward motion of the mid-tropospheric moist air is closely associated with the upper branch of the SMC (see Figure 3.4). This indicates that the SMC does not only produce any mid-tropospheric flow towards the convective region, with the MTNJ being associated with the deep convection. This reveals the opposite impacts of the SMC and the STSJ on the convection and rainfall. For the subtropical southerly jet, the KTL is a critical feature that facilitates the underlying mechanism. In fact, as shown in the previous chapter, a warmer KTL strengthens and enlarges the anomalous anticyclonic vortex over southern Africa (see Figure 2.9). Due to the vorticity conservation, this shrinks and decreases the strength of the Angola low by strengthening the subtropical southerly jet. Due to the absence of the Angola Low, the subtropical southerly jet advects the dry air directly into this convective region while weakening the mid-tropospheric easterly jet (Figure 2.9). This intrusion of the dry air (into the convective region) prevents the convection to deepen further and so, reduces rainfall (Figure 2.9). During the cold phase, the opposite occurs (Figure 2.9). For the SMC, a strong SMC can induce a strong vertical ascending motion, which in turn, enhances the rainfall over the southern Africa (Figure 3.8). This effect can be hampered when the subtropical southerly jet is stronger.

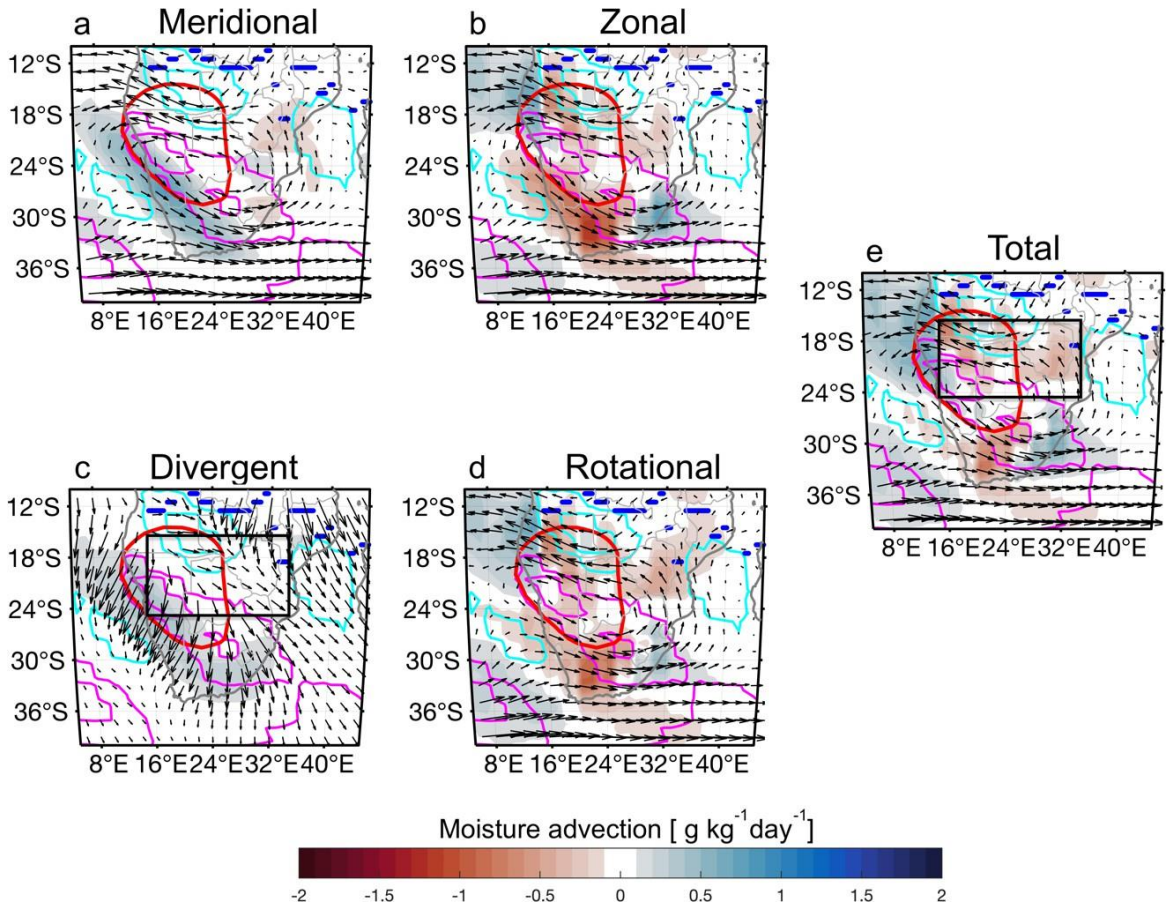

Figure 3.7: Horizontal mid-tropospheric moisture advection (shading, g kg^{-1} day^{-1}) and fluxes (arrows, m/s) over southern Africa for the (a) meridional advection, (b) zonal advection, (c) divergent wind advection ($-\vec{v}_d . \nabla q$), (d) rotational wind advection ($-\vec{v}_r . \nabla q$) and (e) total advection ($-\vec{v} . \nabla q$). Cyan and magenta contours represent the positive and negative relative vorticity at 2.5 and 5 s^{-1} intervals with the first value being -2.5 and 10 s^{-1} respectively. The red isoline shows the Kalahari thermal low (2920-m), while the blue bold contour is the position of the rainfall maximum. The positive and negative values of the horizontal moisture advection indicate the moist and dry air mass.

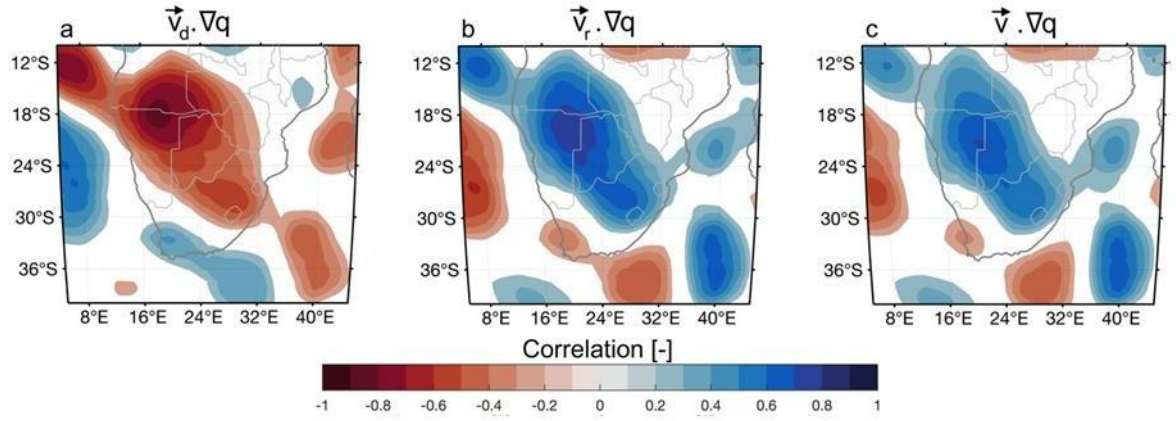

Figure 3.8: Correlation between the horizontal mid-tropospheric moisture advection area-averaged between 15º–30ºE, 15º–25ºS (see black box in Figure 3.7e) and the vertical velocity ($\Delta\omega = \omega_{850} - \omega_{500}$) for (a) $\vec{v}_d.\nabla q$; (b), $\vec{v}_r.\nabla q$ and (c) $\vec{v}.\nabla q$. Only significant correlation at $p < 0.05$ is shown.

3.2.4.2. Contribution of the SMC to the regional moisture budget

The net rainfall distribution over southern Africa needs to satisfy the moisture budget (see equation 3.1). At seasonal timescale, the left side of the equation (3.1) – which is the vertically integrated moisture flux divergence (VIMFD) – can be further expanded as:

$$\text{VIMFD} = < q\nabla.\vec{v} > + < \vec{v}.\nabla q > + < \partial_p(q\omega) > \quad (3.9)$$

where $< q\nabla.\vec{v} >$, $< \vec{v}.\nabla q >$ and $< \partial_p(q\omega) >$ represent the vertically integrated horizontal convergence (VIHMD) term, the vertically integrated horizontal advection term (VIHMA), the vertically integrated vertical advection term (VIVA) term respectively.

We computed the VIMFD and its components using the centred finite differences for the rectilinear latitude-longitude grid. The quantification of the moisture budget terms is constrained by reanalysis products, with the coarser temporal resolution introducing substantial uncertainties (Minallah and Steiner, 2021, Mayer et al., 2021). However, this study, we did not observe substantial disagreements between reanalysis products that could potentially affect the results. Thus, we plotted only the moisture budget terms based on NCEP2.

Over southern Africa, the rainfall is higher over the tropical region than the subtropical region (Figure 3.9a). In most subtropical regions, the rainfall is low (< 1 mm/day). Still,

in southern Africa's eastern escarpment, rainfall is higher than 3 mm/day with limited evaporation (Figure 3.9b).

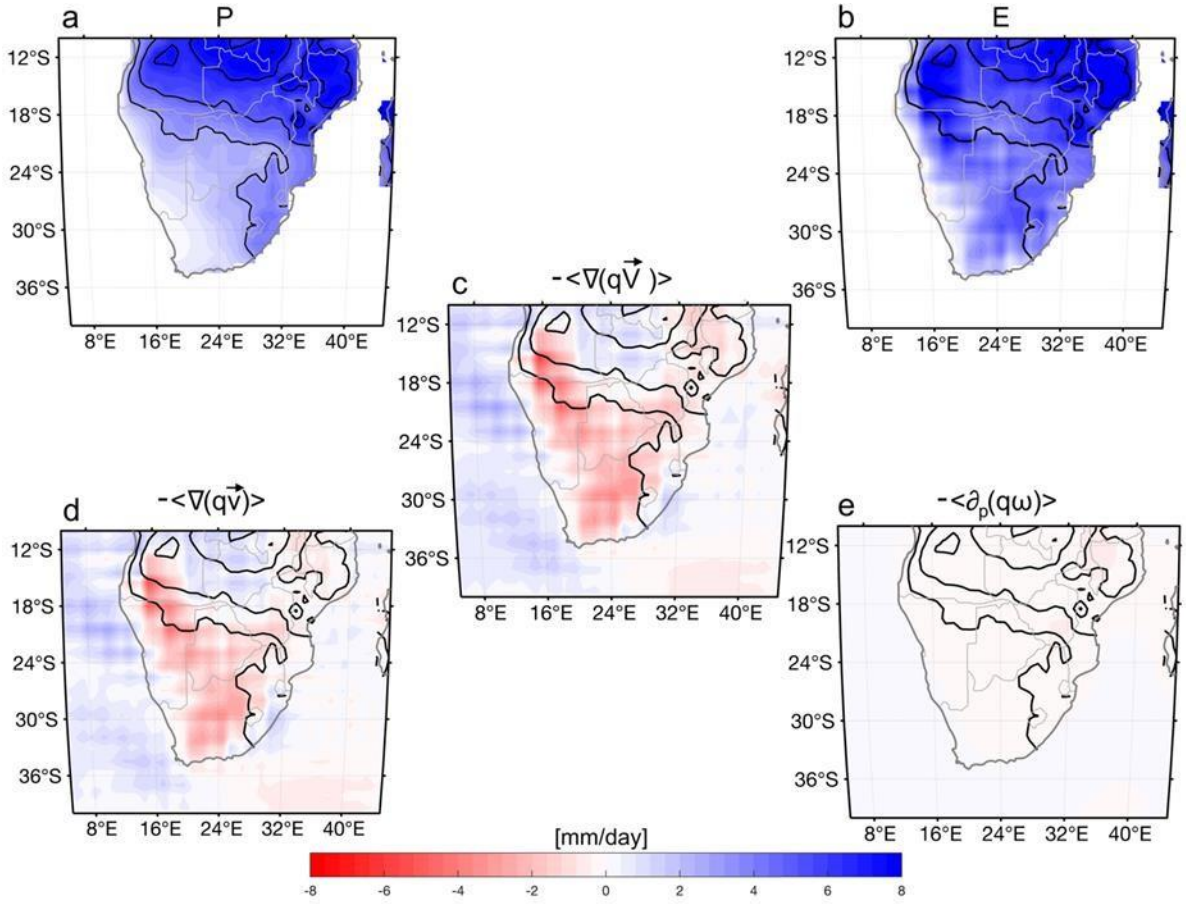

Figure 3.9: Moisture budget over southern African in summer (DJF). (a) Precipitation (mm/day). (b) Evaporation (mm/day). (c) Vertically integrated moisture flux divergence (VIMFD, $< \nabla.(q\vec{V}) >$), (d) vertically integrated horizontal moisture flux convergence (VIHMD, $< \nabla.(q\vec{v}) >$), and (e) vertically integrated vertical moisture advection (VIVA, $< \partial_p(q\omega) >$). Unit: mm/day. In each panel, the black contours represent the rainfall at 2 mm/day interval, with the first value being 3 mm/day. The negative and positive value of the moisture flux divergence indicate the deficit rainfall or surplus rainfall due to moisture export or import respectively.

This zonal rainfall gradient is due to the presence of the horizontal moisture divergence $-< \nabla(q\vec{v}) >$ (Figure 3.9c–d), which plays a more significant role in the supply of moisture to the region where the KTL is dominant. This is consistent with the results discussed in the previous chapter. The vertical moisture advection $-< \partial_p(q\omega) >$ is negligible and does not contribute to the moisture budget (Figure 3.9e). Further decomposition indicates that moisture convergence (VIHMD) term $< q\nabla.\vec{v} >$ – which

arises from wind divergence – is the major contributor term to the moisture budget (Figure 3.10a). However, the horizontal moisture advection (VIHMA) term $-<\vec{v}.\nabla q>$ dominates at ~15°–25°S and over south Africa respectively (Figure 3.10b).

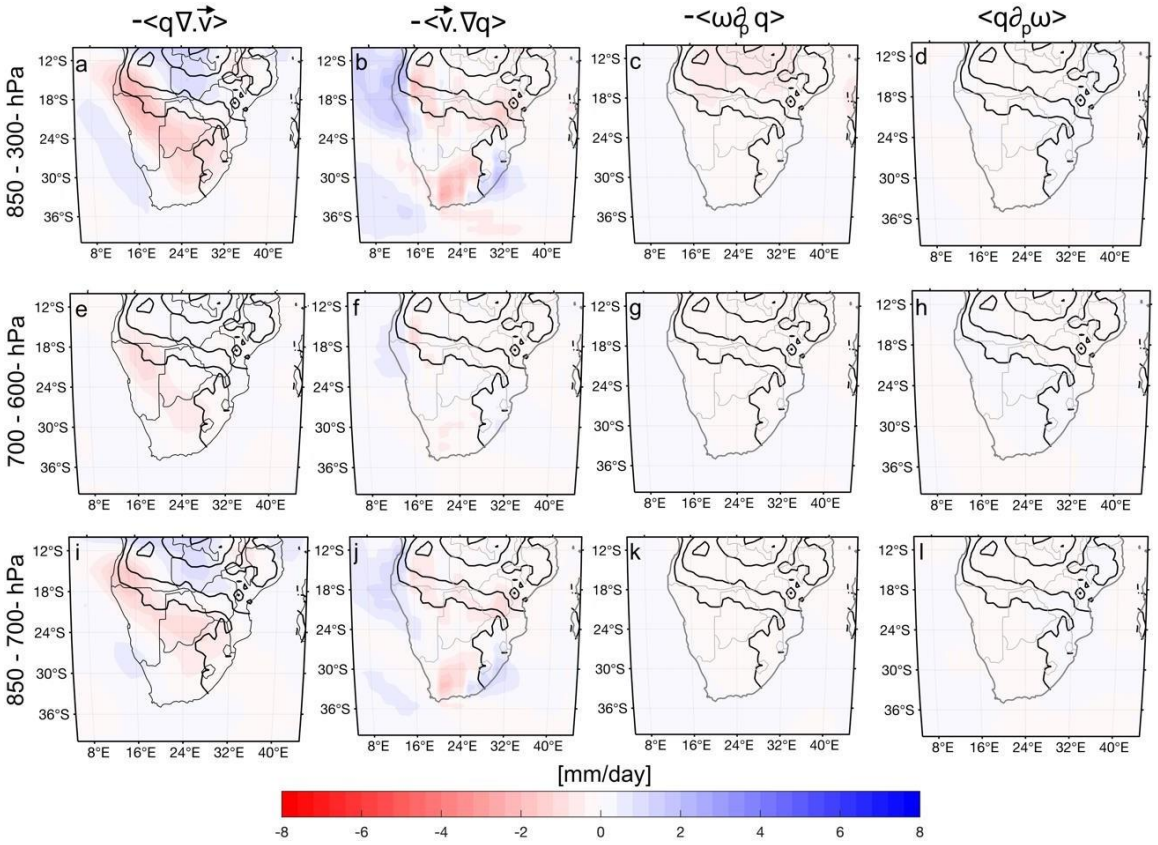

Figure 3.10: Partitioned moisture budget components at different atmospheric layers (top panels) tropospheric column, (middle panels) the mid-troposphere and (bottom panels) the lower troposphere over southern African in summer (DJF). (a, e, i) Moisture convergence $< q\nabla.\vec{v} >$. (b, f, j) moisture advection $-<\vec{v}.\nabla q>$. (c, g, k) $< \omega\partial_p q >$ and (d, h, l) $< q\partial_p\omega >$). Unit: mm/day. In each panel, the black contours represent the rainfall at 2 mm/day interval, with the first value being 3 mm/day.

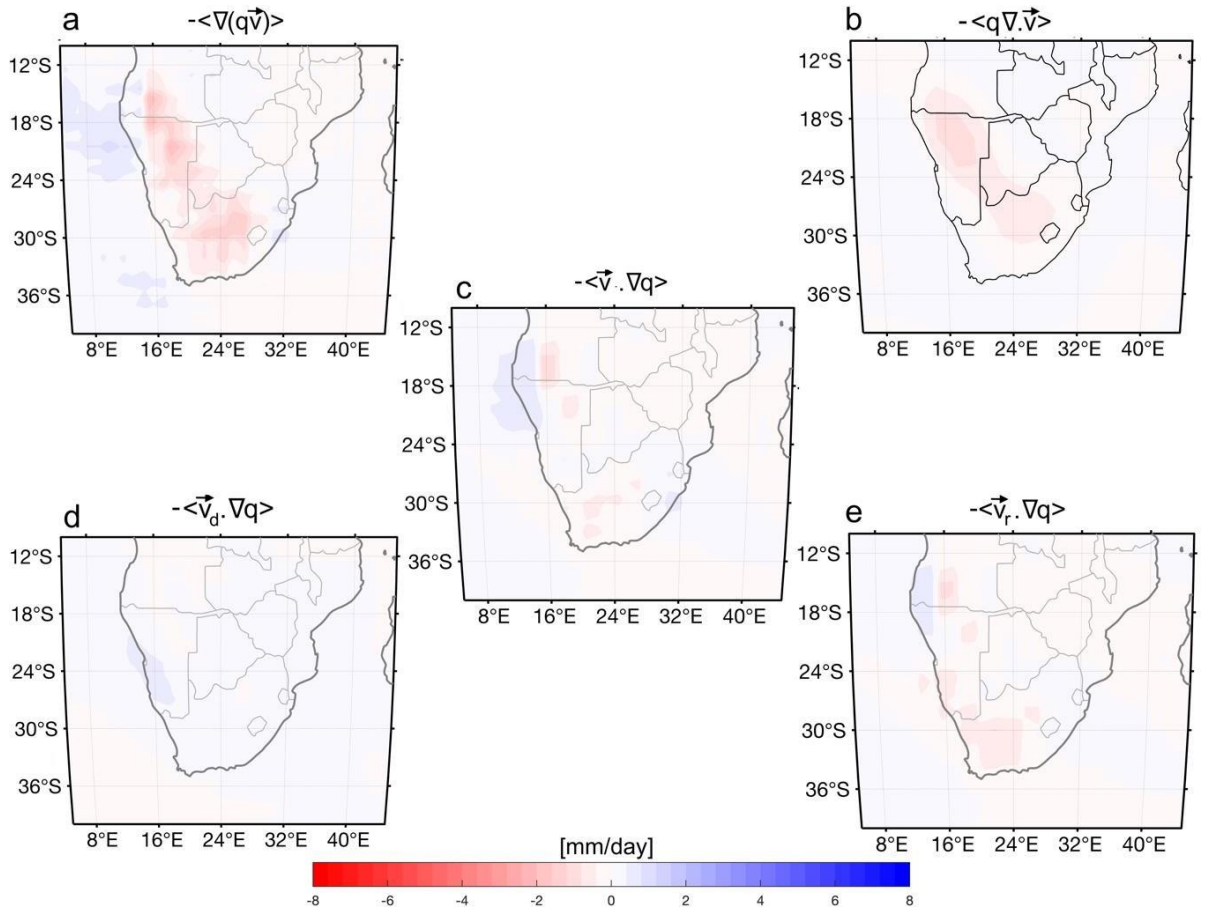

Figure 3.11: Mid-tropospheric (700 – 500 hPa) components of the moisture budget over southern African in summer (DJF). (a) Moisture flux convergence $-<\nabla.(q\vec{v})>$. (b) Moisture convergence $<q\nabla.\vec{v}>$. (c) Moisture advection $-<\vec{v}.\nabla q>$. (d) Moisture advection by the divergent wind $-<\vec{v}_d.\nabla q>$. (e) Moisture advection by the rotational wind $-<\vec{v}_d.\nabla q>$.

To unravel the contribution of the SMC to the regional moisture budget, we plot the contribution of each atmospheric layer to the tropospheric column in Figure 3.10. The bulk (~75%) of the moisture convergence $<q\nabla.\vec{v}>$ occurs at the lower troposphere (i.e., below 700- hPa), as shown in Figure 3.10i. This indicates that the rainfall deficit over the Kalahari region is due to the moisture export associated with the divergent wind that forms the SMC at low levels (Figure 3.3a, e). Meanwhile, the contribution of the low-level moisture advection $<\vec{v}.\nabla q>$ to the moisture budget is less than 10% of the total value, particularly around 15°–25°S (Figure 3.10j). In the mid-tropospheric, the advective terms of the upper branch of the SMC $<\vec{v}_d.\nabla q>$ and the subtropical southerly jet $<\vec{v}_r.\nabla q>$ do not significantly contribute (less than 2%) to the moisture budget (Figure 3.10f). However, the mid-tropospheric moisture convergence

$< q\nabla . \vec{v} >$ related to the upper branch of the SMC represents ~65% of the total value of the moisture budget (Figure 3.10e). Therefore, the results discussed so far identify the moisture convergence $< q\nabla . \vec{v} >$ due to the wind divergence, driven by the KTL, as the important dynamical factor that impacts the rainfall formation in southern Africa. On the other hand, this finding also highlights the limited contribution of the mid-tropospheric advection of dry air $< \vec{v} . \nabla q >$ to the moisture budget. This means that the mechanism that links the mid-tropospheric subtropical southerly jet and the convection is complex and non-linear: the subtropical southerly jet does not directly control the precipitating convection. Therefore, the moisture budget over southern Africa can be written as follow:

$$< q\nabla . \vec{v} > /\rho = E - P \qquad (9)$$

3.3. Summary and discussion

The main objectives of this work were: (i) to document the vertical structure of the large-scale circulation over southern Africa and its zonal counterpart; (ii) to investigate how the SMC interact with the convection and finally, (iii) to examine the contribution of the SMC to the moisture budget. The novel results that emerged from this chapter include:

- The Angola low does not control the monsoon-like circulation from the Atlantic Ocean and driven by the divergent wind.
- The vertical structure of the large-scale dynamics over southern Africa confirms the existence of the SMC, but at the descending branch of the southern Hadley cell due to the presence of the KTL (Figure 3.12). Contrary to the literature, the upper branch of the SMC is constituted by weak mid-tropospheric northerly jet (MTNJ), driven by the divergent wind rather than the STSJ (Figure 3.12).
- There is an existence of a zonal counterclockwise overturning circulation over subtropical southern Africa landmass, with its ascending branch occurring over KTL (Fig. 3.12). Its upper (return) branch is westward, while its subsiding branch occurs over western Atlantic Ocean (Fig. 3.12). Its low-level (closing) branch is constituted by the monsoon-like circulation flowing from Atlantic Ocean towards the landmass (Fig. 3.12).

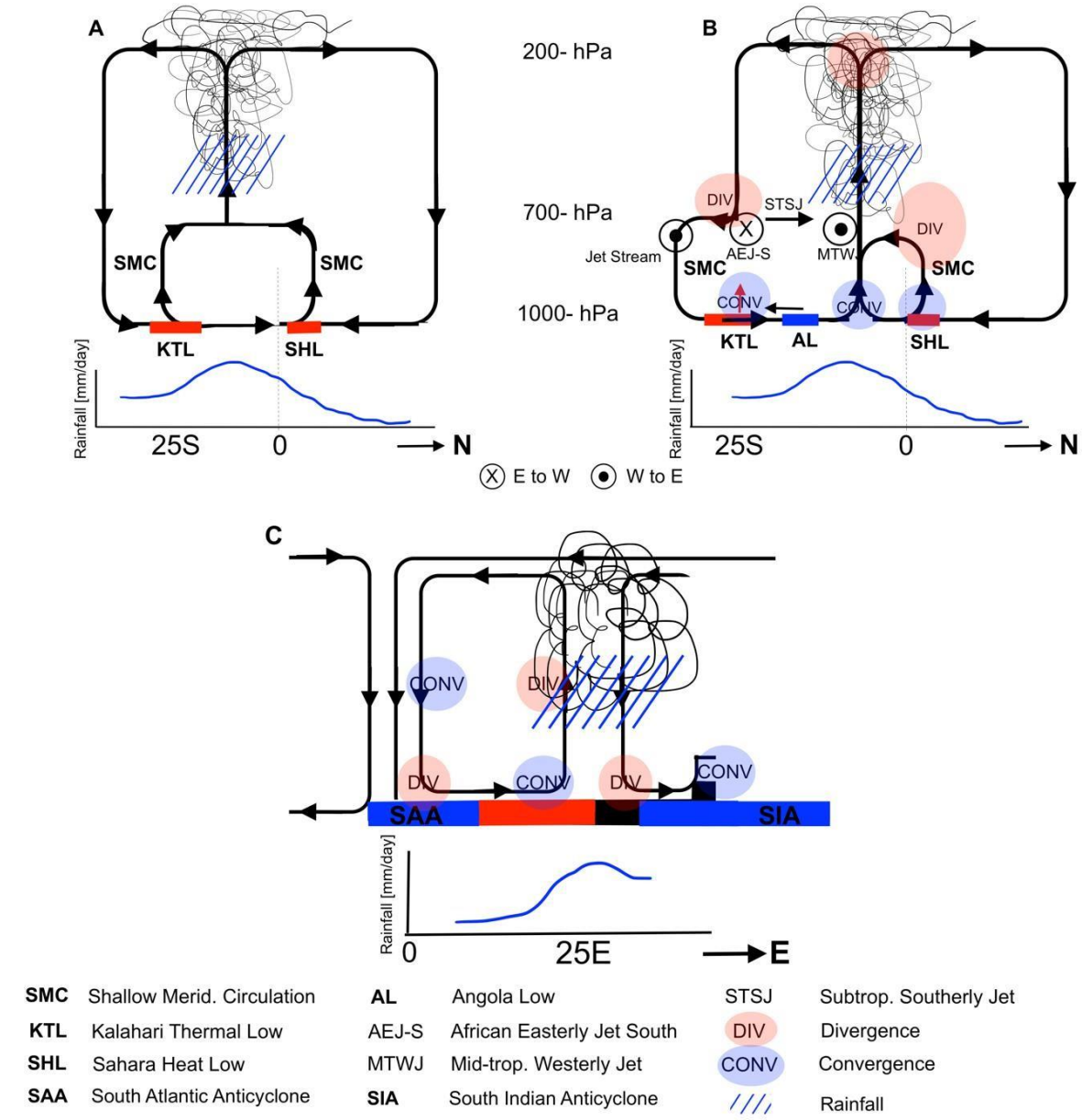

Figure 3.12: Schematic diagram of the vertical structure of the meridional (Hadley) circulation over southern Africa as presented in (A) previous works (Nie et al., 2010; Zhai and Boos 2017) and (B) this study respectively. (C) Vertical structure of the zonal (Walker-like) circulation over subtropical southern Africa.

- The mid-tropospheric dry air is transported westward toward the Atlantic Ocean by the AEJ-S rather than northward toward the convective region by the STSJ as widely reported in the literature.
- The zonal mid-tropospheric outflow related to the anticyclonic circulation, driven by the KTL, is the main conveyor belt over southern Africa. Thus, by its nature

(rotational), it does not contribute to the building-up the moisture convergence, conducive to convection.

- The major rainfall deficit ($-< q\nabla.\vec{v} > \leq 0$) over southern Africa is due to the moisture export related to the SMC. A minor contribution to the moisture budget (i.e., ~15% of the total value) is provided by moisture advection $< \vec{v}.\nabla q >$ associated with the mid-tropospheric wind (AEJ-S and STSJ). As consequence, the STSJ does not directly control the precipitating convection, as reported in the literature.
- The STSJ and the MTNJ have opposing relationships with the convection. The STSJ can initiate a vertical ascent, which later enhances the rainfall. However, the MTNJ builds-up the moisture convergence, which suppresses the convection that reduces rainfall.

4. Process-based Evaluation of the Influence of the Kalahari thermal low and its Induced Dynamics on Regional Precipitation in some CMIP6 GCMs over Southern Africa

4.2. Introduction

Biasutti et al. (2009) used CMIP3 models to analyse the role of Sahara Low on the rainfall variability and change over the Sahelian region. Various models showed that variations in Sahara Heat Low can be both a cause and not just a consequence of rainfall variability on the Sahel region. These results probed for a better understanding of the sources of model discrepancies, which will enable accurate assessment of mechanisms influencing rainfall over a region. Over southern Africa, Dunning et al. (2018) also showed that the future projected changes in KTL may delay the rainfall onset over the subcontinent. Due to expected projected increasing temperatures influenced by human-induced climate change, the KTL is expected to strengthen, and so does its impact on the regional rainfall. Several studies have already indicated a strengthened KTL in recent decades due to increased surface warming trends over the Kalahari region. The circulation associated with the KTL is likely to strengthen in response to increases greenhouse gas emissions in two separated regional model simulations as reported by Engelbrecht et al. (2009) and Cook and Vizy (2013). Therefore, it is very pivotal to investigate the capacity of the recent state -of-the- art climate models to accurately represent the KTL, its driving mechanisms and its impact on the southern Africa hydroclimate during summer.

In this chapter, we use the understanding we developed of the KTL and its induced dynamics to assess the adequacy of a model from the Coupled Model Intercomparison Project Phase 6 (CMIP6; Eyring et al., 2016) to reproduce relevant processes that control the southern Africa's hydroclimate. In return, the historical simulations should confirm the robustness of our theoretical framework in climate models. While not directly translatable into recommendations for model improvements, our results identify processes that are central for better model simulations and projections of the

monsoonal precipitation over southern Africa.

4.3. Data and Methodology

For this study, we are using the historical simulations of nine global climate models (GCMs) from the Coupled Model Intercomparison Project Phase 6 (CMIP6; (Eyring et al., 2016) and summarised in Table 4.1. As observations, we used for precipitation, the Global Precipitation Climatology Centre version 7 (GPCC v7) dataset (Schneider et al., 2014), while for SST, the National Oceanic and Atmospheric Administration's (NOAA) Extended Reconstruction Sea Surface Temperature version 5 (ERSST v5) (Huang et al., 2017) dataset. We also used the ERA5 as a proxy of the tropospheric observations. The variables used are the horizontal wind with its zonal (u), meridional (v) components; the vertical velocity (ω), geopotential height (z), and specific humidity (q), which was obtained from the relative humidity. Note that FIO, GFDL and MCM-UA do not have the vertical velocity component. All the selected variables have been interpolated to a 0.5°×0.5° grid. The time span of all the variables is from DJF 1979/80 to DJF 2013/14.

Table 4.1: A list of CMIP6 models used in this Chapter.

Number	Model Name	Modelling group	Country	Resolution (Lat x Lon)	Vertical levels	References
1	ACCESS-ESM1-5	Australian Community Climate and Earth System Simulator	Australia	192 x144 (192 x 80)	50	(Law et al., 2017) (Ziehn et al., 2017)
2	CanESM5	Canadian Centre for Climate Modelling and Analysis, Environment and Climate Change	Canada	128 x 64 (360 x 300)	49	(Swart et al., 2019)
3	CMCC-ESM2	Euro-Mediterranean Centre on Climate Change (CMCC)	Italy	288 x 192 (362 x 292)	30	(Lovato et al., 2022)
4	CNRM – ESM2 -1	National Centre for Meteorological Research (CNRM)	France	256 x 128 (362 x 294)	91	(Séférian et al., 2019)
5	FIO-ESM-2-0	The first Institute of Oceanography	China	288 x 192 (320 x 384)	30	(Bao et al., 2020)
6	GFDL – ESM4	Geophysical Fluid Dynamics Laboratory Earth System Model	USA	288 x 180 (360 x 180)	75	(Dunne et al., 2020)
7	IPSL – CM6A - LR	Institute of Pierre- Simon Laplace	France	144 x 143 (326 x 332)	79	(Boucher et al., 2018); (Boucher et al., 2020)
8	MRI – ESM2-0	Meteorological Research Institute	Japan	320 x 160 (360 x 180)	48 -80	(Yukimoto et al., 2019)
9	MCM- UA – 1- 0	University of Arizona	USA	96 x 60 (192 x 80)	18	(Stouffer, 2019)

The process-based evaluation assesses the plausibility of climate change projections (James et al., 2015, Howard and Washington, 2020). The procedure consists of, firstly identifying physical processes responsible for the observed climatology and, secondly,

assessing whether models can reproduce them in historical simulations. The main objective of this chapter is to evaluate the capability of the CMIP6 GCMs to represent the KTL, its induced dynamics, and the driving mechanisms of KTL on the regional moisture budget that we developed using observational datasets and highlighted in previous chapters.

4.4. Results

4.4.1. Link between the Botswana high and the Angola tropical Low and the Kalahari Thermal low.

In Figure 4.1, we represented the geopotential thickness (Δz) between 850 and 600 – hPa and the atmospheric circulation in ERA5 and multi-model ensemble (MME). In addition to the atmospheric circulation, we plotted its associated relative vorticity, $\zeta = \nabla \times \vec{v}$. It is important to note that, the low-level circulation is dominated by the monsoon-like circulation that originates from Indian ocean and flows across the near-surface low-pressure systems over the southern Africa landmass (Figure 4.1). Over south Atlantic, the high-pressure system drives the low-level circulation (Figure 4.1). Aloft, the anticyclonic circulation is geostrophic and is controlled by the Botswana high (Figure 4.1). Nevertheless, on the northern flank of the KTL but to the south of the intense convective region, the cyclonic circulation occurs to balance the vorticity as a response to the off equatorial diabatic heating related to the KTL (Figure 4.1), indicative of the Angola tropical low (Cretat et al., 2019, Howard and Washington, 2018, Mulenga, 1999, Pascale et al., 2019) This mid-lower circulation is quite well represented in MME, but with lower magnitudes (Figure 4.1). The lower magnitudes represented is due to large inter-modal variability of KTL displayed in Figure 4.3. For, instance, KTL is overestimated by CMCC– ESM2, ACCESS – ESM1-5, CanESM5 and FIO– ESM – 20. While the KTL is underestimated in MRI-ESM2-0 and GFDL -ESM. Interestingly, CNRM- ESM2-1 and IPSL- CM6A – LR does not capture the KTL at all. Furthermore, The MME also reproduces the KTL position quite well but underestimates its magnitude (Figure 4.1). It realistically captures the Angola low (in terms of its strength, position, and extension), as shown by the mid-tropospheric relative vorticity but overestimates its magnitude and extension when using the 850-hPa geopotential height (Figure 4.1). Similarly, due to the underestimation of Botswana, the mid- tropospheric anticyclonic circulation is well represented (Figure

4.1). As consequence, the strengths of both subtropical southerly jet (STSJ) and African easterly jet (AEJ-S) are underestimated (Figure 4.1). However, induced by the KTL, the response of the Botswana high to the Angola low is also well captured at seasonal and interannual timescales (Figure 4.2c–d).

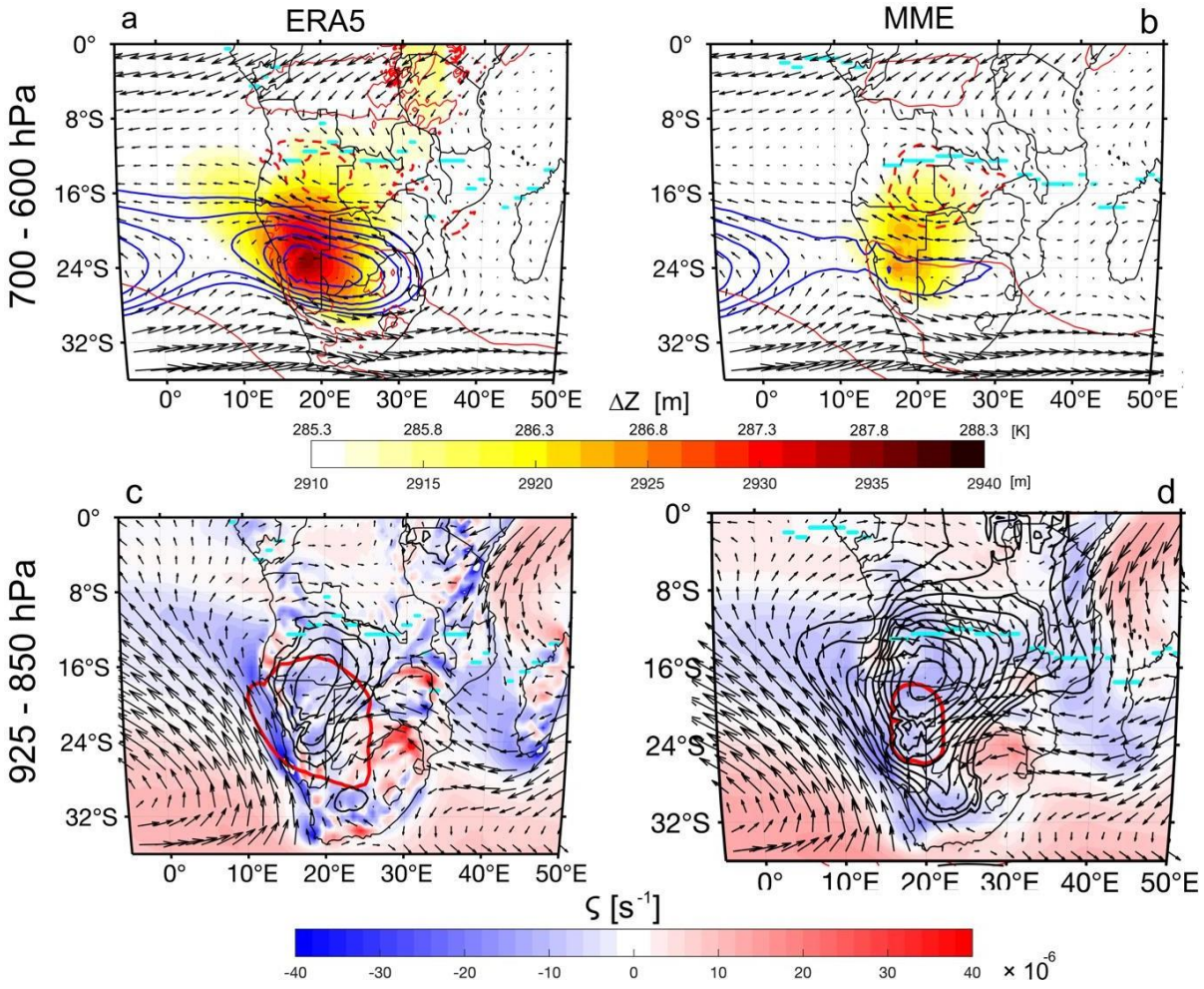

Figure 4.1: (Top panel) The seasonal-mean of the geopotential thickness between 600- and 850- hPa, [Δz (KTL), shading, m], the mid-tropospheric (700–600- hPa) circulation (black arrows, m/s) in summer (DJF). and the 600- hPa geopotential height (blue contours, m) respectively. The cyan contours represent the rainfall. We also plot the mid-tropospheric relative vorticity (ζ, red contours, $\times 10^{-5} s^{-1}$), with the solid and dashed contours indicate the anticyclonic (Botswana high) and cyclonic (Angola low) circulation. (Bottom panels) The Kalahari thermal low is represented by the 2920m red isoline. For details see chapter 2.

At seasonal cycle, the relationship is cubic (Figure 4.2a; Table 4.2) but with weak amplitudes; while it is linear in summer (DJF) such that the KTL contributes to the formation of both the Angola tropical low and Botswana high, with these two atmospheric features depending to each other, as suggested by the strength their linear regression (Figure 4.2b and c). A strong response of Botswana high to the Angola low is also well captured in some CMIP6 GCMs models (Table 4.3). The distribution of the KTL intensity indicates that four models (CNRM, MCM-UA, IPSL and MME) show a rapid increase at colder values, suggestive of negative biases (Figure 4.2b).

Two GCMs (MRI and GFDL) have relatively same magnitude as ERA5 (observations) and four models (FIO, CanESM, CMCC and ACCESS) increase at warmer values (Figure 4.4), favouring positive biases. Likewise, as in Figure 4.3, the magnitude of CNRM, MCM - UA and access are lower than the threshold at 2920 (Figure 4.4) and they all fall below 2900. This explains why they could not capture the KTL within the given minimum value of 2910 (highlighted in the colour bar of Appendix A). Furthermore, there is also a high response of the Botswana high and Angola low to the KTL in all GCMs, except in the UA model in which the Angola tropical low responds weakly to the KTL (Figure 4.5). The GFDL shows the highest model response between the Angola Low and Botswana High to the KTL. All this means that a cold KTL deepens the Angola tropical low and reduces the Botswana high and vice versa (Figure 4.5). More interestingly, there are approximately 65% cases when the above - normal rainfall condition will occur over southern Africa when the KTL is colder (Figure 4.5)

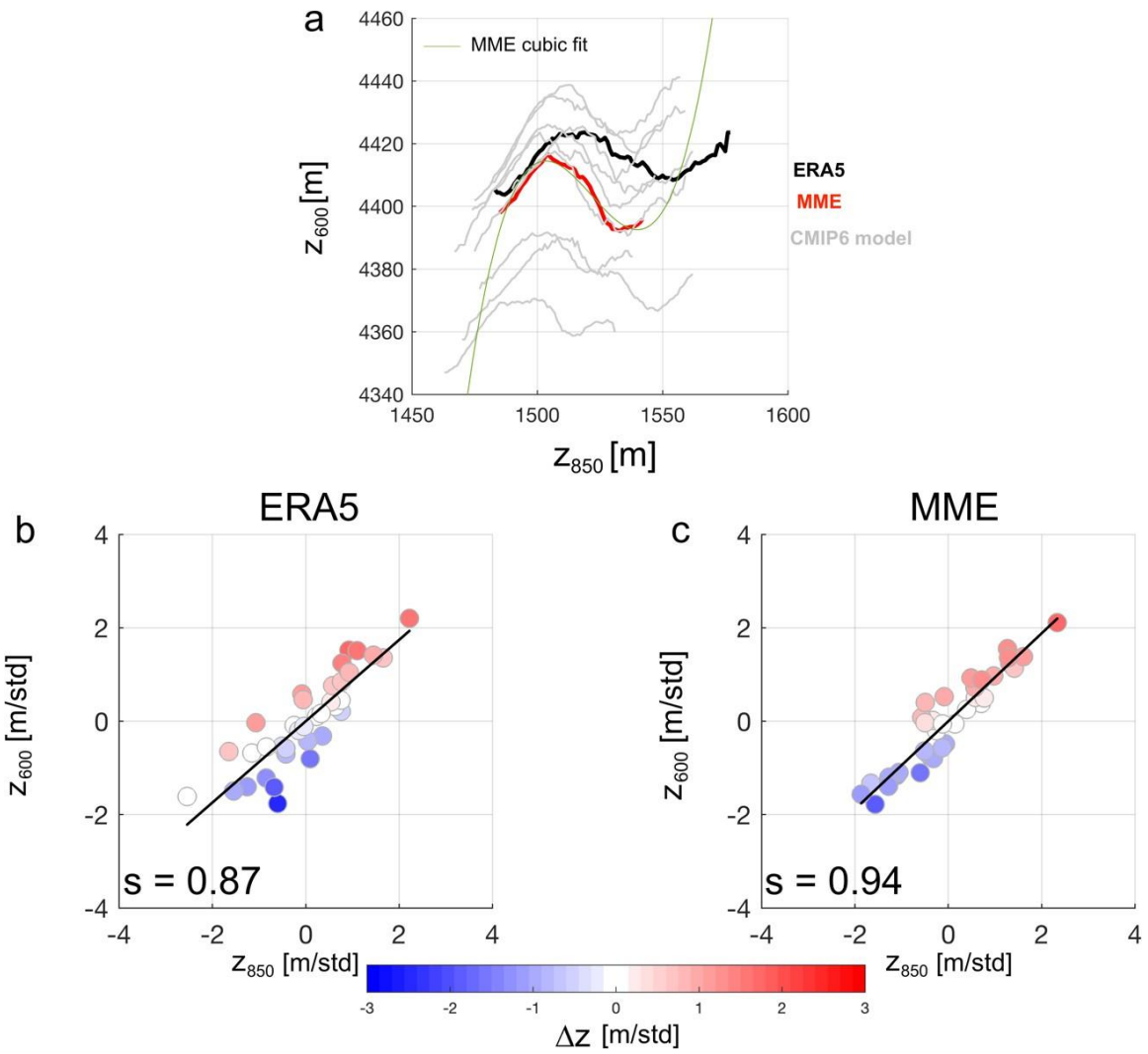

Figure 4.2: (a) Variation of the geopotential height index at 600- hPa (z_{600}) as function of the geopotential height at 850- hPa (z_{850}) area-averaged between 10º–25ºE, 15º–30ºS and 8º–25ºE, 10º–25ºS respectively (see black boxes in Fig. 7a; e) for the study period (January 1979 to December 2014) for ERA5 (black), MME (red) and CMIP6 model (grey) respectively. The cubic fit curve for MME is also shown. (b) Relationship between z_{850} and z_{600}.The shading colour is the Kalahari low index. In (a) and (b) the value of the slope coefficient of the linear regression betweenz_{850} and z_{600} is shown in the left bottom corner.

Table 4.2: Coefficients of determination for the cubit (R^2) fit between the Botswana (z_{600}) high to the Angola low (z_{850}) for ERA5 and MME. z_{600} and z_{850} area-averaged between 10º–25ºE; 15º–30ºS and 8º–25ºE, 10º–25ºS (see black boxes in Figure 4.1) for all months from January 1982 to December 2020. The constants a, b, c d are coefficients of the cubic equation.

	ERA5	**MME**
R^2	0.89	0.93
a ($\times 10^{-3}$ m^{-2})	0.3	0.89
b (m^{-1})	-1.4	-4.1
c ($\times 10^{3}$)	2.1	6.2
d ($\times 10^{6}$ m)	-1.1	-3.1

Table 4.3: Linear response (as slope of the linear fit or regression) of the Botswana (z_{600}) high to the Angola low (z_{850}) in summer (DJF) for ERA5 and some CMIP6 GCMs. z_{600} and z_{850} area-averaged between 10º–25ºE; 15º–30ºS and 8º–25ºE, 10º–25ºS .

Data	**Slope (z_{600}, z_{850})**
ERA5	0.87
MME	0.94
Access	0.87
CanESM	0.88
CMCC	0.92
CNRM	0.83
FIO	0.87
GFDL	0.93
ISPL	0.91
MRI	0.87
UA	0.83

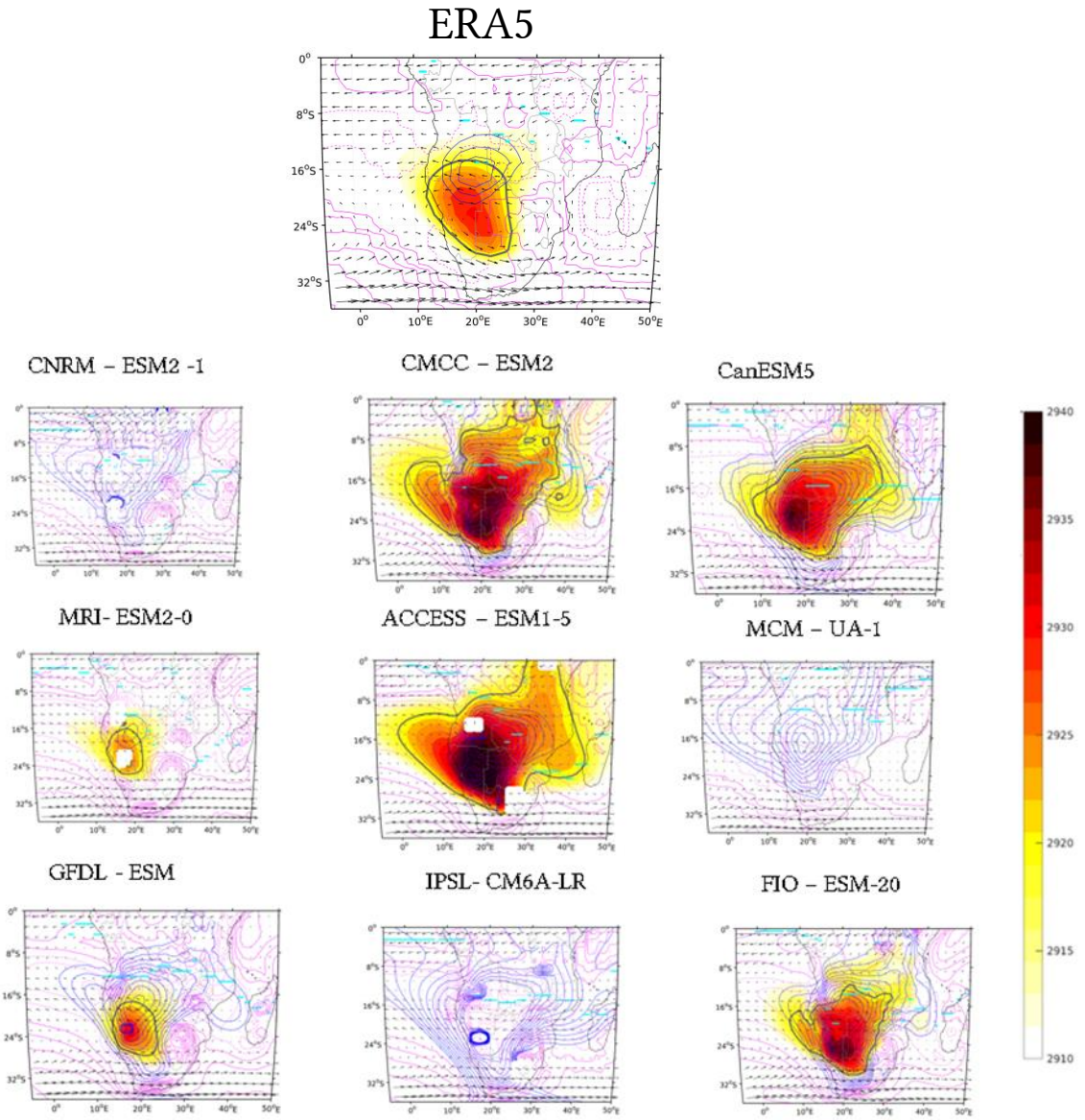

Figure 4.3 : Seasonal-mean atmospheric thickness (Δz) between 600- and 850- hPa, shading, m), the mid-tropospheric (700–600- hPa) circulation (black arrows, m/s) and its associated relative vorticity (red contours, ×10-5 s-1) and the geopotential height at 600- hPa (z600, blue contours, m) in summer for Observation, CNRM-ESM2 -1, CMCC-ESM2, CanESM5,MRI - ESM2- 0, ACCESS- ESM1-5, MCM – UA – 1, GFDL -ESM , IPSL- CM6A-LR and FIO - ESM-20.

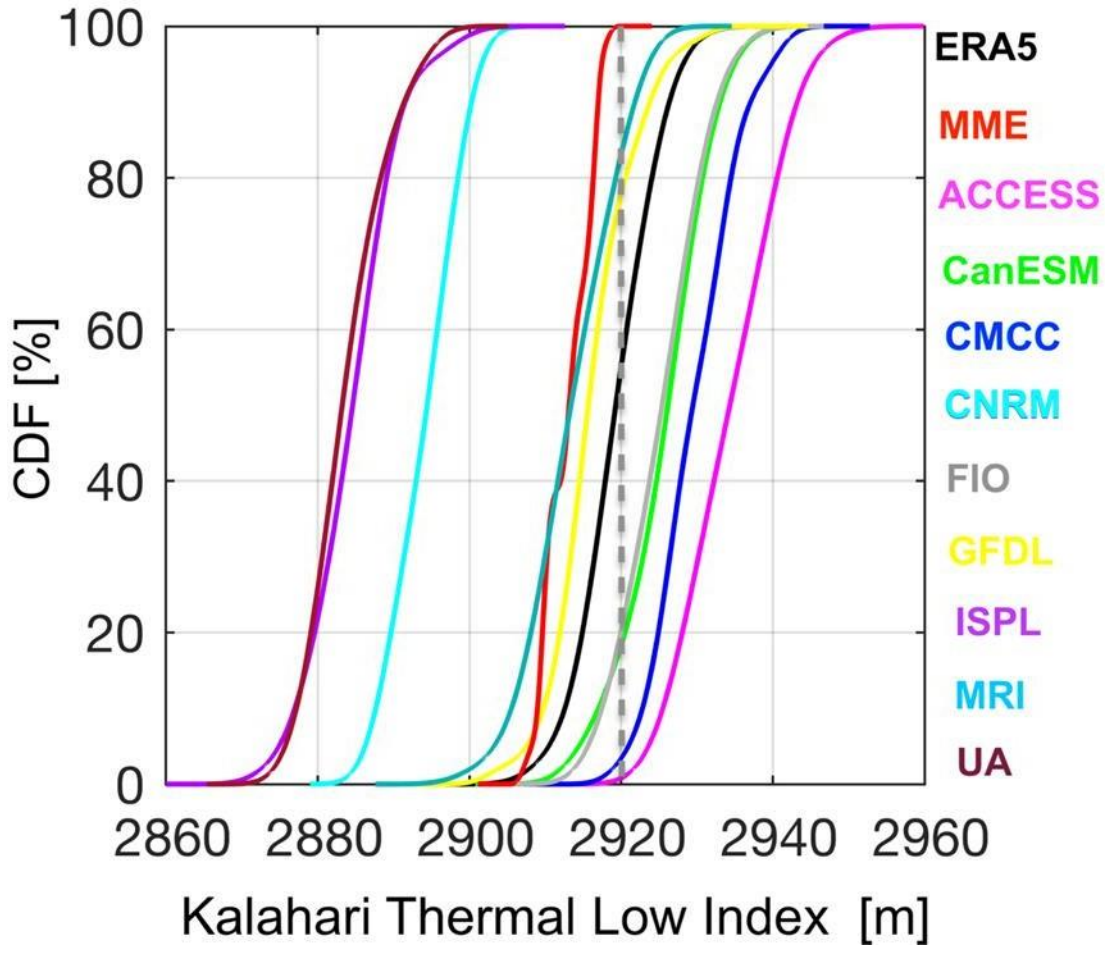

Figure 4.4: Distribution of the Kalahari low in reanalysis products: ERA5 (black); NCEP2 (red); MERRA2 (blue) and JRA55 (green). The vertical dotted gray line marks the ~50%-percentile threshold of the Kalahari low index (10°–25°E, 15°–30°S). Based on equation (2), the unit of the Kalahari low (Δz) index can be m or K.

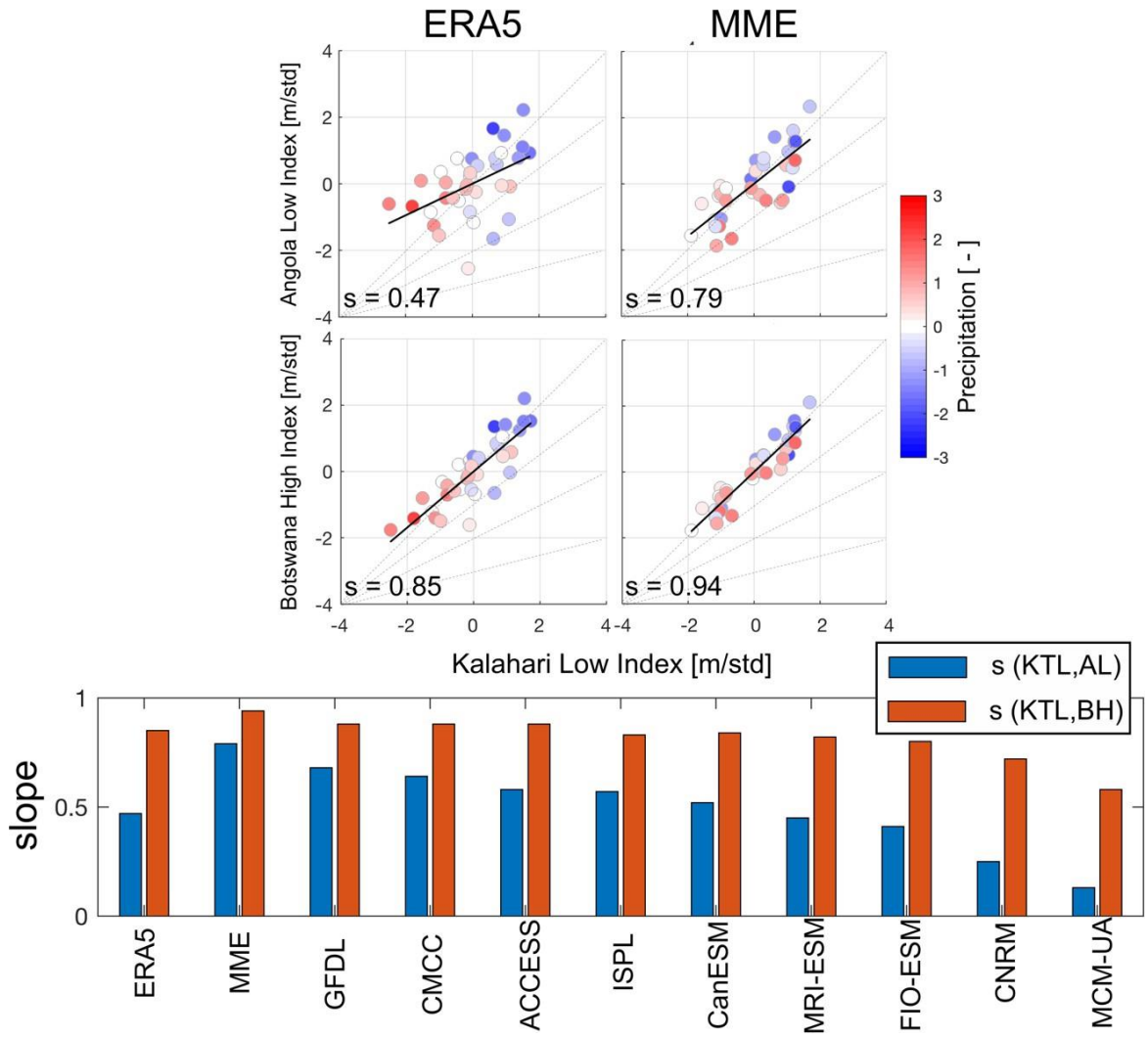

Figure 4.5: (Top panels) Relationship between the Kalahari low index area-averaged between 10º–25ºE, 15º–30ºS and (top panels) the Angola low index (defined as the 850-hPa geopotential height area-averaged between 8º–25ºE, 10º–25ºS) for (left panels) ERA5 and (right panels) MME. (Middle panels) As in top panels, but for the Botswana high (defined as the 600-hPa geopotential height area-averaged between 10º–25ºE, 15º–30ºS). The black straight line is the regression line, with the value of its slope (s) at the left bottom corner. The colour of each dot indicates the corresponding normalized rainfall anomaly area-average over southern Africa. (Bottom panels) Slope coefficient of the linear regression between the Kalahari low and Angola (blue bar) and Botswana High (red bar) for each CMIP6 model. All indexes are normalized by its standard deviation.

4.4.2. Vertical structure of the atmosphere associated with the KTL.

In observations, the vertical structure consists of a recirculation, with a weak

subtropical southerly jet (STSJ) at mid-levels and a weak northerly jet at low levels (Fig, 4.6). This mid- tropospheric STSJ connects the dry subtropical southern Africa to the wet tropical southern Africa (Figure 4.5). The core of the STSJ is located ~600-hPa, 20^{o}S, but at the south of the region of intense convection and seems to be generated by the subsidence induced by the KTL (Figure 4.6).

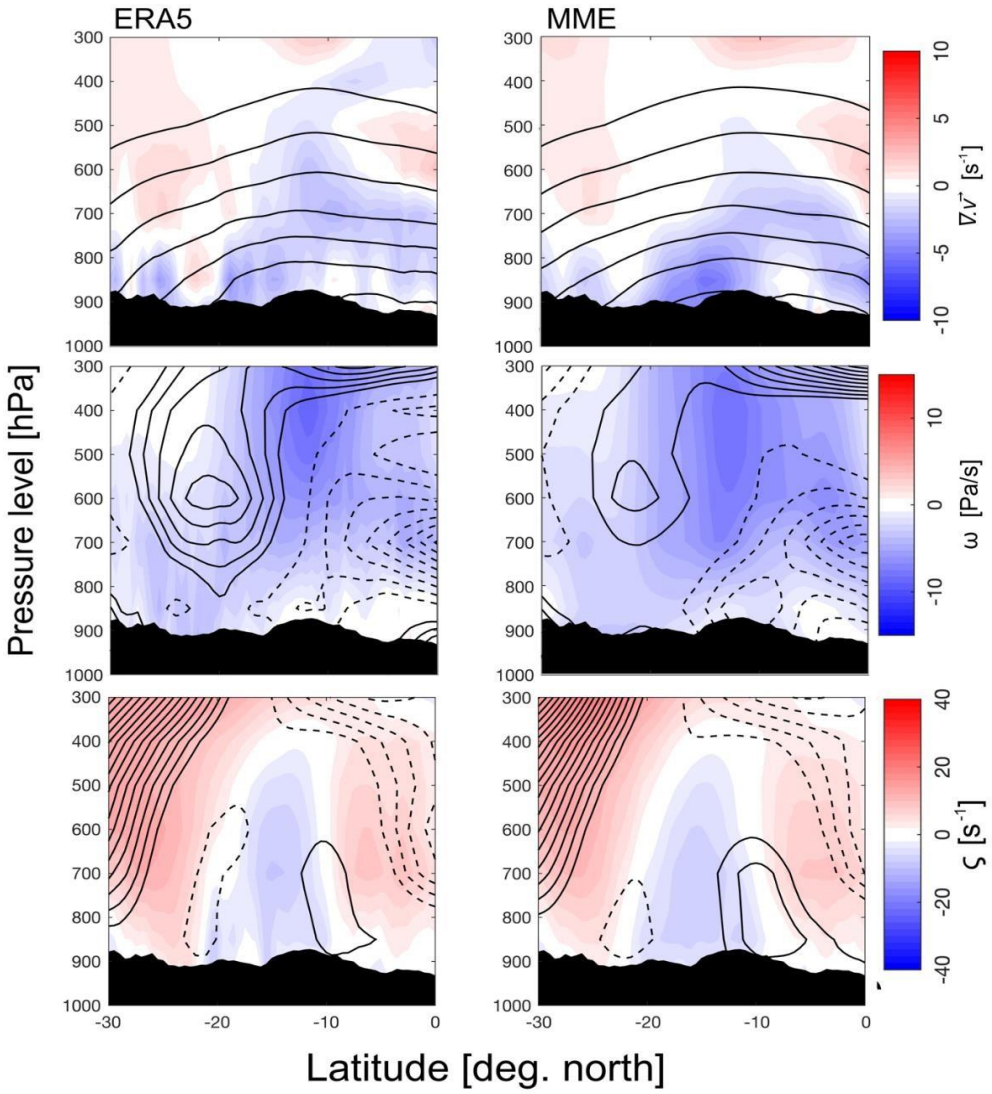

Figure 4.6: Cross-section latitude–pressure of the composite difference between warm and cold phases of KTL for the (a–b) geopotential height (shading, m). The gray contour is for the seasonal-mean geopotential at 1000 m interval. (c–d) wind divergence (shading, s^{-1}) and meridional wind (contours, m/s at 0.25 m/s contour interval). (e–f) vertical velocity (shading, Pa/s) and specific humidity (contours, g/kg at 1 g/kg contour interval). (g–h) relative vorticity (shading, s^{-1}) and zonal wind (contours, m/s at 0.4 m/s contour interval). Only shown $|v| \geq .25$ m/s and $|u| \leq -3$ m/s. The solid and dashed contours represent positive and negative values respectively. In each panel, the vertical black and dotted grey lines mark 15^{o}S and 25^{o}S respectively.

Therefore, the vertical profile of the vertical velocity triggered by the low-level

convergence has a bottom-heavy structure, indicative of the shallow convection (Figure 4.6). However, the deep convection over the tropical southern Africa is driven by the mid-lower northerly divergent flow (Figure 4.6). The underestimation of the STSJ leads to positive bias in MME while equatorward, the negative bias occurs due to stronger mid-lower northerly jet (Figure 4.6). Over the tropical southern Africa, the vertical profile of the vertical velocity associated with the large mid-lower convergence has a top-heavy structure (Figure 4.6). Note that the negative vorticity ($\zeta < 0$) that forms in the mid-lower troposphere favours the setting-up of the cyclonic circulation in its northern flank, indicative of the Angola tropical low (Crétat et al., 2019, Howard and Washington, 2018, Mulenga, 1999, Pascale et al., 2019) and the anti-cyclonic circulation in its southern flank, suggestive of the Botswana high (Figure 4.6). The MME captures quite well this vertical profile of the atmosphere associated with the KTL but underestimates its magnitude; except for the mid-lower westerly jet which is stronger in MME than the observation (Figure 4.6).

4.4.3. Relationship between KTL and regional rainfall

In observations, a strong negative correlation relates the observed southern Africa precipitation and the KTL, while the equatorial central Africa shows a positive correlation (Figure 4.7). This implies that reduced precipitation is caused by warm KTL over southern Africa. Unexpectedly, the MME is unable to represent this relationship, suggesting that the KTL is independent to rainfall variability due to the weakness of their relationship (Figure 4.7). This can also be inferred for ACCESS, GFDL and MRI (Figure 4.7). However, most GCMs do not represent the spatial pattern of the correlation between KTL and the regional rainfall (Figure 4.7). However, depending on the GCM, the KTL could moderately modulate the rainfall variability in different regions of southern Africa (Figure 4.7): the western side in CMCC, FIO and UA; the southern side for CanESM and IPSL; and the eastern side for CNRM .

In the next subsection, we are going to investigate whether the driving mechanisms responsible of the observed correlation between KTL and the regional rainfall is also well reproduced in CMIP6 models.

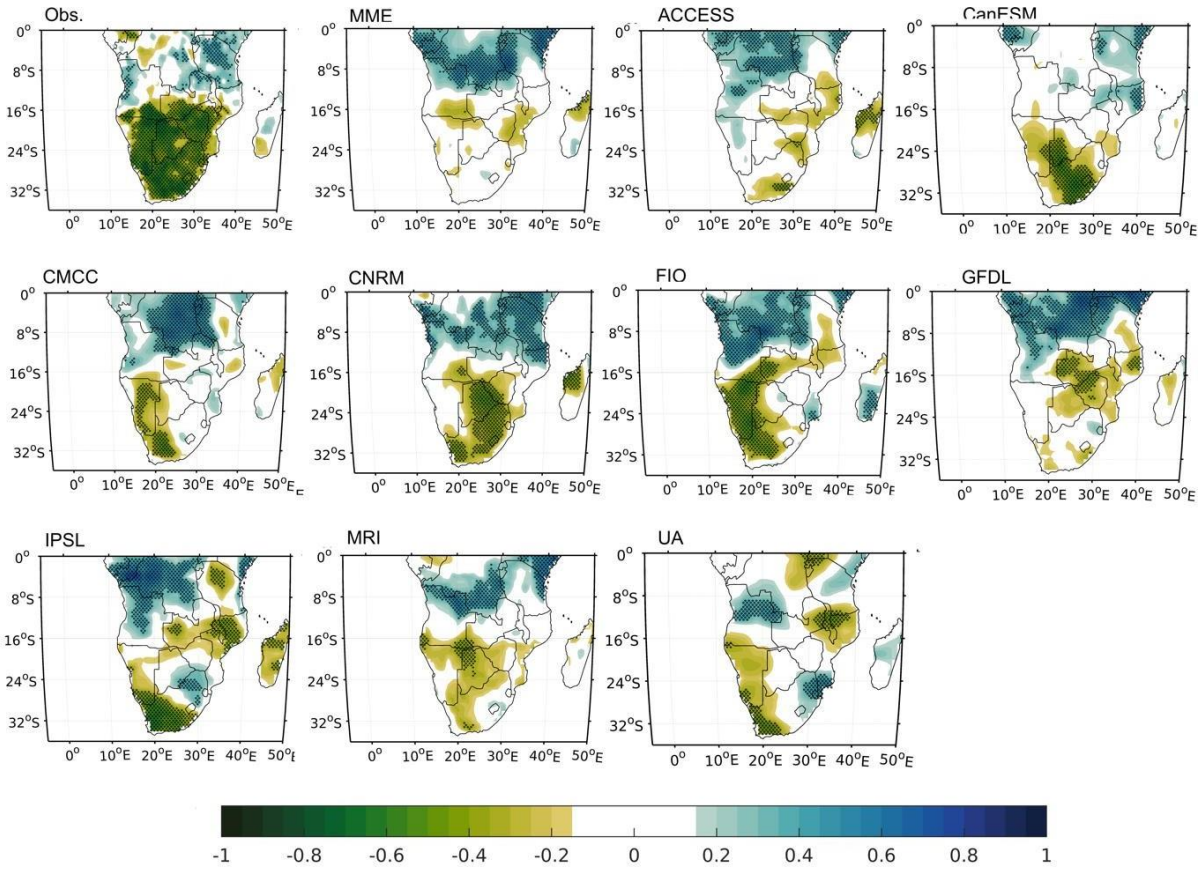

Figure 4.7: Correlation between normalized Kalahari Low index and normalized rainfall anomalies in observation and some CIMP6 GCMs. The stipple indicates correlation that is significant at $p < 0.05$ (t-student test).

4.4.4. Driving mechanisms of the KTL on regional precipitation and moisture transport dynamics

The composite differences between the warm and cold phases of KTL for the geopotential thickness, the relative vorticity, mid-tropospheric circulation, geopotential height at 600 and 850- hPa respectively are shown in Figs. 4.8–4.10. In observation, the anomalous surface warming induces a tropospheric subsidence over southern Africa centred at its core (Figures. 4.8 – 4.10). The surrounding warm air rises but is capped aloft by the subsidence (Figure 4.9). This forces the warm air back to the ground (Figure 4.9). As it sinks, the warm air is compressed and releases more heat, which in turn, loses more moisture through evaporation (Figure 4.9). This further warms the southern Africa region and strengthens the subsidence to form a heat dome that prevents the warm air to escape (Figure 4.9). The MME fails to capture this heat dome formation, with both the anomalous surface warming and its induced anomalous strong subsidence missing (Figure 4.9). All GCMs reproduce quite well the surface warming, although

many of them overestimate its magnitude (Figure 4.8). However, depending on the GCM, the spatial pattern of the anomalous anticyclonic circulation is distorted over the landmass, except CNRM and MRI that appear to well represent both the anomalous surface heating and the mid-tropospheric anomalous vortex quite well (Figure 4.9).

Moreover, the strong subsidence related to the heat dome is associated with a strong anomalous anticyclonic circulation over southern Africa and reinforces both the STSJ and the AEJ-S (Figures. 4.8–4.10). This displaces the anomalous cyclonic circulation equatorward but shrinks it due to balance its vorticity (Figs. 4.8–4.9). As a consequence, the strong anomalous STSJ carries the anomalous dry air further north into the convective region (Figure 4.9), consistent with previous work (Zhai and Boos, 2017).

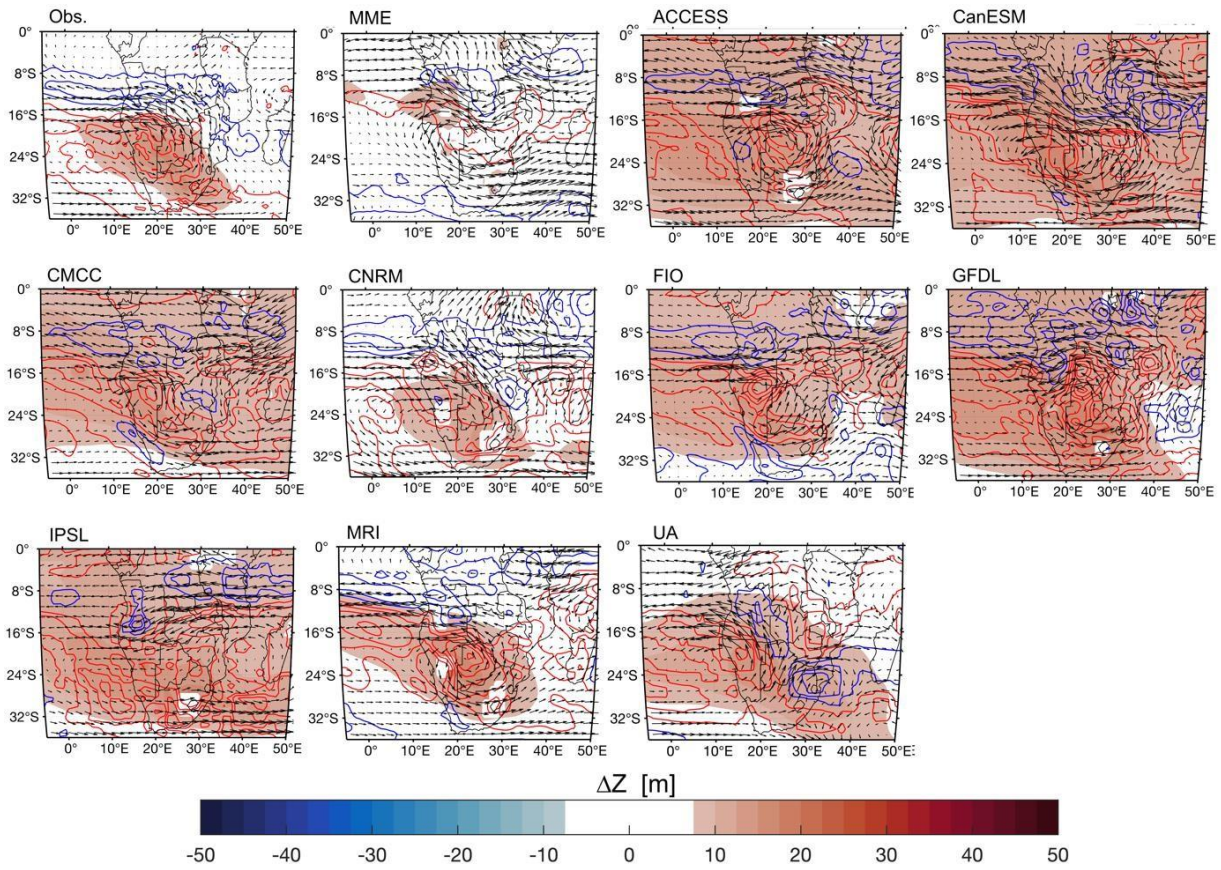

Figure 4.8: Composite difference between the warm and cold phases of KTL for the geopotential thickness (shading, m) and the vertically integrated moisture flux ($< q\vec{v} >$, black arrows, m/s) in the mid-troposphere (700–600- hPa) and its associated relative vorticity. The contour interval for relative vorticity is $0.25\times10^{-6}s^{-1}m$. $<.>$ is the mass-weighted vertical integral (i.e., $\int \frac{dp}{g}$) from 700–600- hPa and g, the gravitational constant.

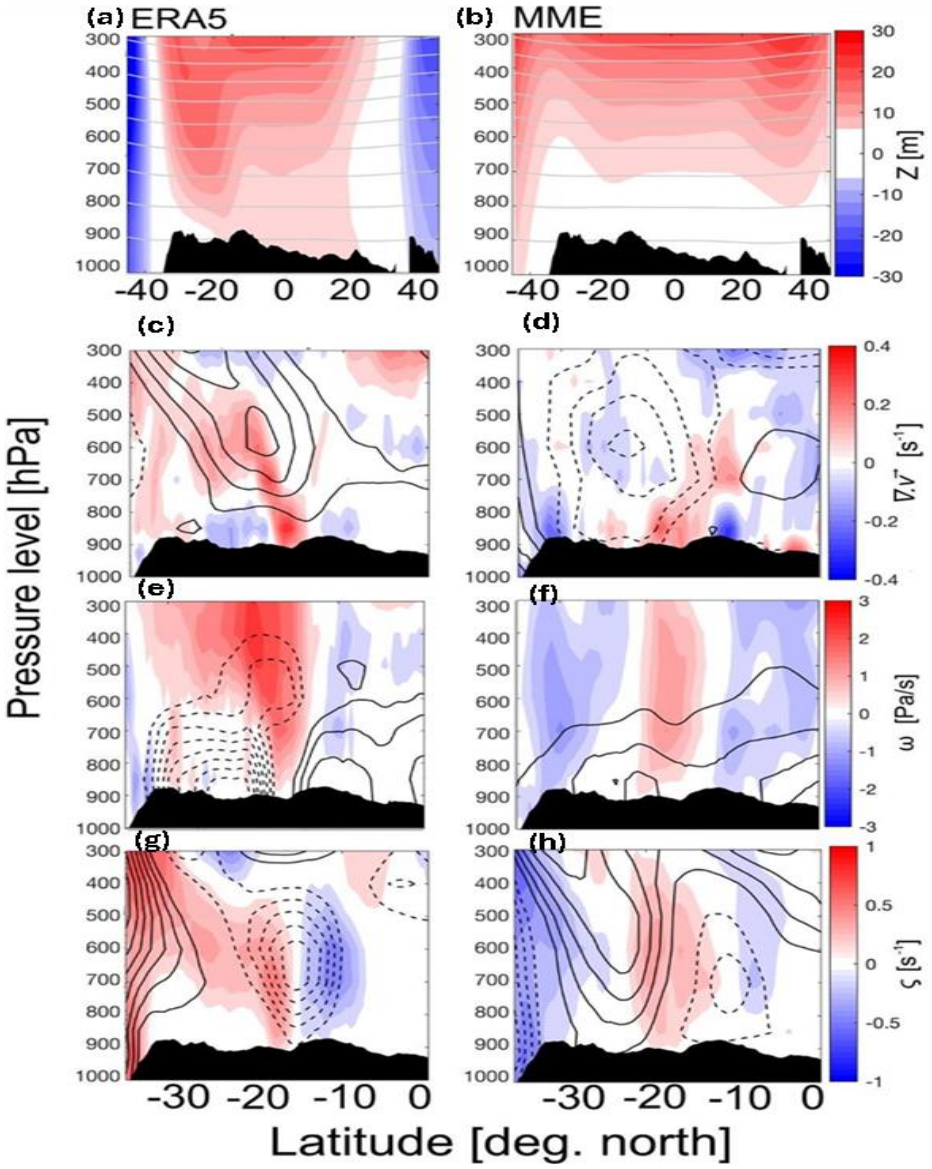

Figure 4.9: Cross-section latitude–pressure of the composite difference between warm and cold phases of KTL for the (a–b) geopotential height (shading, m). The grey contour is for the seasonal-mean geopotential at 1000 m interval. (c–d) wind divergence (shading, s-1) and meridional wind (contours, m/s at 0.25 m/s contour interval). (e–f) vertical velocity (shading, Pa/s) and specific humidity (contours, g/kg at 1 g/kg contour interval). (g–h) relative vorticity (shading, s-1) and zonal wind (contours, m/s at 0.4 m/s contour interval). Only shown |v| ≥ .25 m/s and |u| ≤ −3 m/s. The solid and dashed contours represent positive and negative values respectively. In each panel, the vertical black and dotted grey lines mark 15oS and 25oS respectively.

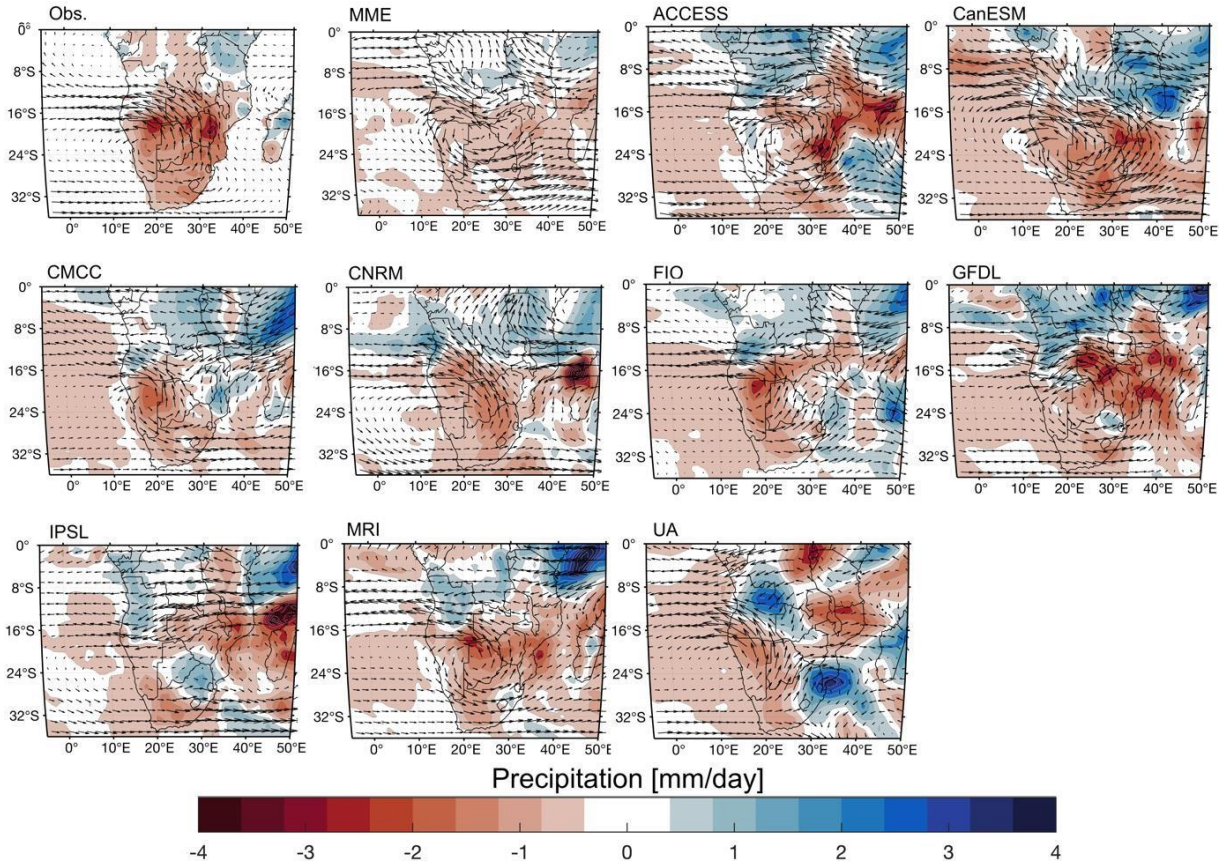

Figure 4.10: The composite difference between the warm and cold phases of KTL for the rainfall (shading, mm/day, the mid-tropospheric circulation (black arrows, m/s) and the vertical velocity ($\Delta\omega$) in the mid-lower troposphere between 850 and 500- hPa. The red and blue contours indicate the positive (subsidence) and convection (negative) respectively.

In MME, the missing strong anomalous subsidence indicates the weakening of the STSJ, suggestive of the southward advection of moist air into the subtropical southern Africa (Figure 4.9). This anomalous northerly jet also favours the development of the anomalous mid-tropospheric convergence in subtropical southern Africa (Figure 4.9). In its northern flank, the wind divergence forms in the tropical southern Africa, indicative of an anomalous subsidence, as shown by the vertical velocity (Figure 4.9). The predominance of the subsidence in the mid-troposphere suppresses the deep convection and reduces the rainfall, with the highest magnitudes between 15° and 25°S (Figure 4.10). All GCMs capture the drought condition quite well, but with different intensities and

spatial patterns (Figure 4.10). The diversity in the rainfall intensity and pattern is governed by the SMC through the horizontal divergence $< \nabla . \vec{v} >$, with the contribution from the mid-tropospheric wind (STSJ and AEJ-S). In the next subsection, we further investigate this assumption.

4.4.5. Mid-tropospheric moisture advection and its contribution to the moisture budget

In the previous chapter, we argued that the mid-tropospheric moisture advection ($\vec{v} . \nabla q$) is carried exclusively by the AEJ-S rather than STSJ as reported in many works (Zhai and Boos, 2017). In addition, the AEJ-S does not control the precipitating convection over southern Africa. Below, Figure 4.12 depicts the mid -tropospheric circulation and its associated moisture advection in ERA5 and MME. For the regional- scale perspective, the AEJ-S advects the mid-troposphere dry air westward towards the Atlantic Ocean in both ERA5 and MME (Figure 4.11). However, due to the weakness of the STSJ, the bulk of the zonal moisture advection ($\vec{v} . \nabla q$) does not directly interact with the convective region which is located equatorward because it is separated by the Angola tropical low, as suggested by the cyclonic circulation (Figure 4.11). Moreover, in MME and all GCMs, the strength of the STSJ is underestimated (Figure 4.11).

Based on chapter 3, the moisture budget over southern Africa should satisfy the following equation at climatological period,

$$E - P \quad = < q \nabla . \vec{v} > / \rho \qquad (4.1)$$

where, P is the rainfall and E is the evaporation, $\vec{v}$ is the horizontal wind; q is the specific humidity and ρ is the density of water. $< A >$ indicates the mass-weighted vertical integral (i.e., $\int A \frac{dp}{g}$).

The GCMs show a widespread value for the rainfall-mean and the evaporation over southern Africa (SA). Except CNRM for SA, but the model overestimated the rainfall, with large positive biases occurring between 15° and 25° S for NSA (Figure 4.12). However, the MME represents the moisture divergence ($< q \nabla . \vec{v} > > 0$) over southern Africa (Figure 4.12), quite well. The rainfall deficit due to moisture divergence $< q \nabla . \vec{v} >$ is overestimated in CanESM. In contrast, a light rainfall surplus is provided by

the moisture convergence in MRI (Figure 4.12). Furthermore, the upper branch of the SMC contributes substantially to the building-up of the moisture convergence in all GCMs, particular over the southern Africa region, where it can range between 50% and 100%, except in MRI (Figure 4.13). However, the contrasted contribution is found in IPSL and MCM-UA in which reduced moisture convergence is produced over north-southern Africa (Figure 4.13).

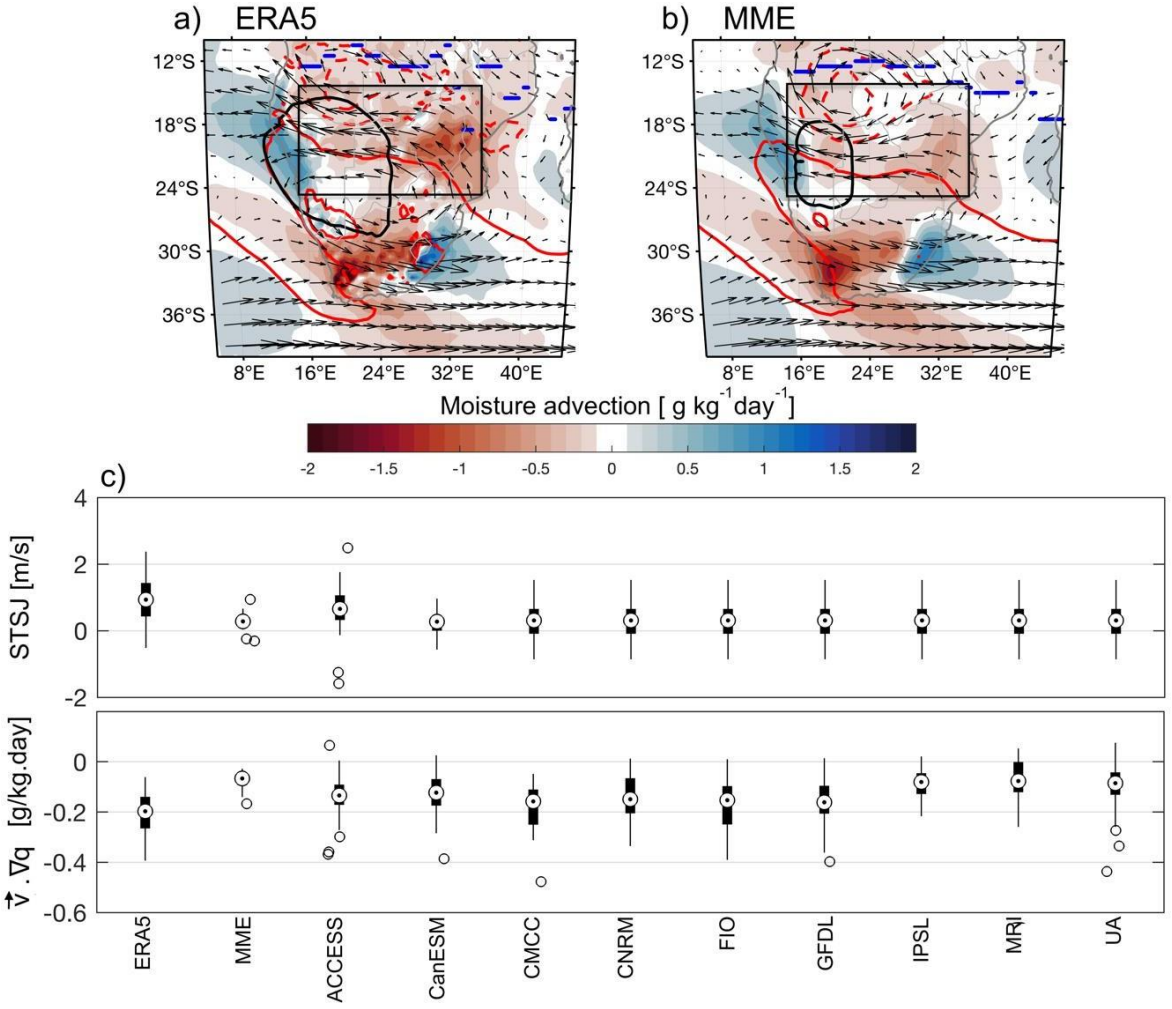

Figure 4.11: (Top panels) Horizontal mid-tropospheric moisture advection (shading, g kg-1 day-1) and fluxes (arrows, m/s) over southern Africa for the (a) meridional advection, (b) zonal advection ($-\vec{v}.\nabla q$) for (a) ERA5 and (b) MME. Red solid and dashed contours represent the positive and negative relative vorticity at 2.5 and 5 s-1 interval with the first value being −2.5 and 10 s-1 respectively. The black isoline shows the Kalahari thermal low (2920-m), while the blue bold contour is the position of the rainfall maximum. The positive and negative values of the horizontal moisture advection indicate the moist and dry air mass. (Middle panels) The subtropical southerly jet (m/s). (Bottom panels) moisture advection (g/kg. day). Both the STSJ and the moisture advection are area-averaged over 15°–35°E, 15°–25°S (black box)

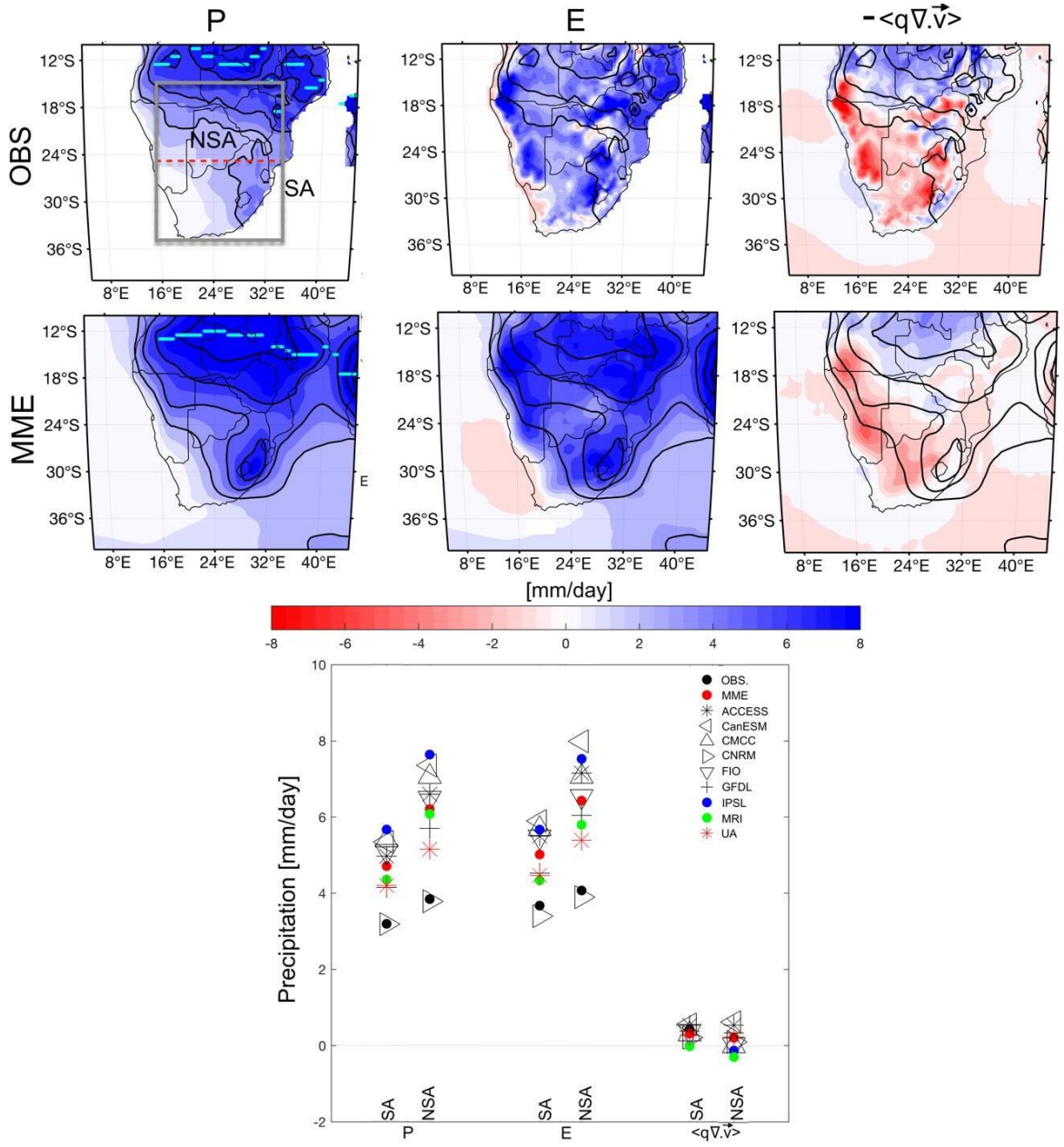

Figure 4.12: Moisture budget components over southern African in summer (DJF). (left panels) Precipitation (P, mm/day); (middle panels) Evaporation (E, mm/day); (right panels) vertically integrated moisture divergence ($< q\nabla.\vec{v} >$ for (top panels) ERA5; (middle panels) MME. Unit: mm/day. In each panel, the black contours represent the rainfall at 2 mm/day interval, with the first value being 3 mm/day. The cyan contour in the left panel indicates the position of rainfall maximum. The negative and positive value of the moisture flux divergence indicate the deficit rainfall or surplus rainfall due to moisture export or import respectively. (Bottom panels) The components of the moisture budget for CMIP6 models over southern Africa (SA) and north-southern Africa (NSA,15°–35°E, 15°–25°S).

Nevertheless, although the contribution is weaker over the southern Africa region as a whole than over its northern part, in MRI, the moisture convergence is built-up. At the same time, it is insignificant over the north-southern Africa (Figure 4.13). Overall, this highlights the crucial role played by the upper branch of the SMC in forming the moisture divergence, which suppresses the deep convection over southern Africa and leads to less rainfall.

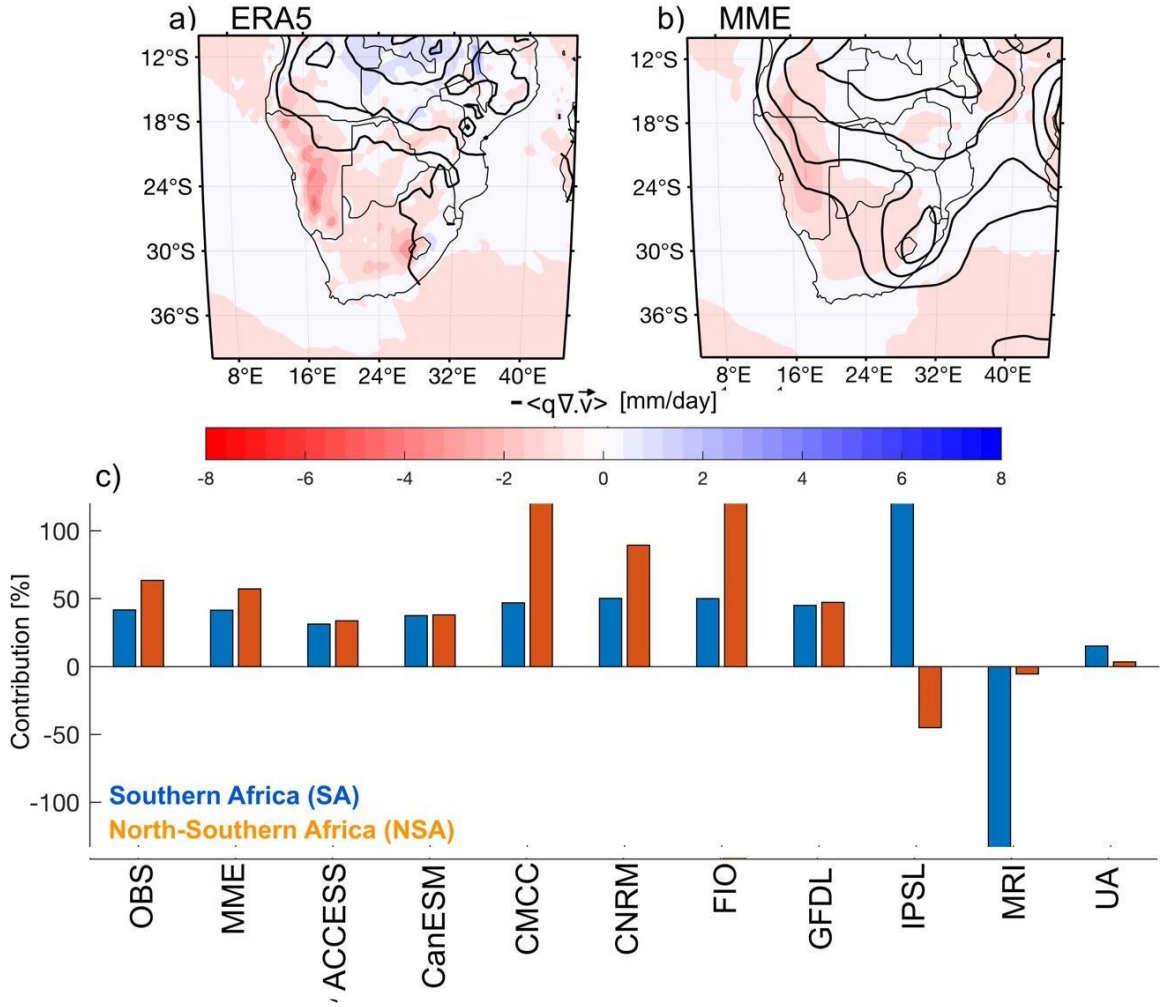

Figure 4.13: (Top panels) Vertically integrated moisture convergence $-<\nabla.(q\vec{v})>$ in the mid-troposphere (700 and 600 - hPa) for (a) ERA5 and (b) MME. (Bottom panels) The contribution of the vertically integrated moisture convergence in the mid-troposphere to the total moisture convergence integrated between 850 and 100- hPa for southern Africa (SA, blue bar) and north-southern Africa (NSA, orange bar).

4.5. Summary and conclusion

CMIP6 simulations of southern Africa have been assessed within the moisture budget and the representation of the KTL and its induced dynamics. We have shown that

CMIP6 failed to realistically capture the spatial structure of the KTL and its intensity, as shown in the MME. However, the capability of KTL to modulate the Angola variability has been found in CMIP6, but its link to the rainfall variability is missed. This may be due to the underestimation of the anomalous surplus surface heating in most of CMIP6 models. This introduces large biases likely to distort the thermally induced anomalous mid-tropospheric anticyclonic circulation over the landmass. The inaccurate representation of the anomalous anticyclonic circulation, with either a missing value or an overestimation of the strength of STSJ, plays a limiting role in the suppression of the deep convection. This why the contribution of the mid-tropospheric circulation in the moisture budget is overestimated. More importantly, the diversity of drought patterns over southern Africa in CMIP6 is due to the horizontal wind divergence, which is controlled by the mid-tropospheric subsidence, as shown by positive vertical velocity anomalies.

Similar analyses should be performed to investigate the future projections change on the regional scale. However, identifying key processes that need to be accurately represented in climate models to capture present-day climate better, as we do in this chapter, is the first step to contribute to efforts towards reducing unprecedented climate change effects through improving historical and future projections over southern Africa and ultimately providing effective guidance to adaptation measures at the regional scale.

5 Conclusion and future works

Many studies investigated the impacts of different drivers on southern Africa's precipitation. Nevertheless, to our knowledge, no study has shown the influence of the Kalahari thermal low (KTL) and its induced atmospheric dynamics on the regional moisture budget over southern Africa by highlighting the physical mechanisms involved. This thesis tried to fill the gap in the literature by addressing the following main concerns:

1. **What is the mean-state structure of the Kalahari Low and the dynamics of its induced SMC during austral summer? What are the physical mechanisms through which the Kalahari low controls the southern African hydroclimate?**

We answered these questions in **Chapter 2**. Firstly, we defined the KTL as the seasonal-mean of the geopotential thickness between 850 and 600 hPa during the core of the summer season (DJF). By doing so, we reconciled the two most important features of the southern African climate – the Angola low and the Botswana high through the Kalahari thermal low. With its oval shape, oriented in the southeast and northwest direction, the KTL is the only heating source in the southern hemisphere, with its core located on the western side of the southern African subcontinent (i.e., the Kalahari region). This spatial structure is robust and semi-annual, forming only from October to March. However, with the underlying Angola low (defined as 850-hPa geopotential height), KTL shows two distinct relationships at different timescales. At the seasonal timescale (annual cycle), the correlation is strongly negative, meaning that the Angola low, driven by the KTL, is also thermal. At the interannual timescale, the reversal of the relationship suggests that the Angola low behaves as a tropical low and forms as a Gill-like response to the diabatic heating related to KTL, as suggested by Mulenga (1999). In addition, the KTL shows a strong negative correlation with southern African rainfall in summer. We found that two physical mechanisms control this teleconnection. During the warm phase of KTL, the heat dome mechanism, in which the moisture divergence is dominant, is conducive to below-normal rainfall conditions over southern Africa. In the cold phase of KTL, the Angola low plays a crucial role in modulating regional precipitation by favouring the moisture convergence

T

h

4

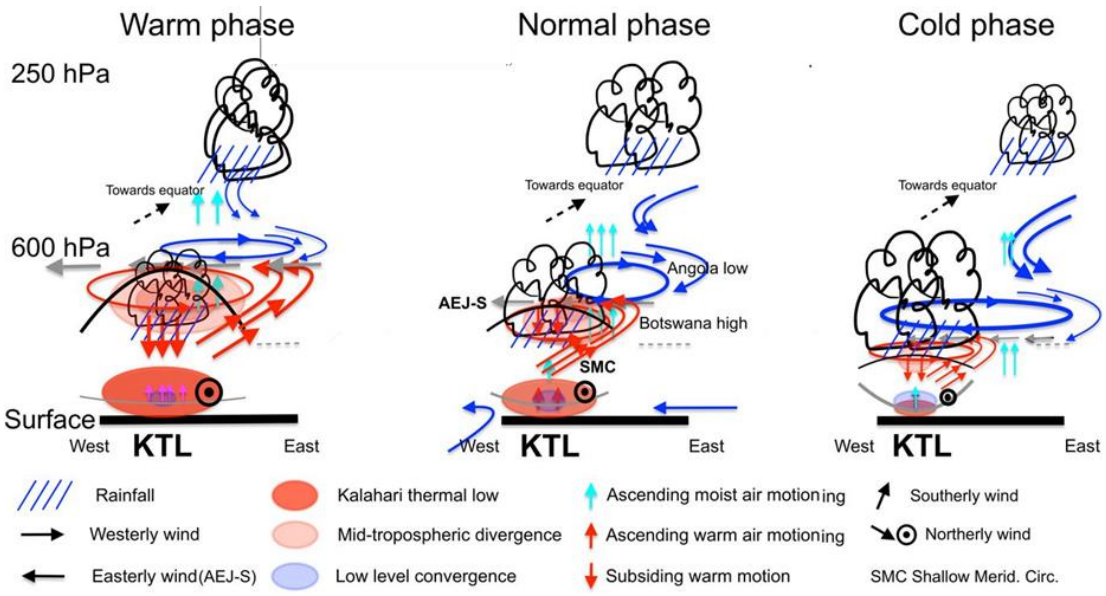

Figure 5.1: Schematic diagram showing the driving mechanisms through which the Kalahari thermal low (KTL) controls the regional precipitation.

2. **How does the thermally driven SMC affect the regional moisture budget over southern Africa?**

Chapter 3 addresses this concern. Using the Helmholtz decomposition, we first partitioned the total circulation into its rotational and divergent components. This helps us to represent the Hadley (meridional) circulation accurately to revisit the vertical structure of the thermally induced circulation. Results show that there is a shallow meridional circulation (SMC) that develops at the descending branch of the southern Hadley cell, with its upper branch flowing southward while its low-level branch is equatorward (see Figure 5.2). Since it is driven by divergent wind, the upper branch of this SMC is crucial in building up the mid-tropospheric moisture divergence responsible for the rainfall deficit over southern Africa. This disagrees with previous works (Nie et al., 2010, Zhai and Boos, 2017), in which the subtropical southerly jet (STSJ) dries up the mid-troposphere by advecting the dry air into the convective

region. This means that the STSJ does not directly control the precipitating convection, as reported in the literature. However, our finding suggests that the mid-tropospheric dry air is predominantly advected zonally by the AEJ-S rather than northward into the convective region by the STSJ. Additionally, the AEJ-S is also the main moist conveyor belt over southern Africa, but it does not contribute to the building-up the mid-tropospheric moisture divergence because it is a rotational flow.

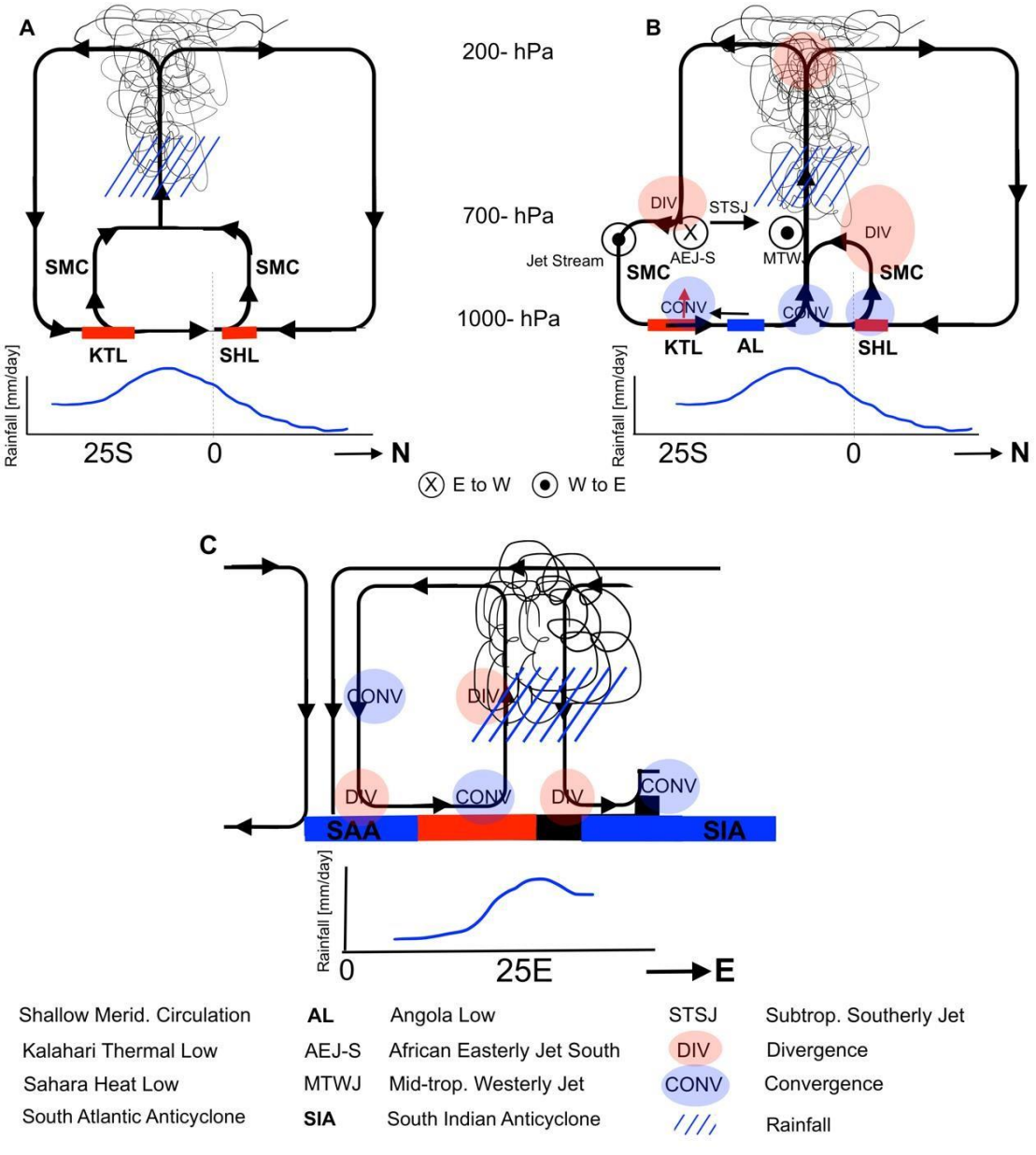

Figure 5.2: Schematic diagram of the vertical structure of the meridional circulation over southern Africa as presented in (A) previous works (Nie et al., 2010; Zhai and Boos 2017; Shekhar and Boos, 2017) and (B) this study respectively. (C) Vertical structure of the Walker-like circulation over subtropical southern Africa.

Furthermore, the major rainfall deficit ($-< q\nabla.\vec{v} > \leq 0$) over southern Africa is due to the moisture export related to the SMC. A minor contribution to the moisture budget is provided by moisture advection $< \vec{v}.\nabla q >$ associated with the mid-tropospheric circulation (i.e., both AEJ-S and STSJ). Finally, we confirmed the existence of a zonal counterclockwise overturning circulation over subtropical southern Africa landmass, with its ascending branch occurring over KTL (Figure 5.2). Its upper (return) branch is westward, while its subsiding branch occurs over western Atlantic Ocean (Figure 5.2). Its low-level (closing) branch is constituted by the monsoon-like circulation flowing from Atlantic Ocean towards the landmass (Figure 5.2). This agrees with Schwendike et al. (2014) but it further completes it by providing a comprehensive picture of its vertical structure. The schematic diagrams describing the vertical structures of the atmospheric circulation over southern Africa are shown in Figure 5.2

3. **How well do some models from the Climate Model Intercomparison Project Six (CMIP6) represent the Kalahari low and its induced circulation as well as its influence on regional precipitation?**

In **Chapter 4**, we used nine of the CMIP6 GCMS to assess the ability of these historical simulations to reproduce the KTL and its induced dynamics over southern Africa. The results suggested that the multi-model ensemble mean (MME) failed to represent the spatial structure and intensity of the KTL. Even so, the CMIP6 models managed to capture the ability of the KTL to modulate the interannual variability of southern Africa rainfall. However, they are unable to reproduce the physical mechanisms responsible for this teleconnection.

More importantly, this dissertation further shed light on how the KTL, through its induced SMC, contributes to drier condition during summer. The sixth assessment report of the IPCC ((IPCC), 2022) stipulated that the mean rainfall in the summer region of southern Africa is projected to decrease by 10–20% with an increase in the number of consecutive dry rainy days under a business-as-usual model. This report also added that more occurrence of heatwaves and drought are going to be experienced with the climate change in southern Africa. This is why this thesis adds a building block to the understanding of current physical mechanisms at the origin of

the current dry climate condition over southern Africa. Further investigations on the driving mechanisms likely to lead to more heatwaves and drought are needed in the context of global warming. Thus, the KTL as one of the key drivers of the southern Africa's climate should be monitored and further investigated to help decisionmakers be more informed about drought and heatwave mitigation measures under a changing climate. Some of the future works may include the evaluation the contribution of KTL on climate extremes over southern Africa such as the droughts and heat waves. Further investigations on the influence of oceanic drivers on KTL have also to be considered.

6 References

(IPCC), I. P. O. C. C. 2022. Africa. In: Climate Change 2022 – Impacts, Adaptation and Vulnerability: Working Group II Contribution to the Sixth Assessment Report of the Intergovernmental Panel on Climate Change.: Cambridge: Cambridge University Pres.

ADEBIYI, A. A. & ZUIDEMA, P. 2016. The role of the southern African easterly jet in modifying the southeast Atlantic aerosol and cloud environments. *Quarterly Journal of the Royal Meteorological Society,* 142**,** 1574-1589.

BAO, Y., SONG, Z. & QIAO, F. 2020. FIO-ESM version 2.0: Model description and evaluation. *Journal of Geophysical Research: Oceans,* 125**,** e2019JC016036.

BARIMALALA, R., BLAMEY, R. C., DESBIOLLES, F. & REASON, C. J. 2020. Variability in the Mozambique Channel trough and impacts on southeast African rainfall. *Journal of Climate,* 33**,** 749-765.

BARIMALALA, R., DESBIOLLES, F., BLAMEY, R. C. & REASON, C. 2018. Madagascar influence on the south Indian Ocean convergence zone, the Mozambique channel trough and southern African rainfall. *Geophysical Research Letters,* 45**,** 11,380-11,389.

BAYR, T., DOMMENGET, D., MARTIN, T. & POWER, S. B. 2014. The eastward shift of the Walker Circulation in response to global warming and its relationship to ENSO variability. *Climate dynamics,* 43**,** 2747-2763.

BEAL, L. M., DE RUIJTER, W. P., BIASTOCH, A. & ZAHN, R. 2011. On the role of the Agulhas system in ocean circulation and climate. *Nature,* 472**,** 429-436.

BEHERA, S. K. & YAMAGATA, T. 2001. Subtropical SST dipole events in the southern Indian Ocean. *Geophysical Research Letters,* 28**,** 327-330.

BIASUTTI, M., SOBEL, A. H. & CAMARGO, S. J. 2009. The role of the Sahara low in summertime Sahel rainfall variability and change in the CMIP3 models. *Journal of Climate,* 22**,** 5755-5771.

BLAKE, D., KRISHNAMURTI, T., LOW-NAM, S. & FEIN, J. 1983. Heat low over the Saudi Arabian desert during May 1979 (Summer MONEX). *Monthly weather review,* 111**,** 1759-1775.

BLAMEY, R. & REASON, C. 2013. The role of mesoscale convective complexes in southern Africa summer rainfall. *Journal of climate,* 26**,** 1654-166

BOLLASINA, M. & NIGAM, S. 2011. The summertime “heat” low over Pakistan/northwestern India: evolution and origin. *Climate dynamics,* 37**,** 957- 970.

BOUCHER, O., DENVIL, S., LEVAVASSEUR, G., COZIC, A., CAUBEL, A., FOUJOLS, M.-A., MEURDESOIF, Y., CADULE, P., DEVILLIERS, M. & GHATTAS, J. 2018. IPSL IPSL-CM6A-LR model output prepared for CMIP6 CMIP piControl-spinup.

BOUCHER, O., SERVONNAT, J., ALBRIGHT, A. L., AUMONT, O., BALKANSKI, Y., BASTRIKOV, V., BEKKI, S., BONNET, R., BONY, S. & BOPP, L. 2020. Presentation and evaluation of the IPSL-CM6A-LR climate model. *Journal of Advances in Modeling Earth Systems,* 12**,** e2019MS002010.

CANE, M. A. 2005. The evolution of El Niño, past and future. *Earth and Planetary Science Letters,* 230**,** 227-240.

COOK, K.H. and VIZY, E.K., 2013. Projected changes in East African rainy seasons. *Journal of Climate*, *26*(16), pp.5931-5948.

COOK, C., REASON, C. J. & HEWITSON, B. C. 2004. Wet and dry spells within particularly wet and dry summers in the South African summer rainfall region. *Climate Research,* 26**,** 17-31.

COOK, K. H. 2000. The South Indian convergence zone and interannual rainfall variability over southern Africa. *Journal of Climate,* 13**,** 3789-3804.

CRÉTAT, J., POHL, B., DIEPPOIS, B., BERTHOU, S. & PERGAUD, J. 2019. The Angola Low: relationship with southern African rainfall and ENSO. *Climate Dynamics,* 52**,** 1783-1803.

CRETAT, J., POHL, B., DIEPPOIS, B., BERTHOU, S. G. & PERGAUD, J. 2019. The Angola Low: relationship with southern African rainfall and ENSO. *Climate Dynamics,* 52**,** 1783-1803.

D'ABRETON, P. & TYSON, P. 1995. Divergent and non-divergent water vapour transport over southern Africa during wet and dry conditions. *Meteorology and Atmospheric Physics,* 55**,** 47-59.

DIEPPOIS, B., POHL, B., ROUAULT, M., NEW, M., LAWLER, D. & KEENLYSIDE, N. 2016. Interannual to interdecadal variability of winter and summer southern African rainfall, and their teleconnections. *Journal of Geophysical Research: Atmospheres,* 121**,** 6215-6239.

DIEPPOIS, B., ROUAULT, M. & NEW, M. 2015. The impact of ENSO on Southern African rainfall in CMIP5 ocean atmosphere coupled climate models. *Climate dynamics,* 45**,** 2425-2442.

DRIVER, P., ABIODUN, B. & REASON, C. 2019. Modelling the precipitation response over southern Africa to the 2009–2010 El Niño using a stretched grid global atmospheric model. *Climate dynamics,* 52**,** 3929-3949.

DRIVER, P. & REASON, C. 2017. Variability in the Botswana High and its relationships with rainfall and temperature characteristics over southern Africa. *International Journal of Climatology,* 37**,** 570-581.

DUNNE, J. P., HOROWITZ, L., ADCROFT, A., GINOUX, P., HELD, I., JOHN, J., KRASTING, J. P., MALYSHEV, S., NAIK, V. & PAULOT, F. 2020. The GFDL Earth System Model version 4.1 (GFDL-ESM 4.1): Overall coupled model description and simulation characteristics. *Journal of Advances in Modeling Earth Systems,* 12**,** e2019MS002015.

DUNNING, C.M., ALLAN, R.P. and BLACK, E., 2017. Identification of deficiencies in seasonal rainfall simulated by CMIP5 climate models. Environmental Research Letters, 12(11), p.114001.

DUTTON, J. A. 2002. *The ceaseless wind: An introduction to the theory of atmospheric motion*, Courier Corporation.

EYRING, V., BONY, S., MEEHL, G. A., SENIOR, C. A., STEVENS, B., STOUFFER, R. J. & TAYLOR, K. E. 2016. Overview of the Coupled Model Intercomparison Project Phase 6 (CMIP6) experimental design and organization. *Geoscientific Model Development,* 9**,** 1937-1958.

ENGELBRECHT, F.A., MCGREGOR, J.L. AND ENGELBRECHT, C.J., 2009. Dynamics of the Conformal-Cubic Atmospheric Model projected climate-change signal over southern Africa. *International Journal of Climatology: A Journal of the Royal Meteorological Society*, 29(7), pp.1013-1033.

FAUCHEREAU, N., POHL, B., REASON, C., ROUAULT, M. & RICHARD, Y. 2009. Recurrent daily OLR patterns in the Southern Africa/Southwest Indian Ocean region, implications for South African rainfall and teleconnections. *Climate Dynamics,* 32**,** 575-591.

FAUCHEREAU, N., TRZASKA, S., ROUAULT, M. & RICHARD, Y. 2003. Rainfall variability and changes in southern Africa during the 20th century in the global warming context. *Natural hazards,* 29**,** 139-154.

FAVRE, A., HEWITSON, B., LENNARD, C., CEREZO-MOTA, R. & TADROSS, M. 2013. Cut-off lows in the South Africa region and their contribution to

precipitation. *Climate dynamics,* 41**,** 2331-2351.

FOGT, R. L. & MARSHALL, G. J. 2020. The Southern Annular Mode: variability, trends, and climate impacts across the Southern Hemisphere. *Wiley Interdisciplinary Reviews: Climate Change,* 11**,** e652.

FONSECA, R., FRANCIS, D., NELLI, N. & THOTA, M. 2022. Climatology of the heat low and the intertropical discontinuity in the Arabian Peninsula. *International Journal of Climatology,* 42**,** 1092-1117.

GARSTANG, M., KELBE, B. E., EMMITT, G. D. & LONDON, W. B. 1987. Generation of convective storms over the escarpment of northeastern South Africa. *Monthly weather review,* 115**,** 429-443.

GELARO, R., MCCARTY, W., SUÁREZ, M. J., TODLING, R., MOLOD, A., TAKACS, L., RANDLES, C. A., DARMENOV, A., BOSILOVICH, M. G. & REICHLE, R. 2017. The modern-era retrospective analysis for research and applications, version 2 (MERRA-2). *Journal of climate,* 30**,** 5419-5454.

GILL, A. E. 1980. Some simple solutions for heat-induced tropical circulation. *Quarterly Journal of the Royal Meteorological Society,* 106**,** 447-462.

HAARSMA, R. J., SELTEN, F. M., WEBER, S. L. & KLIPHUIS, M. 2005. Sahel rainfall variability and response to greenhouse warming. *Geophysical Research Letters,* 32.

HAMMOND, M. & LEWIS, N. T. 2021. The rotational and divergent components of atmospheric circulation on tidally locked planets. *Proceedings of the National Academy of Sciences,* 118**,** e2022705118.

HART, N. C., REASON, C. J. & FAUCHEREAU, N. 2013. Cloud bands over southern Africa: Seasonality, contribution to rainfall variability and modulation by the MJO. *Climate dynamics,* 41**,** 1199-1212.

HERMES, J. & REASON, C. 2005. Ocean model diagnosis of interannual coevolving SST variability in the South Indian and South Atlantic Oceans. *Journal of Climate,* 18**,** 2864-2882.

HERSBACH, H., BELL, B., BERRISFORD, P., HIRAHARA, S., HORÁNYI, A., MUÑOZ-SABATER, J., NICOLAS, J., PEUBEY, C., RADU, R. & SCHEPERS, D. 2020. The ERA5 global reanalysis. *Quarterly Journal of the Royal Meteorological Society,* 146**,** 1999-2049.

HOELL, A. & CHENG, L. 2018. Austral summer Southern Africa precipitation extremes forced by the El Niño-Southern oscillation and the subtropical Indian Ocean dipole. *Climate Dynamics,* 50**,** 3219-3236.

HOELL, A., FUNK, C., ZINKE, J. & HARRISON, L. 2017. Modulation of the southern Africa precipitation response to the El Niño Southern Oscillation by the subtropical Indian Ocean dipole. *Climate Dynamics,* 48**,** 2529-2540.

HOINKA, K. P. & CASTRO, M. D. 2003. The Iberian Peninsula thermal low. *Quarterly Journal of the Royal Meteorological Society: A journal of the atmospheric sciences, applied meteorology and physical oceanography,* 129**,** 1491-1511.

HOWARD, E. & WASHINGTON, R. 2018. Characterizing the synoptic expression of the Angola low. *Journal of Climate,* 31**,** 7147-7165.

HOWARD, E. & WASHINGTON, R. 2020. Tracing future spring and summer drying in southern Africa to tropical lows and the Congo Air Boundary. *Journal of Climate,* 33**,** 6205-6228.

HOWARD, E., WASHINGTON, R. & HODGES, K. I. 2019. Tropical lows in southern Africa: Tracks, rainfall contributions, and the role of ENSO. *Journal of Geophysical Research: Atmospheres,* 124**,** 11009-11032.

HUANG, B., THORNE, P. W., BANZON, V. F., BOYER, T., CHEPURIN, G., LAWRIMORE, J. H., MENNE, M. J., SMITH, T. M., VOSE, R. S. & ZHANG, H.-M. 2017. NOAA extended reconstructed sea surface temperature (ERSST), version 5. *NOAA National Centers for Environmental Information,* 30**,** 25.

HUNG, C. W. & YANAI, M. 2004. Factors contributing to the onset of the Australian summer monsoon. *Quarterly Journal of the Royal Meteorological Society: A journal of the atmospheric sciences, applied meteorology and physical oceanography,* 130**,** 739-758.

HURLEY, J. V. & BOOS, W. R. 2013. Interannual variability of monsoon precipitation and local subcloud equivalent potential temperature. *Journal of Climate,* 26**,** 9507-9527.

HURLEY, J. V. & BOOS, W. R. 2015. A global climatology of monsoon low-pressure systems. *Quarterly Journal of the Royal Meteorological Society,* 141**,** 1049-1064.

IMBOL NKWINKWA, A. S. N., ROUAULT, M., KEENLYSIDE, N. & KOSEKI, S. 2021. Impact of the Agulhas Current on Southern Africa Precipitation: A Modeling Study. *Journal of Climate,* 34**,** 9973-9988.

INNES, H. & PIERREHUMBERT, R. T. 2022. Atmospheric dynamics of temperate sub-Neptunes. I. Dry dynamics. *The Astrophysical Journal,* 927**,** 38.

JAMES, R., WASHINGTON, R. & JONES, R. 2015. Process-based assessment of an ensemble of climate projections for West Africa. *Journal of Geophysical Research: Atmospheres,* 120**,** 1221-1238.

JOHNSON, R. 2003. Thermal low. *Encyclopedia of Atmospheric Science***,** 2269-2273.

JURY, M. R., VALENTINE, H. R. & LUTJEHARMS, J. R. 1993. Influence of the Agulhas Current on summer rainfall along the southeast coast of South Africa. *Journal of Applied Meteorology and Climatology,* 32**,** 1282-1287.

KANAMITSU, M., EBISUZAKI, W., WOOLLEN, J., YANG, S.-K., HNILO, J., FIORINO, M. & POTTER, G. 2002. Ncep–doe amip-ii reanalysis (r-2). *Bulletin of the American Meteorological Society,* 83**,** 1631-1644.

KAWAMURA, R., FUKUTA, Y., UEDA, H., MATSUURA, T. & IIZUKA, S. 2002. A mechanism of the onset of the Australian summer monsoon. *Journal of Geophysical Research: Atmospheres,* 107**,** ACL 5-1-ACL 5-15.

KOBAYASHI, S., OTA, Y., HARADA, Y., EBITA, A., MORIYA, M., ONODA, H., ONOGI, K., KAMAHORI, H., KOBAYASHI, C. & ENDO, H. 2015. The JRA-55 reanalysis: General specifications and basic characteristics. *Journal of the Meteorological Society of Japan. Ser. II,* 93**,** 5-48.

KUETE, G., POKAM Mba, W. and WASHINGTON, R., 2020. African Easterly Jet South: control, maintenance mechanisms and link with Southern subtropical waves. Climate Dynamics, 54(3), pp.1539-1552.

LAVAYSSE, C., FLAMANT, C. & JANICOT, S. 2010. Regional-scale convection patterns during strong and weak phases of the Saharan heat low. *Atmospheric Science Letters,* 11**,** 255-264.

LAVAYSSE, C., FLAMANT, C., JANICOT, S., PARKER, D. J., LAFORE, J.-P., SULTAN, B. & PELON, J. 2009. Seasonal evolution of the West African heat low: a climatological perspective. *Climate Dynamics,* 33**,** 313-330.

LAVENDER, S. L. 2017. A climatology of Australian heat low events. *International Journal of Climatology,* 37**,** 534-539.

LAW, R. M., ZIEHN, T., MATEAR, R. J., LENTON, A., CHAMBERLAIN, M. A., STEVENS, L. E., WANG, Y.-P., SRBINOVSKY, J., BI, D. & YAN, H. 2017. The carbon cycle in the Australian Community Climate and Earth System Simulator (ACCESS-ESM1)–Part 1: Model description and pre-industrial simulation. *Geoscientific Model Development,* 10**,** 2567-2590.

LENSSEN, N.J., GODDARD, L. AND MASON, S., 2020. Seasonal forecast skill of ENSO teleconnection maps. *Weather and Forecasting*, 35(6), pp.2387-2406.

LINDZEN, R. S. & HOU, A. V. 1988. Hadley circulations for zonally averaged heating

centered off the equator. *Journal of Atmospheric Sciences,* 45**,** 2416-2427.

LONGANDJO, G.-N. T. & ROUAULT, M. 2023. Revisiting the Seasonal Cycle of Rainfall over Central Africa.

LOVATO, T., PEANO, D., BUTENSCHÖN, M., MATERIA, S., IOVINO, D., SCOCCIMARRO, E., FOGLI, P., CHERCHI, A., BELLUCCI, A. & GUALDI, 2022. CMIP6 simulations with the CMCC Earth system model (CMCC-ESM2).*Journal of Advances in Modeling Earth Systems,* 14**,** e2021MS002814.

LUTJEHARMS, J. R. 2006. *The Agulhas current retroflection*, Springer.

MACRON, C. M., POHL, B., RICHARD, Y. & BESSAFI, M. 2014. How do tropical temperate troughs form and develop over southern Africa? *Journal of Climate,* 27**,** 1633-1647.

MAHLALELA, P., BLAMEY, R., HART, N. & REASON, C. 2020. Drought in the Eastern Cape region of South Africa and trends in rainfall characteristics. *Climate Dynamics,* 55**,** 2743-2759.

MALHERBE, J., ENGELBRECHT, F. A. & LANDMAN, W. A. 2013. Projected changes in tropical cyclone climatology and landfall in the Southwest Indian Ocean region under enhanced anthropogenic forcing. *Climate dynamics,* 40**,** 2867-2886.

MALHERBE, J., ENGELBRECHT, F. A., LANDMAN, W. A. & ENGELBRECHT, C. J. 2012. Tropical systems from the southwest Indian Ocean making landfall over the Limpopo River Basin, southern Africa: a historical perspective. *International Journal of Climatology,* 32**,** 1018-1032.

MAOYI, M. L. & ABIODUN, B. J. 2021. How well does MPAS-atmosphere simulate the characteristics of the Botswana High? *Climate Dynamics,* 57**,** 2109-2128.

MARTIN, E. R. & THORNCROFT, C. D. 2014. The impact of the AMO on the West African monsoon annual cycle. *Quarterly Journal of the Royal Meteorological Society,* 140**,** 31-46.

MAVUME, A. F., RYDBERG, L., ROUAULT, M. & LUTJEHARMS, J. R. 2009. Climatology and landfall of tropical cyclones in the south-west Indian Ocean. *Western Indian Ocean Journal of Marine Science,* 8.

MAWREN, D., BLAMEY, R., HERMES, J. & REASON, C. 2022. On the importance of the Mozambique Channel for the climate of southeastern Africa. *Climate Dynamics***,** 1-21.

MAYER, J., MAYER, M. & HAIMBERGER, L. 2021. Consistency and homogeneity of atmospheric energy, moisture, and mass budgets in ERA5. *Journal of*

Climate, 34**,** 3955-3974.

MEQUE, A. & ABIODUN, B. J. 2015. Simulating the link between ENSO and summer drought in Southern Africa using regional climate models. *Climate Dynamics,* 44**,** 1881-1900

MINALLAH, S. & STEINER, A. L. 2021. Analysis of the atmospheric water cycle for the Laurentian Great Lakes region using CMIP6 models. *Journal of Climate,* 34**,** 4693-4710.

MORAKE, D. M., BLAMEY, R. & REASON, C. 2021. Long-lived mesoscale convective systems over eastern South Africa. *Journal of Climate,* 34**,** 6421-6439.

MULENGA, H. M. 1999. Southern African climate anomalies, summer rainfall and the Angola low.

MUNDAY, C. & WASHINGTON, R. 2017. Circulation controls on southern African precipitation in coupled models: The role of the Angola low. *Journal of Geophysical Research: Atmospheres,* 122**,** 861-877.

NDARANA, T., MPATI, S., BOPAPE, M. J., ENGELBRECHT, F. & CHIKOORE, H. 2021. The flow and moisture fluxes associated with ridging South Atlantic Ocean anticyclones during the subtropical southern African summer. *International Journal of Climatology,* 41**,** E1000-E1017.

NDARANA, T., RAMMOPO, T. S., CHIKOORE, H., BARNES, M. A. & BOPAPE, M.-J. 2020. A quasi-geostrophic diagnosis of the zonal flow associated with cut-off lows over South Africa and surrounding oceans. *Climate Dynamics,* 55**,** 2631-2644.

NGUYEN, H., HENDON, H., LIM, E.-P., BOSCHAT, G., MALONEY, E. & TIMBAL, B. 2018. Variability of the extent of the Hadley circulation in the Southern Hemisphere: A regional perspective. *Climate Dynamics,* 50**,** 129-142.

NHAMO, G. & DUBE, K. 2021. *Cyclones in Southern Africa*, Springer.

NIE, J., BOOS, W. R. & KUANG, Z. 2010. Observational evaluation of a convective quasi-equilibrium view of monsoons. *Journal of Climate,* 23**,** 4416-4428.

NKWINKWA NJOUODO, A. S., KOSEKI, S., KEENLYSIDE, N. & ROUAULT, M. 2018. Atmospheric signature of the Agulhas Current. *Geophysical Research Letters,* 45**,** 5185-5193.

NOLAN, D. S., ZHANG, C. & CHEN, S.-H. 2007. Dynamics of the shallow meridional circulation around intertropical convergence zones. *Journal of the atmospheric sciences,* 64**,** 2262-2285.

OHISHI, S., SUGIMOTO, S. & HANAWA, K. 2015. Zonal movement of the Mascarene High in austral summer. *Climate Dynamics,* 45**,** 1739-1745.OMAR, S. A. & ABIODUN, B. J. 2020. Characteristics of cut-off lows during the 2015–2017 drought in the Western Cape, South Africa. *Atmospheric Research,* 235**,** 104772.

ONOGI, K., KOIDE, H., SAKAMOTO, M., KOBAYASHI, S., TSUTSUI, J., HATSUSHIKA, H., MATSUMOTO, T., YAMAZAKI, N., KAMAHORI, H. & TAKAHASHI, K. 2005. JRA-25: Japanese 25-year re-analysis project—Progress and status. *Quarterly Journal of the Royal Meteorological Society: A journal of the atmospheric sciences, applied meteorology and physical oceanography,* 131**,** 3259-3268.

PARKER, D. J., WILLETTS, P., BIRCH, C., TURNER, A. G., MARSHAM, J. H., TAYLOR, C. M., KOLUSU, S. & MARTIN, G. M. 2016. The interaction of moist convection and mid-level dry air in the advance of the onset of the Indian monsoon. *Quarterly Journal of the Royal Meteorological Society,* 142**,** 2256-2272.

PASCALE, S., POHL, B., KAPNICK, S. B. & ZHANG, H. 2019. On the Angola low interannual variability and its role in modulating ENSO effects in southern Africa. *Journal of Climate,* 32**,** 4783-4803.

PEIXOTO, J. P. & OORT, A. H. 1992. Physics of climate.

PHILIPPON, N., ROUAULT, M., RICHARD, Y. & FAVRE, A. 2012. The influence of ENSO on winter rainfall in South Africa. *International Journal of Climatology,* 32**,** 2333-2347.

POHL, B., FAUCHEREAU, N., RICHARD, Y., ROUAULT, M. & REASON, C. 2009. Interactions between synoptic, intraseasonal and interannual convective variability over Southern Africa. *Climate Dynamics,* 33**,** 1033-1050.

POHL, B., ROUAULT, M. & ROY, S. S. 2014. Simulation of the annual and diurnal cycles of rainfall over South Africa by a regional climate model. *Climate dynamics,* 43**,** 2207-2226.

PREISSLER, M., REEDER, M. J. & SMITH, R. K. 2002. A case study of a heat low over central Australia. *Aust. Meteor. Mag,* 51**,** 155-163.

RÁCZ, Z. & SMITH, R. K. 1999. The dynamics of heat lows. *Quarterly Journal of the Royal Meteorological Society,* 125**,** 225-252.

RANDLES, C., DA SILVA, A., BUCHARD, V., COLARCO, P., DARMENOV, A., GOVINDARAJU, R., SMIRNOV, A., HOLBEN, B., FERRARE, R. & HAIR, J.

2017. The MERRA-2 aerosol reanalysis, 1980 onward. Part I: Systemdescription and data assimilation evaluation. *Journal of climate,* 30**,** 6823- 6850.

REASON, C. 1996. Topography and the dynamical response to easterly flow in Southern Hemisphere subtropical west coast regions. *Meteorology and Atmospheric Physics,* 61**,** 187-199.

REASON, C. 2001a. Evidence for the influence of the Agulhas Current on regional atmospheric circulation patterns. *Journal of Climate,* 14**,** 2769-2778.

REASON, C. 2001b. Subtropical Indian Ocean SST dipole events and southern African rainfall. *Geophysical Research Letters,* 28**,** 2225-2227.

REASON, C. 2016. The bolivian, botswana, and bilybara highs and southern hemisphere drought/floods. *Geophysical Research Letters,* 43**,** 1280-1286.

REASON, C. 2017. Climate of southern Africa. *Oxford Research Encyclopedia of Climate Science.*

REASON, C. & JAGADHEESHA, D. 2005. A model investigation of recent ENSO impacts over southern Africa. *Meteorology and Atmospheric Physics,* 89**,** 181-205.

REASON, C. & KEIBEL, A. 2004. Tropical cyclone Eline and its unusual penetration and impacts over the southern African mainland. *Weather and forecasting,* 19**,** 789-805.

REASON, C., LANDMAN, W. & TENNANT, W. 2006. Seasonal to decadal prediction of southern African climate and its links with variability of the Atlantic Ocean. *Bulletin of the American Meteorological Society,* 87**,** 941-956.

REASON, C. & PHALADI, R. 2005. Evolution of the 2002-2004 drought over northern South Africa and potential forcing mechanisms. *South African journal of science,* 101**,** 544-552.

REASON, C. J. & SMART, S. 2015. Tropical south east Atlantic warm events and associated rainfall anomalies over southern Africa. *Frontiers in Environmental Science,* 3**,** 24.

REYNOLDS, R. & BANZON, V. 2008. NOAA optimum interpolation 1/4 degree daily sea surface temperature (OISST) analysis, version 2. *NOAA National Centers for Environmental Information,* 10**,** V5SQ8XB5.

RICHARD, Y., FAUCHEREAU, N., POCCARD, I., ROUAULT, M. & TRZASKA, S. 2001. 20th century droughts in southern Africa: spatial and temporal variability, teleconnections with oceanic and atmospheric conditions.

International Journal of Climatology: A Journal of the Royal Meteorological Society, 21**,** 873-885.

ROUAULT, M., FLORENCHIE, P., FAUCHEREAU, N. & REASON, C. J. 2003. South East tropical Atlantic warm events and southern African rainfall. *Geophysical Research Letters,* 30.

ROUAULT, M., POHL, B. & PENVEN, P. 2010. Coastal oceanic climate change and variability from 1982 to 2009 around South Africa. *African Journal of Marine Science,* 32**,** 237-246.

ROUAULT, M. & RICHARD, Y. 2003. Intensity and spatial extension of drought in South Africa at different time scales. *Water Sa,* 29**,** 489-500.

ROUAULT, M. & RICHARD, Y. 2005. Intensity and spatial extent of droughts in southern Africa. *Geophysical research letters,* 32.

ROWSON, D. R. & COLUCCI, S. J. 1992. Synoptic climatology of thermal low-pressure systems over south-western north America. *International journal of climatology,* 12**,** 529-545.

RYOO, J.-M., PFISTER, L., UEYAMA, R., ZUIDEMA, P., WOOD, R., CHANG, I. & REDEMANN, J. 2022. A meteorological overview of the ORACLES (ObseRvations of Aerosols above CLouds and their intEractionS) campaign over the southeastern Atlantic during 2016–2018: Part 2–Daily and synoptic characteristics. *Atmospheric chemistry and physics,* 22**,** 14209-14241.

SCHNEIDER, U., BECKER, A., FINGER, P., MEYER-CHRISTOFFER, A., ZIESE, M. & RUDOLF, B. 2014. GPCC's new land surface precipitation climatology based on quality-controlled in situ data and its role in quantifying the global water cycle. *Theoretical and Applied Climatology,* 115**,** 15-40.

SCHWENDIKE, J., GOVEKAR, P., REEDER, M. J., WARDLE, R., BERRY, G. J. & JAKOB, C. 2014. Local partitioning of the overturning circulation in the tropics and the connection to the Hadley and Walker circulations. *Journal of Geophysical Research: Atmospheres,* 119**,** 1322-1339.

SEAGER, R. & HENDERSON, N. 2013. Diagnostic computation of moisture budgets in the ERA-Interim reanalysis with reference to analysis of CMIP-archived atmospheric model data. *Journal of Climate,* 26**,** 7876-7901.

SÉFÉRIAN, R., NABAT, P., MICHOU, M., SAINT-MARTIN, D., VOLDOIRE, A., COLIN, J., DECHARME, B., DELIRE, C., BERTHET, S. & CHEVALLIER, M.

2019. Evaluation of CNRM Earth System Model, CNRM-ESM2-1: Role of Earth system processes in present-day and future climate. *Journal of Advances in Modeling Earth Systems,* 11**,** 4182-4227.

SINGLETON, A. T. & REASON, C. 2007. Variability in the characteristics of cut-of low pressure systems over subtropical southern Africa. *International Journal of Climatology: A Journal of the Royal Meteorological Society,* 27**,** 295-310.

SPENGLER, T., REEDER, M. J. & SMITH, R. K. 2005. The dynamics of heat lows in simple background flows. *Quarterly Journal of the Royal Meteorological Society: A journal of the atmospheric sciences, applied meteorology and physical oceanography,* 131**,** 3147-3165.

STOUFFER, R. 2019. IPCC DDC: UA MCM-UA-1-0 model output prepared for CMIP6 ScenarioMIP.

SWART, N. C., COLE, J. N., KHARIN, V. V., LAZARE, M., SCINOCCA, J. F., GILLETT, N. P., ANSTEY, J., ARORA, V., CHRISTIAN, J. R. & HANNA, S. 2019. The Canadian earth system model version 5 (CanESM5. 0.3). *Geoscientific Model Development,* 12**,** 4823-4873.

TALJAARD, J. J. 1958. *South African air-masses: their properties, movement and associated weather.*

THORNCROFT, C. D., NGUYEN, H., ZHANG, C. & PEYRILLÉ, P. 2011. Annual cycle of the West African monsoon: regional circulations and associated water vapour transport. *Quarterly Journal of the Royal Meteorological Society,* 137**,** 129-147.

TIM, N., ZORITA, E., HÜNICKE, B. & IVANCIU, I. 2022. The impact of the Agulhas Current System on precipitation in southern Africa in regional climate simulations covering the recent past and future. *Weather and Climate Dynamics Discussions,* 2022**,** 1-21.

TRENBERTH, K. E., STEPANIAK, D. P. & CARON, J. M. 2000. The global monsoon as seen through the divergent atmospheric circulation. *Journal of Climate,* 13**,** 3969-3993.

TYSON, P. D. & PRESTON-WHYTE, R. A. 2000. *Weather and climate of southern Africa*, Oxford University Press.

UNGANAI, L. & MASON, S. J. 2002. Long-range predictability of Zimbabwe summer rainfall. *International Journal of Climatology: A Journal of the Royal Meteorological Society,* 22**,** 1091-1103.

USMAN, M. T. & REASON, C. 2004. Dry spell frequencies and their variability over southern Africa. *Climate research,* 26**,** 199-211.

VAN SCHALKWYK, L., BLAMEY, R., DYSON, L. & REASON, C. 2022. A climatology of drylines in the interior of subtropical southern Africa. *Journal of Climate,* 35**,** 6411-6430.

VIGAUD, N., POHL, B. & CRC)TAT, J. 2012. Tropical-temperate interactions over southern Africa simulated by a regional climate model. *Climate dynamics,* 39**,** 2895-2916.

VIGAUD, N., RICHARD, Y., ROUAULT, M. & FAUCHEREAU, N. 2009. Moisture transport between the South Atlantic Ocean and southern Africa: relationships with summer rainfall and associated dynamics. *Climate Dynamics,* 32**,** 113-123.

VIZY, E.K. and COOK, K.H., 2016. Understanding long-term (1982–2013) multi-decadal change in the equatorial and subtropical South Atlantic climate. Climate Dynamics, 46, pp.2087-2113.

VIZY, E.K., COOK, K.H., CHIMPHAMBA, J. and MCCUSKER, B., 2015. Projected changes in Malawi's growing season. Climate Dynamics, 45, pp.1673-1698.

WILLIAMS, C. J. R., KNIVETON, D. & LAYBERRY, R. 2008. Influence of South Atlantic sea surface temperatures on rainfall variability and extremes over southern Africa. *Journal of Climate,* 21**,** 6498-6520.

YIN, H., WU, Z., FOWLER, H. J., BLENKINSOP, S., HE, H. & LI, Y. 2022. The combined impacts of ENSO and IOD on global seasonal droughts. *Atmosphere,* 13**,** 1673.

YU, B. & ZWIERS, F. W. 2010. Changes in equatorial atmospheric zonal circulations in recent decades. *Geophysical Research Letters,* 37.

YU, B., ZWIERS, F. W., BOER, G. J. & TING, M. 2012. Structure and variances of equatorial zonal circulation in a multimodel ensemble. *Climate dynamics,* 39**,** 2403-2419.

YUKIMOTO, S., KOSHIRO, T., KAWAI, H., OSHIMA, N., YOSHIDA, K., URAKAWA, S., TSUJINO, H., DEUSHI, M., TANAKA, T. & HOSAKA, M. 2019. MRI MRI-ESM2. 0 model output prepared for CMIP6 CMIP historical. *Earth System*

Grid Federation, 10.

ZHAI, J. & BOOS, W. R. 2017. The drying tendency of shallow meridional circulations in monsoons. *Quarterly Journal of the Royal Meteorological Society,* 143**,** 2655-2664.

ZHANG, C. 2005. Madden-julian oscillation. *Reviews of Geophysics,* 43.ZHANG, C., MCGAULEY, M. & BOND, N. A. 2004. Shallow meridional circulation in the tropical eastern Pacific. *Journal of climate,* 17**,** 133-139.

ZHANG, C., NOLAN, D. S., THORNCROFT, C. D. & NGUYEN, H. 2008. Shallow meridional circulations in the tropical atmosphere. *Journal of Climate,* 21**,** 3453-3470.

ZIEHN, T., LENTON, A., LAW, R. M., MATEAR, R. J. & CHAMBERLAIN, M. A. 2017. The carbon cycle in the Australian Community Climate and Earth System Simulator (ACCESS-ESM1)–Part 2: Historical simulations. *Geoscientific Model Development,* 10**,** 2591-2614.